

UNIVERSITY OF THE WITWATERSRAND



CARRIER FREQUENCY OFFSET SYNCHRONIZATION
AND PHASE NOISE COMPENSATION IN COHERENT
OPTICAL OFDM SYSTEMS

BALOGUN, MUYIWA BLESSING

SEPTEMBER 2018

**CARRIER FREQUENCY OFFSET SYNCHRONIZATION
AND PHASE NOISE COMPENSATION IN COHERENT OPTICAL
OFDM SYSTEMS**

DOCTORAL THESIS BY

BALOGUN, MUYIWA BLESSING

**Submitted in fulfillment of the requirements for the degree
of Doctor of Philosophy**

**School of Electrical and Information Engineering,
University of the Witwatersrand**

SEPTEMBER 2018

**SUPERVISORS: PROFESSOR FAMBIRAI TAKAWIRA
DR. OLUTAYO OYERINDE**

The financial support of Société Internationale de Télécommunications Aéronautiques (SITA), United Kingdom and the Center for Telecommunication Access and Services (CeTAS) is hereby acknowledged.

DECLARATION

I, Balogun B. Muyiwa declare that this thesis titled, “Carrier Frequency Synchronization and Phase Noise Compensation in Coherent Optical OFDM Systems” and the work presented in it are my own. I confirm that:

- This work was done wholly or mainly while in the candidature for a research degree at this University.
- Where any part of this thesis has previously been submitted for a degree or any other qualification at this University or any other institution, this has been clearly stated.
- Where I have consulted the published work of others, this is always clearly referenced.
- Where I have quoted from the work of others, the source is always given. Hence, this thesis is entirely my own work, with the exception of such quotations.
- I have acknowledged all main sources of assistance.

Signed: _____

Date: _____

AUTHORIZATION

As the candidate's supervisors, we have approved this thesis for submission.

Name: Professor Fambirai Takawira

Signed:

Date:

Name: Dr. Olutayo Oyerinde

Signed:

Date:

PREFACE

The work presented in this thesis was carried out by Balogun Muyiwa Blessing, under the supervision of Prof. Fambirai Takawira and Dr. Olutayo Oyerinde. The research work was supported by Société Internationale de Télécommunications Aéronautiques (SITA), United Kingdom and the Center for Telecommunication Access and Services (CeTAS), School of Electrical and Information Engineering, University of the Witwatersrand.

The research work centers on techniques for mitigating the effects of carrier frequency offsets and phase noise in optical OFDM networks. Parts of this thesis have been presented at the IEEE AFRICON Conference 2017 in Cape Town, South Africa and published in the IEEE Photonics Journal. Parts of this thesis are also under review for publication in the IEEE Access Journal and the SAIEE Research Journal.

Dedicated to the high and lofty One that inhabits eternity, the Almighty God.

ACKNOWLEDGEMENT

I remain eternally grateful to the Almighty God for his continuous help, mercy, inspiration, and benevolence.

Profound gratitude goes to my amiable supervisor, Professor Fambirai Takawira. He is always there to give valuable advice, support and to meticulously read through all my manuscripts.

Sincere gratitude goes to my supportive co-supervisor, Dr. Olutayo Oyerinde for his immense support. His encouragement and words of advice are greatly appreciated.

Special appreciation goes to my super parents, Mr. and Mrs. I.O Balogun. No dictionary word and description can do them justice –They are simply awesome.

Special thanks also go to my lovely wife and three beautiful sisters for their constant support and prayers.

I am also grateful to all my friends, well-wishers, members of the Center for Telecommunication Access and Services (CeTAS) group and the entire staff members of the School of Electrical and Information Engineering.

Finally, I acknowledge the financial support of Société Internationale de Télécommunications Aéronautiques (SITA), United Kingdom. I also acknowledge the support of CeTAS, School of Electrical and Information Engineering, University of the Witwatersrand.

ABSTRACT

The deployment of optical networks has become inevitably paramount due to the phenomenal advancement in the communications industry and the associated extraordinary demand for high data throughput. Optical networks provide the needed solution and reliability especially in this era where bandwidth-hungry devices are in high demand. The current technical trend seeks to increase the optical networks capacity, flexibility and reconfigurability, in order to effectively support long haul data transportation. The orthogonal frequency division multiplexing (OFDM) technique has been proposed as a viable scheme that can be incorporated so as to greatly enhance the overall output of the existing optical transport networks. The OFDM technique has become a popular scheme in telecommunications due to its support for high data-rate transmission, robustness and spectral efficiency. The scheme is particularly of great interest and very attractive for use in optical transport system due to its tolerance to chromatic dispersion. However, with the introduction of the OFDM scheme comes the attendant challenges of carrier frequency offsets (CFO) and phase noise, which must be adequately addressed in order to ensure optimum performance of the coherent optical OFDM communication system.

This research work therefore, seeks to address the impact of phase noise and carrier frequency offset on a non-simplistic, complex and an all-encompassing optical OFDM system model which considers the influence of polarization mode dispersion, group velocity dispersions, attenuation and other polarization-dependent losses in the optical link. The effectiveness of the algorithms, utilized to combat phase noise and carrier frequency offset based on the simplistic optical OFDM models in the literature, is verified using the non-simplistic comprehensive system model. Also, a closed-form maximum likelihood (ML) method is developed and utilized for phase noise and CFO estimation. First, a closed-form ML estimator is derived and implemented for CFO estimation in coherent optical OFDM (CO-OFDM) system. Thereafter, this is then extended so that the phase noise and the CFO are jointly acquired using the derived closed-form ML method.

The closed-form derivations avoid the traditional exhaustive search associated with the traditional ML methods and ensure low complexity.

In a departure from the pilot-based methods mentioned above, the blind subspace-tracking algorithm is developed and implemented, as countermeasure to address the impact of phase noise in CO-OFDM systems. The subspace-tracking algorithm is based on the fast data projection method (FDPM). The FDPM is uniquely combined with a forward-backward linear predictor to ensure an efficient adaptive way of estimating the phase noise in the optical system. Also, a variable step-size is introduced, which deviates from the constant normalized step-size traditionally utilized for the subspace-based algorithms to ensure an enhanced overall system performance.

Furthermore, an efficient constant modulus method for CFO acquisition is introduced. The method is implemented using a cost function that ensures robustness against fiber impairments. The suitability and efficiency of the constant modulus approach in terms of the system complexity, cost-efficiency and overall performance is implemented and investigated while considering pertinent impairments along the optical fiber link. The method is adequately compared with other prominent methods in terms of system performance and complexity.

Thus, the impact of the CFO and the phase noise are adequately addressed in this research work. The performances of the various methods utilized are verified using computer simulations and documented in this thesis.

TABLE OF CONTENTS

| | |
|--|-----------|
| DECLARATION | i |
| AUTHORIZATION | ii |
| PREFACE | iii |
| DEDICATION | iv |
| ACKNOWLEDGEMENT | v |
| ABSTRACT | vi |
| TABLE OF CONTENTS | viii |
| LIST OF FIGURES | xi |
| LIST OF TABLES | xiv |
| LIST OF ACRONYMS | xv |
| LIST OF NOTATIONS | xviii |
| CHAPTER 1 GENERAL INTRODUCTION | 1 |
| 1.1. Background | 1 |
| 1.2. Research Questions | 5 |
| 1.3. Research Original Contribution | 7 |
| 1.4. Author’s Publications | 8 |
| 1.5. Thesis Organization | 8 |
| CHAPTER 2 THE OPTICAL COMMUNICATIONS SYSTEM | 10 |
| 2.1. Introduction | 10 |
| 2.2. The Optical Transmitter | 11 |
| 2.3. The Optical Receiver | 15 |
| 2.4. The Optical Fiber | 16 |
| 2.4.1. Chromatic Dispersion | 19 |
| 2.4.2. Polarization Mode Dispersion | 19 |
| 2.5. Principles of the OFDM | 20 |
| 2.6. The OFDM Transceiver | 23 |

| | |
|---|-----------|
| 2.7. Major Challenges in OFDM | 24 |
| 2.7.1. Peak-to-Average Power Ratio | 25 |
| 2.7.2. Channel Estimation..... | 26 |
| 2.7.3. Time and Frequency Synchronization | 26 |
| 2.7.3. Phase Noise | 26 |
| 2.8. Optical OFDM System versus RF OFDM System | 27 |
| CHAPTER 3 LITERATURE REVIEW..... | 30 |
| 3.1. Introduction | 30 |
| 3.2. The CO-OFDM System Model | 30 |
| 3.3. CFO Estimation Methods | 34 |
| 3.3.1. FFT Based Algorithm | 34 |
| 3.3.2. CFO Estimation using Phase Difference Method | 35 |
| 3.4. Pilot Aided Techniques | 36 |
| 3.5. RF Based Technique | 38 |
| 3.6. Maximum Likelihood Approach | 40 |
| CHAPTER 4 MAXIMUM LIKELIHOOD APPROACH FOR PHASE NOISE AND CFO ESTIMATION IN CO-OFDM SYSTEMS..... | 42 |
| 4.1. Introduction | 42 |
| 4.2. The ML-Based CFO Estimation | 44 |
| 4.2.1. Traditional ML Estimation Methods | 44 |
| 4.2.2. Proposed ML-Based CFO Estimation | 45 |
| 4.3. The ML-Based CFO and Phase Noise Joint Estimation | 48 |
| 4.4. Simulation and Discussion | 52 |
| 4.4.1. Proposed ML Based CFO Estimation | 52 |
| 4.4.2. Proposed ML-Based CFO and Phase Noise Joint Estimation | 56 |
| 4.5. Computational Complexity | 59 |
| 4.6. Conclusion | 63 |
| CHAPTER 5 EFFICIENT CONSTANT MODULUS BASED CARRIER FREQUENCY OFFSET ESTIMATION..... | 65 |

| | |
|--|------------|
| 5.1. Introduction | 65 |
| 5.2. The System Model | 66 |
| 5.3. Existing Blind CFO Estimation Methods..... | 67 |
| 5.3.1. The Power Difference Estimator | 69 |
| 5.3.2. The Amplitude Difference Estimator | 70 |
| 5.3.3. The Circularly Shifted Covariance Method | 71 |
| 5.4. Proposed Constant Modulus Based Blind CFO Estimation | 72 |
| 5.5. Computational Complexity | 77 |
| 5.6. Simulation and Discussion | 78 |
| 5.7. Conclusion | 85 |
| | |
| CHAPTER 6 ADAPTIVE SUBSPACE METHOD FOR PHASE NOISE ESTIMATION IN CO-OFDM SYSTEMS..... | 86 |
| 6.1. Introduction | 86 |
| 6.2. The Subspace Tracking Algorithm | 88 |
| 6.2.1. Iterative Subspace Computation Technique | 89 |
| 6.2.2. Modification of the Orthogonal Iteration | 90 |
| 6.3. Blind Subspace Phase Noise Estimation for CO-OFDM Systems..... | 91 |
| 6.3.1. The Subspace Problem | 91 |
| 6.3.2. The Prediction Parameter | 94 |
| 6.4. Pilot Aided Subspace Phase Noise Estimation..... | 96 |
| 6.5. Computational Complexity | 96 |
| 6.6. Simulation and discussion | 98 |
| 6.7. Conclusion | 105 |
| | |
| CHAPTER 7 CONCLUSION AND FUTURE WORK..... | 107 |
| 7.1. Conclusion | 107 |
| 7.2. Future work | 109 |
| | |
| APPENDICES | 111 |
| | |
| REFERENCES | 113 |

LIST OF FIGURES

| | |
|---|----|
| Figure 1.1: The direct-detection optical OFDM (DDO-OFDM) | 3 |
| Figure 1.2: Simple research implementation chart | 7 |
| Figure 2.1: A simple block diagram of an optical communication system | 11 |
| Figure 2.2: Block diagram of a simple optical transmitter | 12 |
| Figure 2.3: Typical Mach-Zehnder modulator | 14 |
| Figure 2.4: The IQ Mach-Zehnder modulator | 15 |
| Figure 2.5: Block diagram of a simple optical receiver | 15 |
| Figure 2.6: The basic spectrum-saving concept of OFDM channels as compared with the FDM scheme | 22 |
| Figure 2.7: A typical OFDM transceiver | 24 |
| Figure 2.8: Cyclic extension concept with guard interval N_g | 24 |
| Figure 3.1: The block diagram of a typical CO-OFDM transceiver | 31 |
| Figure 4.1: The frame structure highlighting the data and the pilot positions | 48 |
| Figure 4.2: BER sensitivity for the proposed ML-based estimation algorithms in comparison with existing methods | 54 |
| Figure 4.3: MSE comparison of the ML-based estimators at CFO $\varepsilon = 0.10, 0.20$ | 55 |
| Figure 4.4: MSE performance of the various ML-based estimators under varied fiber impairments | 55 |
| Figure 4.5: MSE versus normalized CFO graph at OSNR = 15 dB | 56 |
| Figure 4.6: CFO estimation MSE for the joint estimation algorithms with laser linewidth of 160 KHz | 60 |
| Figure 4.7: Phase noise estimation MSE for the joint estimation algorithms with CFO $\varepsilon = 0.10$ | 60 |

| | |
|--|-----|
| Figure 4.8: BER sensitivity for the proposed ML-based estimation algorithms in comparison with existing methods | 61 |
| Figure 4.9: MSE performance of the CML/DD-PA and the RF-based joint scheme under fiber impairments | 61 |
| Figure 4.10: CFO estimation MSE comparison at CFO $\varepsilon = 0.25$ with laser linewidth of 250 KHz | 62 |
| Figure 4.11: CFO estimation MSEs versus normalized CFO with laser linewidth of 250 KHz at SNR = 15 dB | 62 |
| Figure 4.12: Complexity comparison of the ML methods in terms of the number of required operations | 63 |
| Figure 5.1: The MSE versus OSNR plot for different values of R | 81 |
| Figure 5.2: MSE plot of the proposed method as a function of R (OSNR = 15 dB, 22 dB) | 80 |
| Figure 5.3: BER sensitivity for the proposed estimator in comparison with existing methods using a compensated fiber link | 81 |
| Figure 5.4: BER plot for varying values of CFO at OSNR = 15 dB | 82 |
| Figure 5.5: MSE plot of the various methods showing range limits (OSNR = 15 dB) | 82 |
| Figure 5.6: MSE performance of the various estimation methods using a fiber link of 8×80 km spans | 83 |
| Figure 5.7: MSE performance of the various estimation schemes under fiber impairments with total haul 1.8×10^3 km | 83 |
| Figure 5.8: MSE performance of the various estimation methods as function of the fiber length at OSNR=15 dB | 84 |
| Figure 5.9: Complexity graph of the various CM methods | 84 |
| Figure 6.1: MSE versus OSNR plot for the SS-FBLP method with varied values of the step-size | 101 |

| | |
|--|-----|
| Figure 6.2: MSE performance of the SS-FBLP-VSS method with varied values of the adjustment variable α | 102 |
| Figure 6.3: BER sensitivity for the proposed estimation algorithms in comparison with the direct SVD method | 102 |
| Figure 6.4: MSE performance of the proposed algorithms with linewidth set to 100 KHz and 400 KHz | 103 |
| Figure 6.5: MSE plot showing the convergence behavior of the proposed algorithms | 103 |
| Figure 6.6: MSE plot showing the convergence behavior of the proposed algorithms with pilots | 104 |
| Figure 6.7: MSE versus linewidth plot for the proposed estimation algorithms | 104 |
| Figure 6.8: Performance of the proposed estimation algorithms with varying fiber length | 105 |
| Figure 6.9: Complexity graph of the proposed methods as compared to the SVD method | 105 |

LIST OF TABLES

| | |
|--|----|
| Table 4.1: Summary of the ML-Based CFO Estimator | 47 |
| Table 4.2: Summary of the Joint ML-Based Algorithm..... | 52 |
| Table 5.1: Summary of the Proposed Algorithm | 77 |
| Table 5.2: Complexity of the various CM methods | 77 |
| Table 6.1: The modified Graam-Schmidt (MGS) orthonormalization procedure | 90 |
| Table 6.2: Orthogonal iteration variant 1 | 90 |
| Table 6.3: Orthogonal iteration variant 2 | 90 |
| Table 6.4: Orthogonal iteration variant 3 | 91 |
| Table 6.5: Computational complexity of the subspace methods | 97 |
| Table 6.6: Summary of the proposed estimation algorithm | 98 |
| Table 6.7: Simulation parameters | 99 |
| Table 6.8: Acronyms and description of techniques | 99 |

LIST OF ACRONYMS

ADC: Analog-to-Digital

ADE: Amplitude Difference Estimator

ASE: Amplified Spontaneous Emission

BER: Bit Error Rate

BPF: Band Pass Filter

BPSK: Binary Phase-Shift Keying

CD: Chromatic Dispersion

CFO: Carrier Frequency Offsets

CML: Closed-Form Maximum Likelihood

CM: Constant Modulus

CO-OFDM: Coherent Optical OFDM

CP: Cyclic Prefix

CPE: Common Phase Error

CSC: Circularly Shifted Covariance

DAB: Digital Audio Broadcasting

DAC: Digital-to-Analog

DDCE: Decision Directed Channel Estimation

DD-PA: Data-Dependent Pilot-Aided

DDO-OFDM: Direct-Detection Optical OFDM

DVB: Digital Video Broadcasting

EAM: Electro-Absorption Modulator

EDFA: Erbium-Doped Fiber Amplifier

FBLP: Forward Backward Linear Prediction

FDM: Frequency Division Multiplexing

FDFM: Fast Data Projection Method
FFO: Fractional Frequency Offset
FFT: Fast Fourier Transforms
FIR: Finite Impulse Response
GVD: Group Velocity Dispersion
HPA: High Power Amplifier
ICI: Inter Carrier Interference
IFFT: Inverse Fast Fourier Transform
IFO: Integral Frequency Offset
ISI: Inter-Symbol Interference
IQ: In-phase Quadrature
LAN: Local Area Network
LED: Light Emitting Diodes
LOs: Local Oscillators
MAN: Metropolitan Area Network
MIMO: Multiple-Input-Multiple-Output
ML: Maximum Likelihood
MSE: Mean Square Error
MSM: Metal-Semiconductor-Metal
MZM: Mach Zehnder Modulator
OFDM: Orthogonal Frequency Division Multiplexing
OOK: On-Off Keying
OSNR: Optical Signal-to-Noise Ratio
PAPR: Peak-to-Average Power Ratio
PDE: Power Difference Estimator
PDF: Probability Density Function

PDL: Polarization-Dependent Losses
PMD: Polarization Mode Dispersion
QAM: Quadrature Amplitude Modulation
QPSK: Quadrature Phase-Shift Keying
RF: Radio Frequency
SFO: Sampling Frequency Offset
SNR: Signal-to-Noise Ratio
SSMF: Standard Single-Mode Fiber
SVD: Singular Vector Decomposition
VLSI: Very Large Scale Integration Technologies
VSS: Variable Step Size
WDM: Wavelength Division Multiplexing

LIST OF NOTATIONS

| | |
|------------------|---------------------------------|
| \hbar | Planck's constant |
| ω | Optical frequency |
| K_B | Boltzmann's constant |
| T_a | Absorption temperature |
| hb | Photon energy |
| β | Propagation constant |
| n_r | Refractive index |
| q_b | Free-state wavelength |
| $\Delta\omega$ | Laser linewidth |
| ω_o | Central optical frequency |
| a_{pf} | Spontaneous emission factor |
| λ_{chp} | Chirp factor |
| q_R | Damping factor |
| Q_R | Relaxation frequency |
| q | Electron charge |
| Δ | Normalized index difference |
| c_{fc} | Fiber core radius |
| $p(\mathcal{J})$ | Normalized propagation constant |
| N | Total number of subcarriers |
| M | Number of used subcarriers |
| ε | Normalized CFO |
| \otimes | Circular convolution |
| $C^{-1}(\cdot)$ | IDFT operation |
| $Z(m)$ | Channel impulse response |

| | |
|---------------------|--|
| δ_p | Birefringence vector |
| τ_p | PDL vector |
| $\vec{\mu}$ | Pauli's vector |
| q_f | Chromatic dispersion |
| ρ_i | Laser phase noise |
| h | Combined laser linewidth |
| T_s | Symbol period |
| N_{CP} | Cyclic prefix length |
| Φ_i | Common phase error |
| σ_{ICI}^2 | Variance of the interference |
| σ_x^2 | Variance of the transmitted information signal |
| σ_G^2 | Variance of the ASE noise |
| \mathbf{X}_n | Data symbols |
| $[\cdot]^T$ | Transpose |
| $\ \cdot\ _F$ | Hilbert-Schmidt norm operation |
| \odot | Entry-wise product |
| $\mathbb{E}[\cdot]$ | Expectation operator |
| \angle | Phase angle |
| $[\cdot]^*$ | Complex conjugate transpose |

CHAPTER ONE

GENERAL INTRODUCTION

1.1. Background

The need for high data rate transmission due to the advent of bandwidth-hungry applications has necessitated various studies aimed at the provision of reliable, quality and efficient services to the satisfaction of communication system's users. Modern means of signal transmission through light wave dates back to about six decades ago after the possibilities were first demonstrated using lasers [1]. The use of optical transmission was seen as a viable and promising option due to the phenomenal rise in demand for telecommunication services. Coupled with the huge bandwidth offered by the optical transmission system, Kao and Hockham stated in 1966 [2], that the then fiber loss of 1000 dB/km, could be reduced to 20 dB/km. This encouraged a burst of research into this promising field of communications.

However, the first commercial fiber-optics transmission system only came to actualization after another decade. Around the close of the twentieth century, the first transatlantic optic-fiber cable was installed. Although a lower fiber loss was achieved few years later, the need for regeneration after short distance of propagation continued to be a great challenge [3, 4]. After the introduction of the Erbium-doped optical amplifiers and wavelength division multiplexing, the optic fiber technology asserted itself as an appropriate solution for long-haul high capacity transmission. Presently, research into this robust field has grown to meet the ever-increasing demand for Internet, which doubles in traffic every year. The fiber-optics transmission presents a technology with a large available bandwidth. This bandwidth is utilized and shared among multiple consumers, using the Wavelength Division Multiplexing (WDM) [5]. The WDM scheme allows the simple upgrade of the system capacity and various ways are still being explored to effectively

utilize the available bandwidth. There have been numerous studies towards this direction in recent years aiming at the possibility of transmitting several Tb/s over one optical fiber.

The optical communication networks have to contend with issues such as dispersion along the transmission link. A dispersion control scheme was being utilized, where dispersion compensation modules are placed at the amplifier site to mitigate the impact of dispersion along the propagation line [6]. However, the mitigation scheme only performs well when transmitting at about 10Gb/s or lower, as the scheme proves inefficient during transmission at a higher rate [7, 8]. In order to address this inefficiency, electronic equalizers were proposed as alternatives to the dispersion compensation modules [9, 10]. Although the deployment was successful to a large extent, the major step forward came early in the twenty-first century with the introduction of predistortion equalizers. The predistortion equalizers thus enabled transmission over a long distance using the standard single-mode fiber (SSMF) without any dispersion compensation [11, 12]. The introduced equalizers consist mainly of some potent silicon chip encircling a digital finite impulse filter (FIR) with taps, high-speed digital-to-analog converter and an optical in-phase quadrature (IQ) modulator. This breakthrough therefore encouraged more research into digital signal processing based optical network transmission as well as the use of coherent detection in optical network systems [13]-[16].

Recently, the introduction of orthogonal frequency division multiplexing (OFDM) scheme into the existing optical communication system was proposed and two major types of optical OFDM schemes were proposed to support long-distance transmission without the need of the traditional dispersion management. They are the direct-detection optical OFDM (DDO-OFDM), as shown in Figure 1.1, and the coherent optical OFDM (CO-OFDM), which shall be discussed further in Section 3.2 [17, 18]. Both solutions were promising although the CO-OFDM offers a superior performance in terms of polarization-dispersion resilience and spectral efficiency [18, 19]. The main advantage of the DDO-OFDM is the ease of implementation, which is simpler and less complicated, compared to its CO-OFDM counterpart. [17].

The incorporated OFDM in the CO-OFDM system has grown in popularity and the technique has been extensively deployed in various communication schemes and standards. Based on some communication preferences, some countries have elected to stick to either the single-carrier transmission or the multicarrier transmission mode. However, as extensively discussed in [20], the multicarrier transmission offered by the CO-OFDM scheme provide useful advantages in areas which are of vital importance in transmission systems, such as bandwidth scalability, computation complexity, tight bonding of spectral components, sampling rate and tolerance to system imperfection, among others. Hence, the coherent OFDM-based optical system is adopted in this research work.

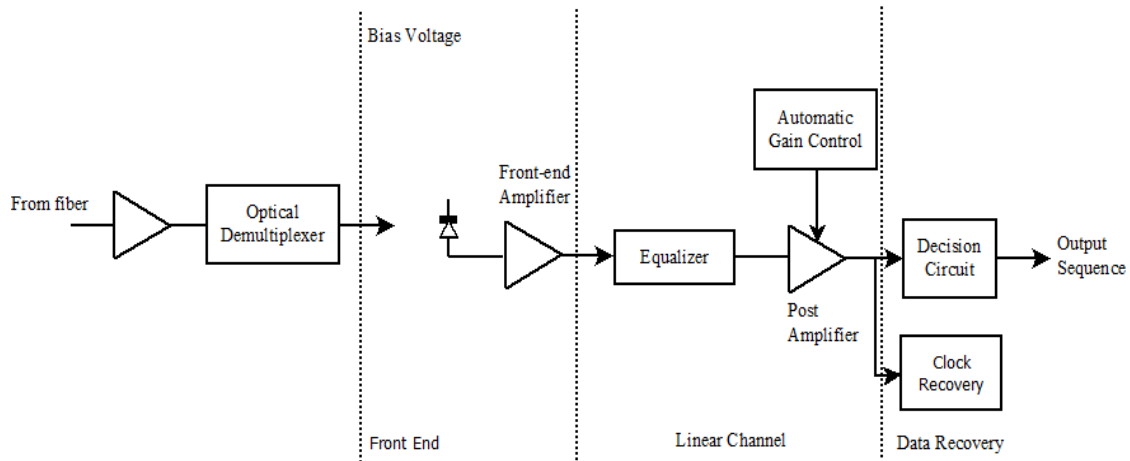


Figure 1.1: The direct-detection optical OFDM (DDO-OFDM) receiver.

Although the proposed incorporation of the OFDM technique into the traditional optical system offers useful and pertinent advantages, it however brings in a different measure of challenges, which include carrier frequency offset errors and phase noise. OFDM is highly vulnerable to these challenges due to its relatively long symbol length compared to that of the single carrier. Also the OFDM is highly sensitive to phase noise which originates from the transmit and the

receive lasers, which becomes even severe in long haul transmission. To avoid these degrading and undesirable challenges, appropriate estimation algorithms and compensation measures need to be put in place to achieve the desired system efficiency, robustness and reliability.

Various algorithms have been proposed in the literature to address the degrading impacts of the CFO and phase noise as will be discussed later in this thesis. Methods such as the pilot-aided technique, the decision-aided technique, the RF-based scheme as well as the maximum likelihood approach, have been utilized for phase noise and CFO estimation in CO-OFDM systems. However, these methods come with their inherent challenges such as increased system overhead and computational complexity.

Among the algorithms proposed in this work is a simplified maximum likelihood (ML) method, which utilizes only two long training symbols to achieve CFO estimation. Thereafter, a joint ML approach is implemented for both CFO and phase noise estimation. This approach is derived in a closed-form, to avoid the exhaustive search associated with the traditional ML methods, thereby ensuring low-complexity implementation.

Also, blind algorithms including a subspace-tracking algorithm as well as a constant modulus based estimator are developed and implemented as counter-measures for phase noise and CFO in optical OFDM systems. The subspace algorithm is implemented adaptively using a forward backward linear prediction (FBLP) technique. Also, to achieve enhanced system stability and performance, a variable step-size is introduced. The constant modulus algorithm is based on a robust cost-function similar to the Godard's method for blind channel equalization. The algorithm is clearly derived and implemented in such a way that only three trial values are required for estimation, thus ensuring low complexity and system efficiency.

1.2. Research questions

As stated earlier, the proposed introduction of the OFDM technique into the core optical transport networks is laudable as well as inevitable for scalability, robustness and efficiency. However, the inherent drawbacks in the OFDM scheme could greatly hamper all these desired elements if not adequately addressed. For the purpose of this research work, the carrier frequency offset error and phase noise will be adequately addressed.

The pertinent questions in this research work, therefore, center on the incorporated OFDM scheme in the optical network scenario and how the inherent drawbacks of these hybrid optical communications scheme can be addressed. Thus, the following questions are highlighted:

- a) There are simple CFO and phase noise estimation schemes based on fast Fourier transforms (FFT) and simple correlation methods reported in the literature, but the optical system models considered by those authors are very simplistic and not comprehensive.
 - How will these existing proposed schemes for CFO and phase noise estimation fare in a non-simplistic, complex and an all-encompassing system model?
- b) Methods employed so far for carrier frequency estimation and phase noise compensation in optical transmission mainly rely on pilot symbols, which result in increase in system overhead.
 - How would an ML-based estimator perform using only two long training symbols and how effectively will the estimator address the impact of frequency offset in optical networks?
 - How suitable and efficient is the use of blind algorithm-based methods in terms of system complexity, performance and cost-efficiency especially taking into account the fast rate of change of phase noise?

- Can the impact of phase noise and frequency offset be addressed jointly? Is the overall system performance improved if a different technique is utilized for a first stage phase noise estimation before the eventual acquisition of the CFO?

Since the focal point of the research work is phase noise compensation and carrier frequency offset estimation in optical OFDM systems, a thorough survey and analyses of the algorithms utilized so far to combat their degrading impacts is conducted. Thereafter, improved, efficient, and cost-effective algorithms are therefore proposed and implemented, to address the undesirable effects of carrier frequency offsets and phase noise on the optical OFDM scheme. These drawbacks are addressed independently and jointly, using various cost-effective and efficient algorithms. The analytical and mathematical models developed are executed using the Optilux (an optical network simulation platform), and the MATLAB software. A simple research implementation chart is shown in Figure 1.2.

Thus, for the purpose of this research work, the objectives include:

- a) Developing a comprehensive system model for the OFDM-based optical network.
- b) Investigating the impact of carrier frequency offset errors and phase noise, on the overall performance of the optical OFDM scheme.
- c) Implementing and investigating the efficiency of existing estimation and compensation schemes, which have been utilized to address the impact of carrier frequency offset errors and phase noise on the OFDM-based next generation optical networks.
- d) Developing and implementing a better and more efficient analytical model and estimation-based algorithm to independently and jointly combat the impacts of the carrier frequency offset errors and phase noise in the optical OFDM systems.
- e) Developing efficient blind estimation based algorithms to tackle the degrading effects of carrier frequency offsets and phase noise on the OFDM-based next generation optical networks.

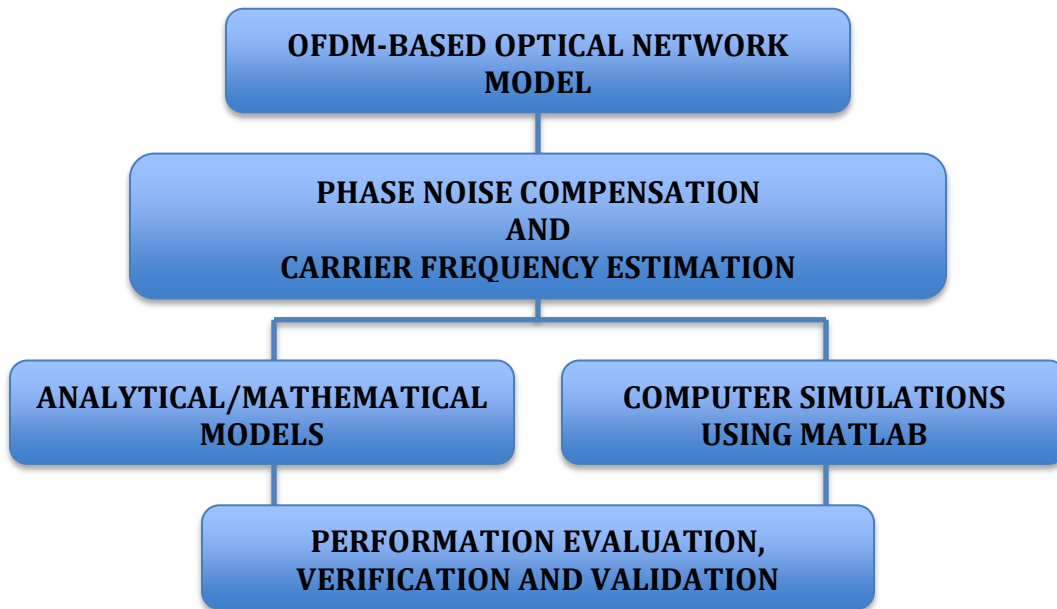


Figure 1.2: Simple research implementation chart.

1.3. Research Original Contribution

- Derivation, implementation and analysis of a closed-form ML-based estimation for both CFO and phase noise acquisition.
- Derivation and analysis of a constant modulus method, considering the influence of impairments along the optical fiber link, for CFO estimation in CO-OFDM systems.
- Derivation and implementation of a robust cost function to achieve an efficient blind estimation in CO-OFDM systems. Also, the performance analysis of an adaptive fast subspace algorithm for blind estimation in a practical optical OFDM system is carried out. The impact of a variable step-size and a forward-backward linear prediction (FBLP) parameter, on the convergence speed, stability and the overall performance of the subspace- tracking algorithm is investigated.

1.4. Author Publications

The following are peer-reviewed journals and conference publications from this research work.

- **M.B. Balogun**, O.O. Oyerinde and F. Takawira, “Performance of ML-Based Carrier Frequency Offset Estimation in CO-OFDM Systems,” in Proceedings of 2017 IEEE AFRICON, Cape Town, South Africa, pp. 175-180, Sept. 2017.
- **M.B. Balogun**, O.O. Oyerinde and F. Takawira, “Efficient Constant Modulus Based Carrier Frequency Offset Estimation for CO-OFDM Systems,” in IEEE Photonics Journal, vol. 9, no. 5, pp. 1–15, Oct. 2017.
- **M.B. Balogun**, O.O. Oyerinde and F. Takawira, “Adaptive Subspace Method for Phase Noise Estimation in CO-OFDM systems,” Accepted for publication in the IEEE Access Journal.
- **M.B. Balogun**, O.O. Oyerinde and F. Takawira, “Simplified ML-Based Carrier Frequency Offset and Phase Noise Estimation for CO-OFDM Systems,” under review for publication in the SAIEE Research Journal.

1.5. Thesis Organization

The rest of this thesis is organized as follows:

Chapter two presents the overview of the optical communication system. The major constituents of the optical system such as the optical transmitter, the optical receiver, the optical fiber channel, are highlighted. Also, a review on the principles of the OFDM technique and the associated challenges is presented in this chapter.

In Chapter three, a survey on the various prominent methods for CFO and phase noise estimation as reported in the literature, is carried out. Methods such as the FFT-based estimation technique,

the RF-based scheme, the subspace tracking algorithms as well as the constant modulus technique are reviewed.

Chapter four presents the maximum likelihood approach for the phase noise and CFO estimation in CO-OFDM systems. First, a closed-form approach for CFO estimation is derived and implemented. Thereafter, a joint approach for the estimation of both the phase noise and the CFO is described and implemented.

In Chapter five, an efficient constant modulus scheme for CFO acquisition in CO-OFDM systems is presented. The mathematical analysis as well as the derivation is clearly described.

Chapter six presents a blind subspace method for phase noise estimation. This chapter includes the adaptive implementation of a fast subspace-tracking algorithm, the introduction of the forward backward linear prediction technique as well as the incorporation of the variable step-size parameter, to achieve enhanced system performance.

Chapter seven provides the general conclusion based on all the methods presented in this research work as well as possible future research directions.

CHAPTER TWO

THE OPTICAL COMMUNICATION SYSTEM

2.1. Introduction

Generally, communication systems always demand that stringent structures, models and parameters are effectively put in place, in order to achieve a set quality of service and reliability. The optical communication networks is no exception, and the system's parameters as well as the components have to be effectively planned and implemented to achieve the best possible from the system. The general designing and modeling also entail effectively addressing various generic challenges whose effects may lead to the degradation of signal during modulation, transmission and detection process. Typically, the bit error rate (BER) and the signal to noise ratio (SNR) are used as figure of merit and for transmission quality assessment in telecommunications. Therefore, in a typical optical transport networks, optical signal parameters that determine the signal level such as the optical amplification gain, optical transmitter output power, photodiode responsivity, and optical noise parameters that determine the BER, must be carefully addressed. The common impairments to contend with in optical systems include chromatic dispersion (CD), fiber attenuation, polarization mode dispersion (PMD), fiber-nonlinearities, polarization-dependent loss (PDL), insertion loss and frequency chirp [20, 21]. Therefore, a deliberate and effective design is required to address these challenges during transmission, propagation and detection. The major components of the optical communication system as shown in Figure 2.1, will be considered in details.

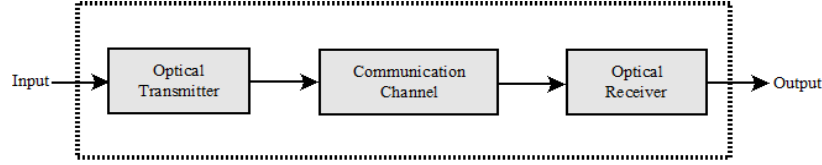


Figure 2.1: A simple block diagram of an optical communication system.

2.2. The Optical Transmitter

Optical transmitters convert the original input, which is an electrical signal, to an optical signal. The main activity of the optical transmitter is to generate the optical signal, modulate, and send the modulated signal into the fiber link. Optical transmitters, as shown in Figure 2.2, contain semi-conductor components through which the light-generation process is achieved under direct biasing, by the recombination of electrons and holes in p-n junctions. Semiconductor light sources can be classified, depending on the mode of recombination, as either light-emitting diodes (LEDs), where the recombination process is mainly spontaneous, or semiconductor lasers, in which the recombination process is achieved through stimulated emission. The three main processes in semiconductor materials through which light relates with matter include absorption, spontaneous emission and stimulated emission. Considering normal conditions, the number of electrons in ground state S_1 with energy U_1 is greater than the number of electrons in excited state S_2 with energy U_2 and their ratio follows the Boltzmann's statistics in the thermal equilibrium [23]:

$$\frac{S_2}{S_1} = \exp\left(\frac{\hbar\omega}{K_B T_a}\right) = \exp\left(\frac{U_2 - U_1}{K_B T_a}\right), \quad (2.1)$$

where the product $\hbar\omega$ is the photon energy, \hbar is the Planck's constant and ω is the optical frequency proportional to the energy difference in the energy levels U_2 and U_1 , K_B is the Boltzmann's constant, and T_a is the absorption temperature.

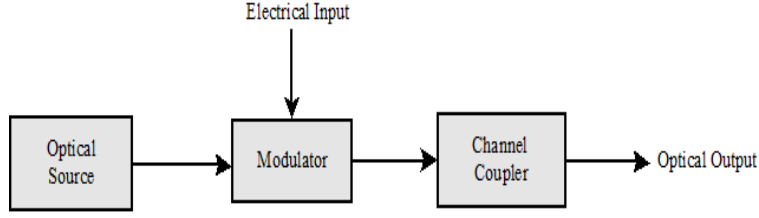


Figure 2.2: Block diagram of a simple optical transmitter.

The spontaneous emission rate is given as $dS_{2,spont}/dt = V_1 S_2$ and the stimulated emission rate is given as $dS_{2,stim}/dt = A_1 \rho(\nu) S_2$, where V_1 is the spontaneous emission coefficient, A_1 denotes the stimulated emission coefficient and $\rho(\nu)$ is the spectral density of the electromagnetic energy [23]. The spontaneous emission rate and the stimulated emission rate are equalized with an absorption rate $dS_{1,abs}/dt = V_2 \rho(\nu) S_1$, where V_2 is the absorption coefficient. However, the spontaneous emission always dominates over the stimulated emission in the visible or near-infrared region, in thermal equilibrium at room temperature.

The condition for which the stimulated emission rate can exceed the absorption rate is when S_2 is greater than S_1 and this is referred to as population inversion, although this cannot be achieved for systems in thermal equilibrium. This condition called population inversion is an essential prerequisite for laser operation. The three main modules needed to sustain stimulated emission and to form useful laser output are: the pump source, the active medium and the feedback mirrors. The pump can be electrical, like the case of semiconductor lasers, optical or chemical. The pump accomplishes the population inversion and the active medium can be of any primary state. The gain and the phase matching condition must be attained for the lasing process to be sustainable and the intensity inside the cavity can be represented as [20]:

$$C(I) = C_o \exp[(\eta(\nu) - \varphi_s)I], \quad (2.2)$$

where $\eta(v)$ and φ_s describe the gain and the scattering in the active medium respectively. Also the resultant phase matching condition to be attained is described as:

$$\exp[-j2\beta\mathcal{L}] = 1, \quad 2\beta\mathcal{L} = 2\pi r, \quad (2.3)$$

where \mathcal{L} is the length of the active medium, r is an integer for satisfying the phase matching condition, and β is the propagation constant given as:

$$\beta = 2\pi n_r / \varrho, \quad (2.4)$$

where n_r is the refractive index of the active medium and ϱ is the free-state wavelength. Also, the Lorentzian shape equation can be used to describe the spectral curve of the single-mode lasers, which is due to the transition between discrete energy levels. The equation is given as [22, 23]:

$$\mathfrak{X}(\omega) = \frac{\Delta\omega}{2\pi [(\omega - \omega_o)^2 + (\Delta\omega/2)^2]}, \quad (2.5)$$

where ω_o denotes the central optical frequency and $\Delta\omega$ denotes the laser linewidth, which can be expressed as [20]:

$$\Delta\omega = \frac{a_{pf} B (1 + \lambda_{chp}^2)}{4\pi \mathfrak{U}}, \quad (2.6)$$

where a_{pf} is the spontaneous emission factor, B represents the net rate of stimulated emission, \mathfrak{U} is the output power and the amplitude-phase coupling parameter is represented as λ_{chp} .

For the semiconductor laser, the small-signal frequency response is determined by the following expression [20, 22]:

$$H_s(\omega) = \frac{\mathfrak{Q}_R^2 + \mathfrak{d}_R^2}{(\mathfrak{Q}_R + \omega - j\mathfrak{d}_R)(\mathfrak{Q}_R - \omega + j\mathfrak{d}_R)}, \quad (2.7)$$

where \mathfrak{d}_R is the damping factor and \mathfrak{Q}_R is called the relaxation frequency [20].

The relaxation frequency is used to determine the modulation bandwidth, although the direct modulation of semiconductor lasers causes frequency chirp. Frequency chirp is an instantaneous frequency shift from steady-state frequency and can be expressed mathematically as:

$$\delta v(t) = \frac{\lambda_{chp}}{4\pi} \left[\frac{\delta \ln F(t)}{\delta t} + \mathcal{V}F(t) \right], \quad (2.8)$$

where $F(t)$ denotes the time variation of the output power, \mathcal{V} represents the constant related to the material and design parameters, while λ_{chp} is the amplitude-phase coupling parameter [23]. However, external modulation is employed as a way of addressing the chirp problem. The Mach-Zehnder modulator (MZM), as shown in Figure 2.3, and the electro-absorption modulator (EAM) are the two main types of external modulators utilized for this purpose. The material used for the MZM possesses electro-optical properties by which the phase of the optical wave propagating through it receives a phase modulation proportional to the applied electrical field. Thus, the optical power P_{out} depends on the phase difference between the arms of the modulator. In the case of a CO-OFDM system, the IQ MZM is typically used, which consists of two null-biased MZMs arranged as shown in Figure 2.4. Also, viable modulation schemes such as the binary phase-shift keying (BPSK), quadrature phase-shift keying (QPSK), differential QPSK and on-off keying (OOK) with zero/nonzero chirp can be used with these external modulators [20, 22].

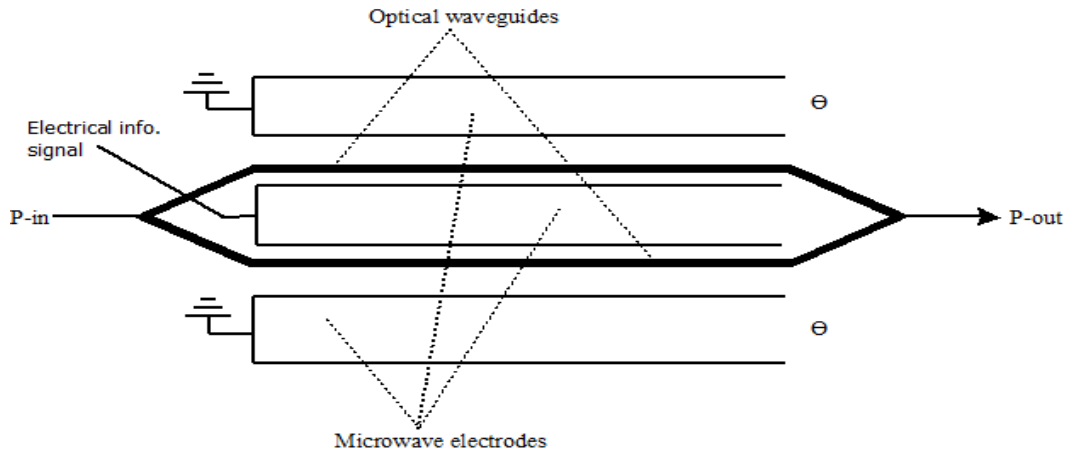


Figure 2.3: Typical Mach-Zehnder modulator.

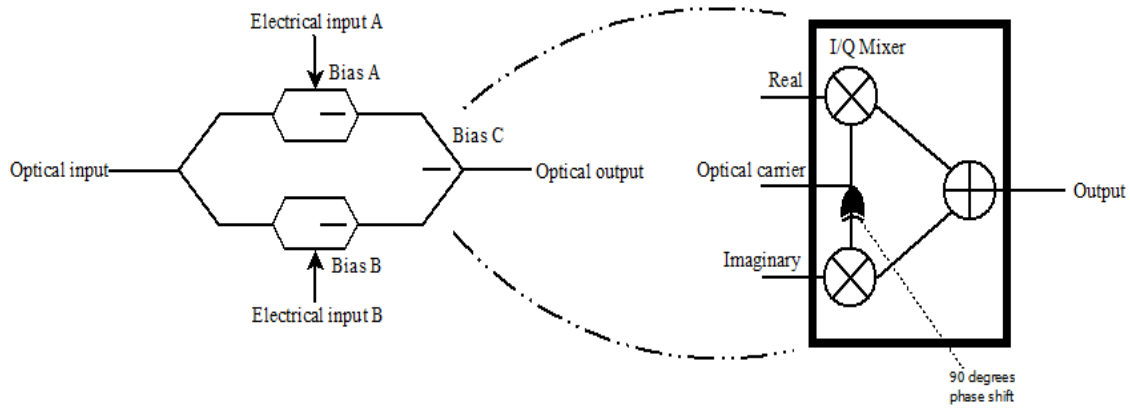


Figure 2.4: The IQ Mach-Zehnder modulator [22].

2.3. The Optical Receiver

The receiver in the optical communication system, as shown in Figure 2.5, serves to convert signals from the optical domain to the electrical domain and to effectively recover the transmitted signal. The typical optical receiver consists mainly of three stages, namely: the front-end stage, the linear channel stage and the data recovery stage. Photo-detectors and preamplifiers are the core components of the front-end stage. The high impedance front-end and the trans-impedance front-end are the two commonly used schemes in this stage. Also, the photodiodes are important part of the front-end stage as they are responsible for the absorption of photons in the incoming optical signal and convert them back to the electrical domain. This process achieved by the photodiodes is the exact opposite of what takes place in semiconductor lasers.

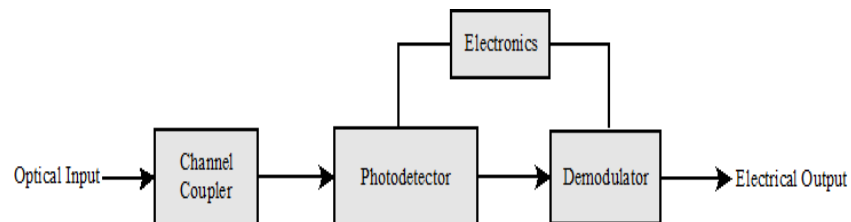


Figure 2.5: Block diagram of a simple optical receiver.

In optical communications, the popular photodiodes are the avalanche photodiodes, p-n photodiodes, p-i-n photodiodes, and the metal-semiconductor-metal (MSM) photo-detectors [22]. The p-n photodiodes, which are typically of reverse biased p-n junction, have the thickness of their depletion region less than the absorption depth for incident length. Thus, the photons are absorbed outside the depletion region, resulting in slow response speed. The avalanche photodiodes are similar to the p-i-n photodiodes, which have intrinsic regions crammed between p- and n- type layers, but operated at a very high reverse bias. The MSM photo-detectors utilize inter-digitized Schottky barrier contacts on one face of the device, which are compatible with optoelectronic integration and planar processing. The channel coupler focuses the optical signal onto the photodetector as described in Figure 2.5. Usually, an intrinsic layer is introduced to the p-i-n photodiode structure to increase the depletion region as well as to reduce the diffusion current component. The p-i-n photodiode can act as a current source, generating the photocurrent proportional to the incoming optical signal power, due to the fact that it is reverse biased and has very high internal impedance [20].

The responsivity of photodiodes is related to the quantum efficiency ϕ , which can be stated as the ratio of the number of generated electrons and the number of incident photons. This can be expressed mathematically as [20]:

$$\mathcal{D}_R = \phi q / hb , \quad (2.9)$$

where q represents an electron charge and hb denotes the photon energy. At the receiver, a drift occurs due to the lasers, causing the introduction of phase noise in the optical system.

2.4. The Optical Fiber

The optical fiber serves the main purpose of conveying optical signals from source to the required destination. The typical modern optical fiber has extremely large bandwidth and a low-loss characteristic, which enhances high-speed transmission over long distance. The major material in the manufacture of the low-loss optical fiber is the pure silica, which is further mixed with other

dopants to regulate the refractive index of the fiber. The optical fiber is made of two waveguide layers, which are the core and the cladding, both protected by a buffer coating. The core houses the majority of the power although some portions do extend to the cladding. Thus, the ray will be completely reflected from the core-cladding interface provided the condition below is satisfied [20]:

$$n_o \sin \theta_i < \sqrt{n_1^2 - n_2^2}, \quad n_o = 1, \quad (2.10)$$

where n_1 and n_2 are the refractive indices of the core and the cladding respectively and θ_i is the angle of incidence. The light-gathering capacity of an optical fiber is defined by $\max(n_o \sin \theta_i)$.

This is called the numerical aperture, and can be expressed as:

$$NA = \sqrt{n_1^2 - n_2^2} \approx n_1 \sqrt{2\Delta}, \quad \Delta \ll 1, \quad (2.11)$$

where Δ denotes the normalized index difference, which is given as $\Delta = n_1 - n_2/n_1$. Thus, it can be said that a series of total internal reflections, which take place at the core-cladding interface, enables light propagation through optical fibers.

The multimode optical fiber and the single-mode optical fiber are the two major types of optical fiber [20]. The multimode optical fiber achieves light transfer through a collection of spatial transversal modes. These modes take distinct paths along the fiber link. They are defined through a given combination of electrical and magnetic components and occupy different cross section of the fiber core. Signal distortion occurs in multimode fiber due to the difference in mode path lengths, which causes a difference in arrival times at the receiving point. This occurrence is termed as multimode dispersion. However, in single-mode optical fiber, the occurrence of multimode dispersion is eliminated, as the number of propagating modes is basically limited to one. The radial distribution of the single-mode, which occupies the central part of the optical fiber, can be approximated by a Gaussian curve. Therefore, the total number of modes that can

propagate through a given optical fiber is determined by the normalized frequency \mathcal{T} : $M_n = \mathcal{T}^2/2$, where M_n is the number of modes while \mathcal{T} is large and can be expressed as:

$$\mathcal{T} = \frac{2\pi c_{fc}}{\lambda} \sqrt{n_1^2 - n_2^2}, \quad (2.12)$$

where c_{fc} is the fiber core radius and λ is the carrier wavelength. The propagation constant ς defines the path for each mode propagating through the fiber link and the dependence of the electric and magnetic fields on axial coordinate z , is described through the factor $\exp(-j\varsigma z)$. Thus, the following condition must be satisfied by the propagation constant [20]:

$$2\pi n_2/\lambda < \varsigma < 2\pi n_1/\lambda. \quad (2.13)$$

The transmission characteristic of the optical fiber can be estimated when the fundamental dependence of the mode propagation constant on the optical signal wavelength is known. Hence, the normalized propagation constant for this purpose is given as:

$$p = \frac{\varsigma^2 - (2\pi n_2/\lambda)^2}{(2\pi n_1/\lambda)^2 - (2\pi n_2/\lambda)^2}. \quad (2.14)$$

The normalized propagation constant p is related to the normalized frequency described earlier as it is expressed as [22]:

$$p \approx (1.1428 - 0.9960/\mathcal{T})^2, 1.5 \leq \mathcal{T} \leq 2.5. \quad (2.15)$$

To address the multimode dispersion, the number of propagation modes is limited to a fundamental one: $\mathcal{T} \leq \mathcal{T}_c \approx 2.405$, with \mathcal{T}_c being the cutoff frequency, which is controlled by keeping the core radius small and the normalized index difference $\Delta = n_1 - n_2/n_1$ between 0.2% and 0.3% [20].

2.4.1 Chromatic Dispersion

Chromatic dispersion is an impairment that characterizes the single-mode optical fiber. This results from the differences in velocities among different spectral components in the same mode. Chromatic dispersion has two components, namely: material dispersion and waveguide dispersion. Indeed, the spectral components of the modulated signals travel at different speeds in the fiber-link. This results in some wavelengths arriving before others and therefore causes the signal pulse to broaden. The material dispersion is as a result of the refractive index being a function of the wavelength, described by the Sellmeier equation [22]:

$$n(\lambda) = \left(1 + \sum_{i=1}^M \frac{B_i \lambda^2}{\lambda^2 - \lambda_i} \right), \quad (2.16)$$

where M is the number of modes that can effectively propagate through an optical fiber, with typical B_i and λ_i parameters for pure silica being $B_1 = 0.6921663$ at $\lambda_1 = 0.0684043 \mu\text{m}$, $B_2 = 0.4079426$ at $\lambda_2 = 0.1162414 \mu\text{m}$, $B_3 = 0.8974794$ at $\lambda_3 = 0.896161 \mu\text{m}$ [22].

Due to the fact that the value of the normalized index difference Δ is usually small, the refractive indices of the core cladding are nearly equal. Thus, the light is not strictly confined in the fiber core, and the fiber modes are said to be weakly guided. This results in waveguide dispersion. However, the general challenge posed by chromatic dispersion may be addressed by changing the power distribution across the cross-sectional area through the use of multiple cladding layers [20].

2.4.2 Polarization Mode Dispersion

Polarization mode dispersion (PMD) has its origin in optical birefringence. In a perfect fiber, both orthogonal polarizations have the same group delays. However, in a practical scenario, fibers have some amount of asymmetry due to imperfections in the manufacturing process as well as mechanical stress on the fiber after manufacture. The asymmetry breaks the degeneracy of the orthogonally polarized modes, resulting in birefringence and a difference in the phase and group

velocities of the two modes. In a CO-OFDM, for the m th OFDM subcarrier, a typical single-mode fiber optical link is usually modeled appropriately in the frequency domain for the two polarization components in the fiber, described as [20, 22]:

$$Z(m) = e^{j\phi(m)} \prod_{p=1}^L \exp \left\{ \left(-\frac{1}{2} j \cdot \vec{\delta}_p \cdot f_m + \frac{1}{2} \vec{\tau}_p \right) \cdot \vec{\mu} \right\} \quad (2.17)$$

where $\phi(m)$ is the phase dispersion due to the fiber chromatic dispersion effect, L represents the number of PMD/PDL cascading elements described by their birefringence vector $\vec{\delta}_p$ and polarization-dependent loss (PDL) vector $\vec{\tau}_p$ and $\vec{\mu}$ is the Pauli's vector as detailed in [20]. The dispersion $e^{j\phi(m)}$ for this channel can be first estimated and factored out for channel estimation. The dispersion can be reduced effectively to a summation of only a few taps of the finite impulse response (FIR) model, if its mean PMD value is known. Therefore, channel estimation, dependent on the PMD value and the data rate, can be greatly simplified for the optical OFDM system [20].

2.5. Principles of the Orthogonal Frequency Division Multiplexing

The orthogonal frequency division multiplexing (OFDM) technique dates back to about some four decades ago when a paper published on the synthesis of band-limited orthogonal signals for multichannel data transmission was published by Chang [24], which was later patented in 1966. He proffered a principle where messages are transmitted via a linear band-limited channel without inter-carrier interference and inter-symbol interference. A year later, Saltzberg presented a performance analysis of effective signal transmission in parallel form [26]. There were other important contributions to OFDM in the following years by Weinstein and Ebert [26], Peled and Ruiz [27] among others. However, Cimini first proffered the OFDM technique as a wireless communication solution, in 1985 [28]. The OFDM is currently being employed in several wireless technologies and standards such as digital audio broadcasting (DAB), digital video broadcasting (DVB), high-rate wireless LAN standard [29] (IEEE 802.11a) and the IEEE

802.16a metropolitan area network (MAN) standard. In recent time, it has been found useful in the optical communication systems.

Orthogonal frequency division multiplexing is a multicarrier modulation technique. Essentially, high data rate streams are divided into N parallel streams, each of a lower data rate, which are modulated by N different sub-carriers while the symbol duration is being prolonged N times. The lower data rate streams are transmitted in parallel, over multiplexed subcarriers, which are mutually orthogonal. As long as orthogonality is maintained, there will be no interference between sub-carriers i.e. inter-carrier interference (ICI). As shown in Figure 2.6, unlike the conventional Frequency Division Multiplexing (FDM) scheme, the spectra of the different modulated sub-carriers overlap in OFDM. This makes OFDM an appropriate scheme for optimum and efficient use of valuable spectrum. Also, the conversion of frequency-selective fading channel into a collection of parallel flat fading sub-channels makes the structure of the receiver of OFDM system quite simple.

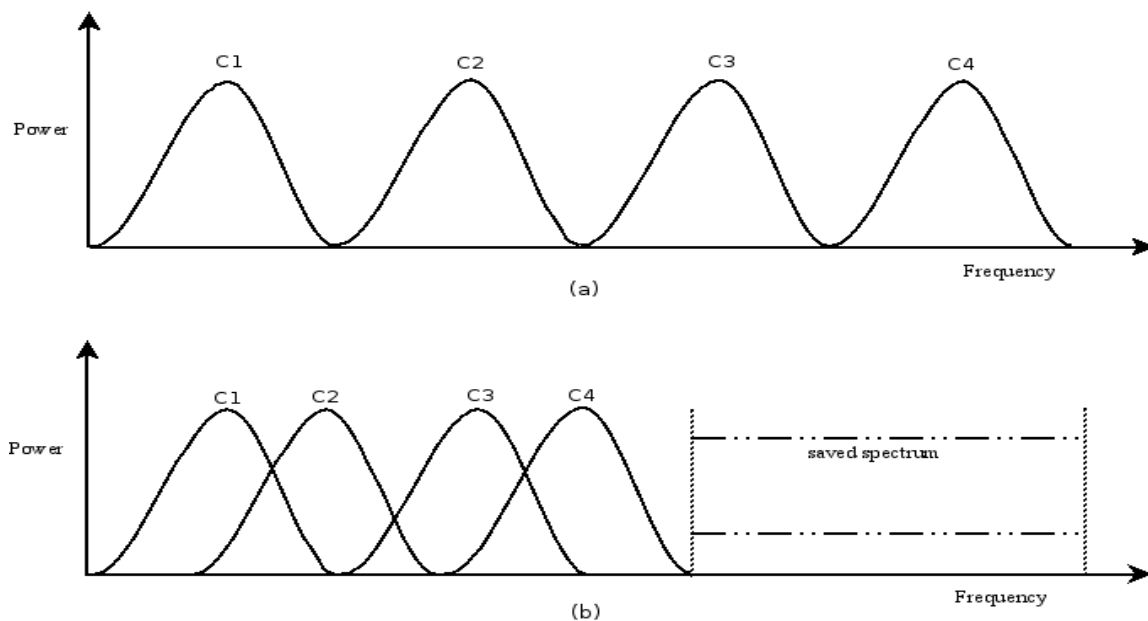


Figure 2.6: The basic spectrum-saving concept of OFDM channels (b) as compared with the FDM scheme (a).

Local Oscillators (LOs) were used earlier in OFDM implementation. However, the associated complexity and high cost made real-life implementation unsuitable. The idea behind the analog implementation was extended to the digital domain by using the DFT and IDFT [26], being employed majorly to transform data between time domain and frequency domain. The introduction and the eventual use of the discrete Fourier transform and its inverse was a major breakthrough in OFDM implementation. In practice, however, OFDM systems are implemented using a combination of FFT and inverse FFT (IFFT) blocks that are mathematical equivalent versions of the DFT and IDFT, respectively, but more efficient to implement. Recent advances in very large scale integration technologies (VLSI) also have ensured an easy, cheap and fast implementation using FFTs and IFFTs. In this approach, the data stream is divided into blocks of N symbols. Each block of data is then subjected to an IFFT and then transmitted. The immediate output of the IFFT has to be transmitted one at a time, hence, a parallel to serial conversion after the operation. This process, however, is reversed (i.e. serial to parallel conversion) and an inverse operation FFT is performed at the receiver.

2.6. The OFDM Transceiver

Figure 2.7 illustrates the adaptation of the baseband OFDM transceiver IEEE standard 802.11a. Each sub-carrier is modulated in phase and amplitude by the data bits in the OFDM system. One or more bits are being used in the modulation of each sub-carrier, depending on the kind of modulation method adopted (QPSK, 16/64 QAM, BPSK are most commonly used). Different coding schemes are used to achieve low SNR and to obtain better system efficiency. In the mapping process, modulated data are assigned to sub-carriers based on sub-carrier assignment information obtained from sub-carrier level sensing [30]. These are then serial-to-parallel converted and fed into the IFFT, which transforms the data from frequency domain to time domain. Each time-domain OFDM symbol is extended by the so-called cyclic prefix (CP) [31] or

guard interval in order to combat inter-symbol interference. Typically, guard interval or the cyclic prefix of not more than 10% (shown as N_g) of the OFDM symbol duration, as seen in Figure 2.8, is employed and later discarded at the receiver. Passing through the Digital-to-Analog (DAC) converter, the signal is amplified and up-converted to desired center frequency before transmission in the frequency selective fading channel in wireless communication scenario. At the receiver, the CP symbols are removed after analog to digital conversion. A crucial synchronization process is carried out to estimate and correct carrier frequency offsets of the received signal as well as to find the symbol boundaries to prevent inter-symbol interference (ISI) and ICI. The FFT of the signal is taken before channel estimation is carried out to evaluate the time and frequency domain response, in order to correctly detect and recover the transmitted data. The reverse of the other processes at the transmitter is executed at the receiver, before the final process of decoding takes place in order to give the binary output signal.

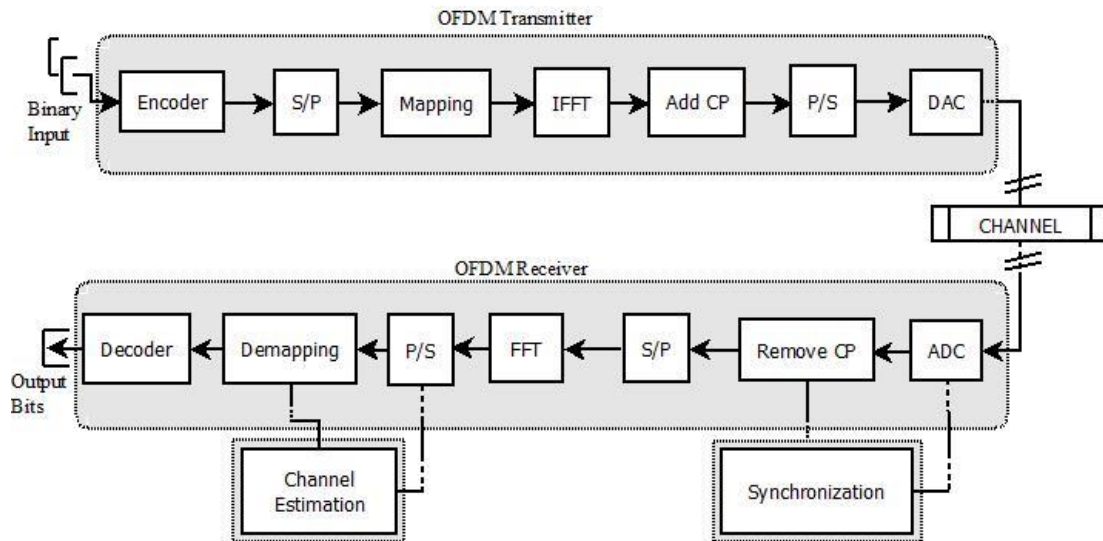


Figure 2.7: A typical OFDM transceiver.

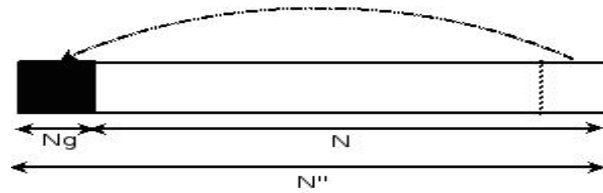


Figure 2.8: Cyclic extension concept with guard interval N_g .

2.7. Major Challenges in OFDM

Despite the laudable attributes of OFDM, which has resulted in its wide popularity as a modulation scheme for high-speed transmission, some major difficulties and drawbacks require effective handling and special attention to obtain the best operation possible out of this scheme. In subsequent sub-sections, three major issues common in the radio frequency (RF) scenario that include; 1) Peak-to-average power ratio (PAPR), 2) Time and frequency synchronization and 3) Channel estimation, are discussed.

2.7.1 Peak-to-average power ratio

Peak-to-average power ratio, which originates from the fact that an OFDM signal is the superposition of a number of modulated sub-carrier signals, is a scenario in OFDM where the peak amplitude of the emitted signal is considerably higher than the average amplitude [32]. This is a major drawback in OFDM systems, as it causes the digital-to-analog converter in the transmitter to be more complex while the efficiency of the power amplifier is reduced and the performance of the system degraded.

Non-linearity of the high power amplifier (HPA) causes in-band distortion, which leads to an increase in the bit-error rate (BER) and also out-of-band emission (emission immediately outside the necessary bandwidth), causing interference with neighboring channels.

These drawbacks, therefore, have necessitated a search for a viable technique to combat PAPR. Several techniques have been proposed, to date, which include majorly; clipping and filtering [33]-[35], coding [36], inter-leaver technique [37] and peak windowing [38]. In [33], review of some major techniques is presented. In the review paper, it is stated that although the criteria for selecting a PAPR technique involves many aspects such as PAR reduction capacity, power increase, BER increase and complexity, a main consideration is that the cost of extra complexity for PAR reduction is lower than the cost of power inefficiency. In [37], a data randomization technique is presented, where it is submitted that by interleaving a data frame, the peaks in the associated OFDM signal can be compressed. In all of these techniques, PAPR reduction is basically carried out at the transmitter.

2.7.2 Channel Estimation

Before the demodulation of the OFDM signals at the transmitter, a reliable and accurate estimation of the channel state information (CSI) is expedient, since the radio channel is frequency selective and time-varying in nature for wideband mobile communication systems [39]. Channel estimation is necessary for coherent symbol detection in an OFDM receiver.

Many techniques, which include pilot-based technique, decision direct channel estimation and blind channel estimation techniques, have been proposed for dynamic channel estimation with their own merits, demerits, and limitations. The blind channel estimation technique is studied in [40]-[42]. In [43], block-type and comb-type pilot based channel estimation techniques are described. Also, [44] pointed out the downsides of previous works on channel estimation and proposed an efficient pilot tone placement scheme applicable to OFDM systems regardless of time variation in the channel. Three pilot-aided doubly selective channel estimation schemes that exploit the proposed pilot-tone placement were presented.

In [45]-[47], Decision Directed Channel Estimation (DDCE) schemes are developed. The schemes employ both the pilot symbols as well as the detected message symbols for channel

estimation. This gives the proposed schemes an edge over previous pilot-based channel estimation techniques as the DDCE schemes benefit from the availability of about hundred percent symbols, in the absence of symbol errors by employing the detected symbols in combination with the sparsely available pilot symbols [48, 49].

2.7.3 Carrier Frequency Offset

Despite the robustness of OFDM against frequency selective fading channels, it is sensitive to carrier frequency offset errors. Carrier frequency offset error occurs when there is a frequency offset or mismatch between the transmitter carrier frequency and the receiver carrier frequency. Also, CFO can arise due to relative motion between the transmitter and the receiver. In practical systems, the mismatch of the transmitter and the receiver oscillators arises due to oscillator instability, which can be as a result of aging, temperature, humidity, pressure and electromagnetic interference. Thus, with the frequency offset, the receiver cannot sample correctly at the center frequencies of the subcarriers. This leads to ICI, which degrades system performance.

Many synchronization schemes have been proposed to combat the degrading impact of CFO in OFDM systems [50]-[55]. Some of these schemes exploit the redundancy in the cyclic prefix as in [50, 51], while the data-aided synchronization technique is also employed in some schemes [52, 53]. In [51], conventional carrier frequency synchronization is summarized. It consists of four major steps, which include frame detection, coarse frequency offset estimation, and fine frequency offset estimation [54, 55]. Some prominent methods used for CFO estimation in the literature will be discussed later in this thesis.

2.7.4 Phase noise

Phase noise $\rho(t)$ generated at both transmitter and the receiver oscillators is generally described as a continuous time Brownian motion process or a random Wiener process expressed as [57]

$$\rho(t) = \int_0^t u(t) dt \quad (2.18)$$

where $u(t)$ is a white Gaussian process with zero mean and variance $\sigma^2(t) = 2\pi ht$, while h is the combined laser linewidth. As a random Wiener process, phase noise has independent Gaussian increments and its power is a monotonically increasing function of time. This means that its power could be infinitely large as time increases. However, the phase noise can be modeled as a filtered Gaussian random variable if restricted to a finite period. For the purpose of analysis and simulation in CO-OFDM systems, the discrete noise model is utilized. As presented in [57], the phase noise can be described by a discrete process, which for the n^{th} , ($n = 0, 1, 2 \dots N$) sample of the i^{th} OFDM symbol, is given by

$$\rho_i(n) = \rho_{i-1}(n-1) + \sum_{v=-N_{CP}}^n u(i(N+N_{CP})+v), \quad (2.19)$$

where $u(v)$ denotes the independently incremental movement of the phase noise at time instant v and N_{CP} is the cyclic prefix (CP) length.

2.8. Optical OFDM system versus RF OFDM system

The optical OFDM system has its uniqueness and a clear understanding of this enables an appropriate and efficient system design for CO-OFDM system. The RF OFDM system has been studied extensively for the past two decades, however, due to the peculiarity of the optical system and the optical channel, the widely studied RF-OFDM may not be literally translated into the optical scenario. The parameters associated with CO-OFDM systems and its channel vis-a-vis RF-OFDM systems are discussed below using the typical case of the single-mode fiber optical system and the wireless OFDM scheme.

- a) Channel nonlinearity: Nonlinearity does not pose a serious challenge in the wireless channel since it is in free space. However, the fiber link is fairly nonlinear. In addition to the fiber dispersion, PMD and PDL effects, the optical channel is arguably more

complicated than the typical wireless channel. Oftentimes, there is no close-form analytical solution for nonlinear transmission in the fiber link. As a result, the numerical solutions to the nonlinear Schrodinger equation, which describes the nonlinear wave propagation in the fiber, are needed to analyze the performance [56]. The OFDM scheme is plagued with high peak-to-average power ratio, and could be thought as inappropriate for the optical fiber link with high nonlinearity. However, the chromatic dispersion in the link serves a good purpose of mitigating the nonlinearity [57] and it has been shown through experiments, the successful transmission of high Gb/s CO-OFDM over long distance fiber link [58, 59].

- b) Tolerance to out-of-band emission: The RF channel in wireless systems is closely packed as much as possible, due to the scarcity of the spectrum. Strict out-of-band requirements are therefore enforced in the wireless OFDM system. However, the wavelength division multiplexing devices are usually employed to combine multiple wavelengths in optical systems. Thus, any out-of-band emission from the CO-OFDM transmitter is effectively removed. Therefore, the CO-OFDM system is more tolerant to the out-of-band emission. The knowledge of this is useful for effective design and for addressing challenges such as the peak-to-average power ratio in CO-OFDM systems [20].
- c) Time variation of the channel characteristics: Time selectivity or dispersion is also a determining factor as important as the frequency dispersion of the channel [60, 61]. The changing rate of the channel characteristics is termed time dispersion and it is described in the wireless system as the Doppler frequency from the fast-moving mobile users. On the other hand, in the fiber-optic systems, it is characterized as the polarization motion resulting from the mechanical disturbance of the optical link. The product of the Doppler frequency in wireless systems and the OFDM symbol length defines the extent of the time selectivity, while in the optical scenario, it is defined by the product of the polarization rotation rate and the OFDM symbol length. Hence, the optical link can be

seen as quasistatic. Efficient and appropriate channel estimation can be adopted by taking advantage of this important fact.

- d) Amplifier nonlinearity: The major source of nonlinearity in wireless systems is the power amplifier, making it important to either have high saturation power RF amplifier or operate at a sufficient back-off [20]. On the other hand, the predominant amplifier utilized in optical systems is the erbium-doped fiber amplifier (EDFA), which is perfectly linear. The reason is because the response duration of the EDFA is milliseconds, thus any nonlinearity faster than milliseconds would literally vanish. The importance of this comes in the design of CO-OFDM systems, when confronted with the trade-off between the optical loss and the RF loss. The former would be chosen because it is more linear. During CO-OFDM transmitter design, for example, it would be more viable to minimize the RF drive voltage to the optical IQ modulator and optically amplify the signal to compensate for the excess loss of the optical IQ modulator [20].

CHAPTER THREE

LITERATURE REVIEW

3.1. Introduction

As stated earlier, the focus of this research work is the estimation of phase noise and CFO in coherent optical OFDM systems. This chapter therefore presents methods in the literature that have been utilized for phase noise as well as CFO estimation in optical OFDM systems. Methods such as the FFT-based estimation scheme, pilot-based schemes, RF-based estimation schemes and the maximum likelihood algorithm are reviewed. Also, blind schemes such as the constant modulus methods as well as the subspace algorithms are reviewed. These reviewed methods constitute the main schemes in the literature that are related to the research work reported in this thesis.

3.2. The coherent optical OFDM system

The block diagram of a typical coherent optical OFDM system is shown in Fig. 3.1. The binary inputs to the RF-OFDM transmitter are first encoded, and serial-to-parallel converted. The serial-to-parallel converted data are mapped and converted to time domain signals by the IFFT operation. The resulting signals are digital-to-analog converted and then undergo the filtering process, using the low pass filter to address aliasing. The RF-to-optical up-converter block transforms the transmit signal from the electrical domain to the optical domain using an optical in-phase/quadrature (IQ) modulator, which consists of two Mach-Zehnder modulators (MZMs) with a 90 degree phase offset [20].

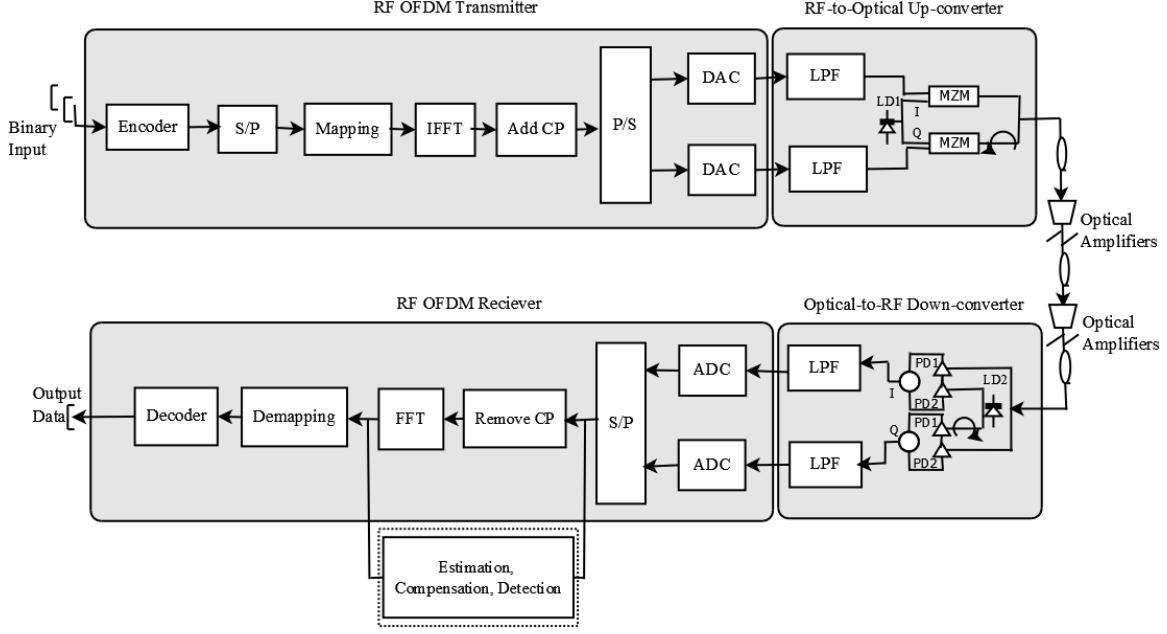


Figure 3.1: The block diagram of a typical CO-OFDM transceiver.

The baseband transmitted OFDM signal after inverse FFT (IFFT) is given as:

$$x_i(n) = \frac{1}{\sqrt{N}} \sum_{m=0}^{M-1} X_i(m) e^{\frac{j2\pi nm}{N}}. \quad (3.1)$$

where $x_i(n)$ represents the n^{th} sample of the i^{th} OFDM symbol, N is the total number of subcarriers, M is the number of used subcarriers and $X_i(m)$ represents the data symbol transmitted on the m^{th} data subcarrier. The received signal after passing through the optical channel can be written as:

$$y_i(n) = e^{\frac{j2\pi \epsilon n}{N}} e^{j\rho_i(n)} [x_i(n) \otimes C^{-1}(Z(m))] + g_i(n) \quad (3.2)$$

where ϵ , \otimes and $C^{-1}(\cdot)$ represent the normalized CFO, the circular convolution and IDFT respectively, while $g_i(n)$ is the total ASE noise generated from inline optical amplifiers. The connotation $Z(m)$, which is the holistic channel impulse response of the fiber link encompassing

the polarization mode dispersion, and other polarization dependent losses, is given by (2.17) and repeated here as [20]:

$$Z(m) = e^{j\phi(m)} \prod_{p=1}^L \exp \left\{ \left(-\frac{1}{2} j \cdot \vec{\delta}_p \cdot f_m + \frac{1}{2} \vec{\tau}_p \right) \cdot \vec{\mu} \right\} \quad (3.3)$$

where the number of the PMD/PDL cascading elements in the entire fiber link is denoted as L , with each section represented by its birefringence vector $\vec{\delta}_p$ and PDL vector $\vec{\tau}_p$ as detailed in [20]. Also, the term $\vec{\mu}$ represents the Pauli's vector, while quadratic dependence on frequency is assumed. The representation $\phi(m)$ is the group velocity dispersion (GVD), which is primarily a phase shift due to distortion in the fiber link and is expressed mathematically as:

$$\phi(m) = \pi \cdot c \cdot q_f \cdot \frac{f_m^2}{f_o^2}, \quad (3.4)$$

where q_f denotes the chromatic dispersion in the link, f_m is the frequency for the m^{th} subcarrier while f_o is the center optical frequency. The laser phase noise $\rho_i(n)$ is modeled as a Weiner-Levy process as expressed in (2.19) as [62]:

$$\rho_i(n) = \rho_{i-1}(N-1) + \sum_{v=-N_{CP}}^n u(i(N+N_{CP})+v), \quad (3.5)$$

where $u(v)$ denotes the independently incremental movement of the phase noise at time instant v and can be described as Gaussian distributed with zero mean and variance $\sigma^2 = 2\pi h T_s$, where h is the combined laser linewidth, T_s is the symbol period and N_{CP} is the cyclic prefix (CP) length.

The expression in (3.2) can be rewritten as:

$$y_i(n) = e^{\frac{j2\pi\epsilon n}{N}} e^{j\rho_i(n)} s_i(n) + g_i(n) \quad (3.6)$$

where

$$s_i(n) = x_i(n) \otimes C^{-1}(Z(m)) \quad (3.7)$$

The FFT is performed to recover the received OFDM information symbol, which is given as [63]-[65]:

$$Y_i(m) = e^{\frac{j2\pi\epsilon m}{N}} \cdot B_i(0)X_i(m)Z(m) + ICI_i(m) + G_i(m), \quad (3.8)$$

where

$$ICI_i(m) = \sum_{k=0, k \neq m}^{N-1} X_i(k) \cdot Z(k) \cdot B_i(k - m). \quad (3.9)$$

and $B_i(m)$ is a function of the distortion due to the laser phase noise, which can be expressed as:

$$B_i(m) = \frac{1}{N} \sum_{n=0}^{N-1} e^{j\rho_i(n)} \cdot e^{\frac{-j2\pi n m}{N}}. \quad (3.10)$$

Also, in (3.8),

$$B_i(0) = \frac{1}{N} \sum_{n=0}^{N-1} e^{j\rho_i(n)} \cong e^{j\Phi_i}, \quad (3.11)$$

and it denotes the phase evolution, which corresponds to the time-average of the laser phase noise over the i^{th} OFDM symbol.

Thus (3.8) becomes

$$Y_i(m) = e^{\frac{j2\pi\epsilon m}{N}} e^{j\Phi_i} \cdot X_i(m)Z(m) + W_i(m), \quad (3.12)$$

where

$$W_i(m) = ICI_i(m) + G_i(m). \quad (3.13)$$

Also, the effective signal-noise-ratio (SNR') is expressed as [66]:

$$SNR' = \frac{E\{B_i(0)X_i(m)Z(m)\}^2}{E\{ICI_i(m)\}^2 + E\{G_i(m)\}^2} = \frac{\sigma_x^2 Z^2(m)}{\sigma_x^2 \sum_{k=0, k \neq m}^{N-1} B_i^2(k - m) Z^2(k) + \sigma_G^2}, \quad (3.14)$$

$$SNR' = \frac{Z^2(m)}{\sum_{k=0, k \neq m}^{N-1} B_i^2(k - m) Z^2(k) + \frac{\sigma_G^2}{\sigma_x^2}}, \quad (3.15)$$

where σ_x^2 is the variance of the transmitted information signal, σ_G^2 is the variance of the ASE noise. Also, $\sigma_w^2 = \sigma_x^2 \sum_{k=0, k \neq m}^{N-1} B_i^2(k-m)Z^2(k) + \sigma_G^2$ is the variance of the interference plus ASE noise while $SNR = \frac{\sigma_x^2}{\sigma_G^2}$ is the original channel SNR without the effect of $ICI_i(m)$. The SNR is related to the optical SNR (OSNR) by the expression [16]

$$OSNR \text{ (dB)} = 10 \log_{10}[SNR] + 10 \log_{10} \frac{B_f}{R_s}, \quad (3.16)$$

where B_f is the central bandwidth while R_s is the symbol rate [16].

From the above expressions, the received signal can be analyzed and the impact of the phase noise as well as the CFO can be estimated, evaluated and compensated.

3.3. CFO ESTIMATION METHODS

As stated earlier the efficient estimation of the CFO in CO-OFDM systems is vital for the overall system performance. In the optical domain, the prominent schemes among the methods utilized so far for CFO estimation, as related to this research work, are reviewed in this section.

3.3.1 FFT Based Algorithm for CFO Estimation

In [67, 68], an FFT-based algorithm was proposed for frequency offset estimation in CO-OFDM systems. The algorithm has been utilized earlier in [68] but with more computational burden. The FFT-based algorithm in [67] therefore implements the algorithm with an improved computational complexity. In the paper, only the frequency offset error was considered for estimation, while the phase noise error was neglected. Also, the impact of chromatic dispersion as well as the influence of polarization mode dispersion was not put into consideration.

Considering (3.12) in the absence of phase noise, the FFT-based frequency offset (FO) algorithm as proposed in [68] is designed as follows:

1. Compute FO estimate $|\hat{\epsilon}|$ using

$$\begin{cases} |\hat{\varepsilon}| = 1/4 \varepsilon_{peak} & (3.17) \\ \varepsilon_{peak} = \arg \max_{\varepsilon} [|Y(m)|] & (3.18) \end{cases}$$

2. Assume $\varepsilon > 0$, after compensating $Y(m)$ using $|\hat{\varepsilon}|$, then

$$Y'(m) = Y(m) \exp\left(\frac{-j2\pi m |\hat{\varepsilon}| T_s}{N}\right). \quad (3.19)$$

3. Repeat the first step once more to get the residual absolute of the FO, $|\hat{\varepsilon}'|$.

4. Compare $|\hat{\varepsilon}'|$ with $|\hat{\varepsilon}|$ to determine the sign of FO. This gives,

$$\hat{\varepsilon} = \text{sign}\{|\hat{\varepsilon}| - |\hat{\varepsilon}'|\} |\hat{\varepsilon}|. \quad (3.20)$$

The FO estimation range of the algorithm in [68] is of bound $[-R_s/12, R_s/8]$, where R_s is the symbol rate. However [67] proposed an improved algorithm, whose estimation range can be up to $[-R_s/8, R_s/8]$. Therefore in [67], (3.20) is replaced by (3.21) given as:

$$\hat{\varepsilon} = \text{sign}\{|\hat{\varepsilon}'|_{th} - |\hat{\varepsilon}'|\} |\hat{\varepsilon}|, \quad (3.21)$$

where $|\hat{\varepsilon}'|_{th}$ denotes the judging threshold for $|\hat{\varepsilon}'|$ and is given as [67]:

$$|\hat{\varepsilon}'|_{th} = 1/2 [|\hat{\varepsilon}'|_{(\varepsilon>0)} + |\hat{\varepsilon}'|_{(\varepsilon<0)}]. \quad (3.22)$$

where $|\hat{\varepsilon}'|$ is the residual absolute of the FO as stated earlier.

3.3.2 CFO Estimation Using the Phase Difference Method.

In [54], an estimation scheme based on the phase-difference method is used for the acquisition of CFO in a CO-OFDM system. However, the impacts of the chromatic dispersion and other fiber impairments were not considered. The expression in (3.6) is modified for the MPSK symbol containing CFO, phase noise and the ASE noise as:

$$y_i(n) = e^{j(\rho_i(n) + 2\pi\varepsilon n + \eta_i(n))} + g_i(n) \quad (3.23)$$

$$= r_i(n) e^{j(\rho_i(n) + 2\pi\varepsilon n + \eta_i(n) + \vartheta_i(n))}, \quad (3.24)$$

where $\eta_i(n)$ is the transmitted data phase, $\rho_i(n)$ is the phase noise, ε is the normalized CFO, $g_i(n)$ is the ASE noise, $r_i(n)$ is the overall signal modulus while $\vartheta_i(n)$ represents the ASE induced phase error, which is assumed to be Gaussian distributed. The CFO estimation algorithm

is achieved by averaging the phase difference between adjacent modulation-free symbols [64]. The M^{th} -order power operation, which is used to remove modulated data phase, is employed [13]-[15]. Hence, $y_i(n)$ is raised to the M^{th} power, where $M = 2^d$ ($d = 2, 3, 4 \dots$) is the power index. For different types of modulation formats, different values of M are required to remove the modulated data phase. The resulted signal is expressed as [54]:

$$y_i^M(n) = r_i^M(n) e^{(jM(\rho_i(n)+2\pi\epsilon n+\vartheta_i(n)+\eta_i(n)))}. \quad (3.25)$$

Then by multiplying $y_i^M(n)$ with the conjugate of its N^{th} previous signal $y_i^M(n - N)$, the CFO induced phase difference signal can be obtained as [54]:

$$d_i(n) = r_i^M(n)r_i^M(n - N) e^{(jM(\rho_i(n)-\rho_i(n-N)+2\pi\epsilon n+\eta_i(n)-\eta_i(n-N)))} \quad (3.26)$$

Thus, $d_i(n)$ is obtained by multiplying $y_i^M(n)$ in (3.25) with the conjugate of its previous signal $y_i^M(n - N)$ while the phase noise here is assumed to be constant for a few symbol duration, so that the term $\rho_i(n) - \rho_i(n - N)$ in (3.26) can be ignored. Hence, $d_i(n)$ represents the CFO signal corrupted with ASE noise induced phase $\vartheta_i(n) - \vartheta_i(n - N)$ and (3.26) is rewritten as:

$$d_i(n) = r_i^M(n)r_i^M(n - N) e^{(jM(2\pi\epsilon n+\vartheta_i(n)-\vartheta_i(n-N)))}. \quad (3.27)$$

Therefore the normalized CFO estimation is obtained as:

$$\hat{\epsilon} = \frac{\arg(\sum_{n=1}^N d_i(n))}{2\pi MN}. \quad (3.28)$$

where $\arg(\cdot)$ is the phase angle.

The complexity of the M^{th} power is greatly increasing along with N . Also, when the power number M increases, the required multiplication operations increase as well. This drawback leads to the M^{th} power operation not being applicable to high order modulation formats [14].

3.4. Pilot Aided Techniques for Phase Noise Estimation

The estimation of the phase noise is pertinent to achieve an efficient CO-OFDM system performance. Pilot-aided methods are the most prominent techniques utilized for the acquisition

of phase noise in CO-OFDM systems. This is due to the random nature of the phase noise as described by the Wiener process. In [69]-[72], pilot-aided methods are proposed for phase noise estimation and compensation in CO-OFDM systems. Pilot-aided and data-aided phase estimation were proposed and compared for coherent optical systems in [69, 70]. In the papers, it was shown that as few as five subcarriers are sufficient for pilot-aided phase estimation.

In all the methods examined in [69]-[71], only the phase noise effect is considered while the frequency offset is assumed perfect. Also, in [69]-[71], all the fiber link dispersions, including the chromatic dispersion, group velocity and the polarization mode dispersion, were neglected.

Considering the pilot-aided method employed in [69], the received signal is as described in (3.2) while neglecting the CFO in the system. The first step of the pilot-aided method is to compute the phase angle difference between the received and the transmitted pilot subcarriers. Then the laser phase drift of each OFDM symbol is obtained by averaging the phase difference across all the pilot subcarriers. The estimated phase drift can be expressed as:

$$\Phi_i = 1/N_p \sum_{n=1}^{N_p} \{arg(y_i(n)) - arg(\hat{x}_i(n))\}, \quad (3.29)$$

where $arg(\cdot)$ is the phase angle of the symbol, $\hat{x}_i(n)$ is the known transmitted pilot subcarrier while N_p is the number of pilot subcarriers.

Now considering the case where data subcarriers are used together with the M^{th} -power operation, where N_{sc} is the number of data subcarriers and $M = 2^d$ ($d = 2, 3, 4 \dots$) is the power index, the received signal remains the same as described in (3.2) in the absence of CFO. After averaging across all the subcarriers in the OFDM symbol, the estimated phase drift can be written as [73]:

$$\Phi_i = 1/N_{sc} \sum_{n=1}^{N_{sc}} \{arg(y_i(n)^M) / M\}. \quad (3.30)$$

Also, as implemented in [71], by transmitting a few pilot symbols $\hat{x}_i(n)$, the common phase error (CPE) can be estimated as in pilot-aided methods as [71]:

$$\Phi_i = \arg \left(\frac{1}{N_p} \sum_n^{N_p} \frac{y_i(n) \cdot \hat{x}_i(n)}{|y_i(n)| \cdot |\hat{x}_i(n)|} \right), \quad (3.31)$$

where $\arg(\cdot)$ is the phase angle of the information symbol, $\hat{x}_i(n)$ is the known transmitted information symbol and N_p is the number of pilot symbols.

3.5. RF-Based Technique for Joint CFO and Phase Noise Estimation

In [74], the RF-pilot based estimation method is proposed. The RF-based method is implemented in such a way that the CFO can be easily estimated by searching the peak of the spectral samples. The system model employed was also simplistic, without considering fiber dispersions and attenuations. The pilot scheme utilized introduces some overhead into the system.

Joint carrier frequency offset and phase noise using RF-based technique is detailed in [75]. In order to obtain the optimum compensation performance with low computing cost when combining the RF-phase estimation and RF-frequency offset estimation, the joint compensation scheme is developed in such a way that the only integral part frequency offset (IFO), needs to be estimated by the RF-frequency offset estimates based on the aid of the pre-estimation of the fractional part of frequency offset (FFO). After that, RF-phase estimation utilizes a band-rejection filter (BRF) filter and compensates all the phase impairments. Three computational steps are taken into consideration according to [75]:

1. The signal discrete spectrum is obtained by performing FFT on N received samples. The intensity of signal discrete spectrum can thus be formulated as:

$$|Y(m)|^2 = \left| \sum_{n=0}^{N-1} y(n) \exp \left(\frac{-j2\pi nm}{N} \right) \right|^2, \quad (3.32)$$

2. In order to observe spectral shift and estimate FO conveniently, the discrete spectrum is reshaped based on the frequency distribution characteristics of the FFT.

3. The FO can therefore be estimated by finding an index of the sample that has the maximum intensity value, i.e.:

$$\hat{\varepsilon} = \left(\underset{m=1,2,\dots,N}{\text{find max}}(|Y'(m)|^2) - N/2 - 1 \right) \cdot f_{sc}, \quad (3.33)$$

where $\hat{\varepsilon}$ denotes the estimated FO value, $Y'(m)$ stands for the discrete spectral samples after reshaping, $\text{find max}(A)$ represents the operation of “finding the index number corresponding to the maximum value of A” and f_{sc} represents the spectral resolution.

To achieve the joint CFO and phase noise estimation, the correlation function is first obtained, which is further utilized to estimate the FFO. Thus, the estimate for the FFO is given by [75, 76]:

$$\hat{\varepsilon}_{FFO} = \frac{\arg(P(d))}{\pi} \cdot f_{sc}, \quad (3.34)$$

where $P(d)$ is the correlation function given as,

$$P(d) = \sum_{n=0}^{N/2-1} y^*(d+n)y(d+n+N/2), \quad (3.35)$$

where d denotes the maximum timing metric [76],

$$C(d) = \frac{|d|^2}{\left(\sum_{n=0}^{N/2-1} |y(d+n)|^2 \right) \left(\sum_{n=0}^{N/2-1} |y(d+n+N/2)|^2 \right)}, \quad (3.36)$$

and $(.)^*$ stands for the complex conjugate operation.

In order to avoid unnecessary repeat operations for phase compensation, the estimated FO value $\hat{\varepsilon}$ is directly set as the central frequency for the BPF instead of employing a low pass filter (LPF) to filter the RF-pilot after IFO correction. In this case, the extracted RF-pilot will include all the phase impairments, which are induced not only by the laser phase noise, but the IFO as well as residual FFO. The combined phase impairments can be calculated as [75]:

$$\exp(j(2\pi n\hat{\varepsilon} + \hat{\rho}(n) + \hat{\vartheta}_i(n))) = \frac{y'_{BPF}(n)}{\text{abs}(y'_{BPF}(n))}, \quad (3.37)$$

where $\text{abs}(\cdot)$ represents the absolute value of the input element, y'_{BPF} is the filtered signal (namely the extracted RF-pilot), $\hat{\varepsilon}$ is the estimated FO, $\hat{\rho}(n)$ and $\hat{\vartheta}_i(n)$ represent the estimated

phase noise of laser linewidth and ASE induced phase error respectively. All the phase impairments can therefore be compensated as [75]:

$$\hat{y}(n) = \bar{y}(n) \cdot \exp\left(-j(2\pi n\hat{\varepsilon} + \hat{\rho}(n) + \hat{\vartheta}_i(n))\right). \quad (3.38)$$

where \bar{y} denotes the digital samples after FFO compensation.

3.6. Maximum likelihood Method for Phase Noise and Channel Estimation

In [65], a maximum likelihood (ML) phase estimation and channel estimation for CO-OFDM was proposed. The focus was on phase estimation and channel estimation, while the frequency offset error was not considered. The use of ML for joint phase and frequency estimation was also not considered. The system model employed does not consider the holistic fiber dispersion and distortions like the polarization mode dispersion as well as the chromatic dispersion in the system. The proposed algorithm is however, a hybrid method as it combines ML with pilot-assisted method for optimal performance. Assuming perfect frequency synchronization and FFT window, the received signal is described in (3.12) as:

$$Y_i(m) = e^{j\Phi_i} \cdot X_i(m)Z(m) + W_i(m), \quad (3.39)$$

Also, it is assumed that the channel transfer function and the noise variance δ_m^2 of the combined noise interference $W_i(m)$ are known.

Thus, the search for the optimal phase Φ_i becomes an ML problem, that is, the minimization of the following likelihood function given by [65]:

$$\Lambda_i = \delta_m^{-2} \sum_{m=1}^{N_p} |Y_i(m) - Z(m)X_i(m)e^{j\Phi_i}|^2. \quad (3.40)$$

where N_p represents the number of pilot subcarriers.

In (3.40), the expression can be expanded as

$$\Lambda_i = \delta_m^{-2} \sum_{m=1}^{N_p} (Y_i(m) - Z(m)X_i(m)e^{j\Phi_i})(Y_i(m) - Z(m)X_i(m)e^{j\Phi_i})^* \quad (3.41)$$

Therefore, by expanding (3.40), the minimization of Λ_i with respect to the common phase noise Φ_i results in [65]:

$$\Phi_i = \arg \left(\delta_m^{-2} \sum_m^{N_p} Y_i(m) Z(m)^* X_i(m)^* \right). \quad (3.42)$$

Following the same approach as in (3.40) and (3.42), the ML channel estimate is obtained according to [65] by:

$$\hat{Z}(m) = \frac{\sum_{i=1}^N Y_i(m) X_i(m)^* e^{-j\Phi_i}}{\sum_i^N |X_i(m)|^2}. \quad (3.43)$$

In (3.43), it is assumed the phase noise has been obtained from (3.42). If the effect of noise variance δ_m^2 is ignored, (3.42) will reduce to the least square (LS) method of [64]. The ML method may be preferred over LS method in optical OFDM systems. In wireless system, the noise is dominated by the detection circuit thermal noise, which can be assumed constant across all subcarriers. However, in the optical system, the dominant noise is the amplified-spontaneous noise distributed along many fiber spans. Due to the interaction of PMD and PDL, the noise for individual carriers can be different or ‘colored’. Therefore, it is advantageous to use the ML method that includes the effect of the colored noise variance [65]. As seen from this ML approach, the same procedure can also be assumed in the case of the acquisition of both the CFO and the phase noise in CO-OFDM systems.

CHAPTER FOUR

MAXIMUM LIKELIHOOD APPROACH FOR PHASE NOISE AND CFO ESTIMATION IN CO-OFDM SYSTEMS

4.1. Introduction

Various techniques and algorithms have been proposed to separately combat the degrading impact of phase noise and CFO in CO-OFDM systems [68]-[74]. In [69, 70], pilot techniques were utilized for phase estimation in CO-OFDM systems. Also, an M^{th} -power law data-aided estimator was implemented in [69]. However, the overall performance of this approach is grossly affected by the phase ambiguity associated with the M^{th} -power law method. The RF method was presented for phase noise estimation and compensation in [74]. In the RF estimation approach, the phase acquisition is realized by placing an RF-pilot tone in the middle of the OFDM transmit spectrum, which is then utilized at the receiver end to reverse any phase noise impairments in the system. Also, [75] presents a joint RF-based frequency offset and phase noise compensation scheme, in which the frequency offset is split into the integral part (IFO) and the fractional part (FFO). During implementation, the IFO was estimated based on the pre-acquisition of the FFO. In the approach, the signal discrete spectrum is acquired by performing the fast Fourier transforms (FFT) on the received samples. The discrete spectrum is reshaped based on the frequency distribution properties of the FFT and the frequency offset is estimated by obtaining an index of the sample that has the maximum intensity value. In [67, 68], an FFT-based frequency estimation technique was proposed. The technique was implemented by first obtaining the estimated absolute value of the frequency offset by identifying the frequency of peak value in the signal spectrum. The sign of the frequency offset is then obtained using a piecewise linear function of the absolute value of the estimated frequency offset as the judging threshold [68].

In [65], the maximum likelihood (ML) scheme was utilized to estimate the channel and the phase noise. Also, [63] implemented a joint carrier frequency offset (CFO) and sampling frequency offset (SFO) ML scheme where two long training symbols were utilized for the entire estimation in the wireless domain. However, for the estimation of CFO and phase noise, the CFO can be assumed to vary slowly, therefore will remain constant across a frame, but the evolution of the phase noise within a frame results in fast variation and pilot subcarriers are required for efficient estimation.

The focus of this chapter is therefore in two folds. The first part focuses on the estimation of only the CFO using ML-based techniques. An ML estimation of the CFO, based on the method in [63], is proposed. The proposed method utilizes only two identical training symbols for CFO estimation in the frequency domain. The estimation is achieved by exploiting the phase shift between the two training symbols. Solving and obtaining a simplified expression for the CFO removes the need for the commonly required exhaustive search. Thus, a closed-form solution is derived and presented to address the high computational burden associated with ML methods [94]-[97]. This reduces system complexity while ensuring an enhanced system performance and overall efficiency. The derived ML-based method for CFO estimation in CO-OFDM systems is compared with existing ML methods in terms of performance and system complexity.

The second part considers the acquisition of both the CFO and the phase noise using the closed-form ML-based estimator, with a cost function that includes the effect of the dominance of the amplified spontaneous emission (ASE) noise along the optical fiber link. To achieve this, an initial approach, where the closed-form ML algorithm is utilized to acquire both the phase noise and the CFO, is considered. Thereafter, another approach, where the derived CML estimator is combined with a data dependent technique for the acquisition of both the CFO and the phase noise, is then considered. The data-dependent pilot-aided technique differs from the conventional pilot aided method where pilot subcarriers are predetermined. This approach is implemented in such a way that the phases of the pilot subcarriers are dependent and correlated to the phase of the

data subcarriers. The hybrid technique is aimed at improving the overall system performance and efficiency, without the additional overhead that is associated with conventional pilot-aided methods [71]. The results are compared with prominent existing methods such as the pilot-based methods, the FFT-based method and the RF-based method. Pertinent impairments along the fiber link such as polarization mode dispersion (PMD), group velocity dispersion (GVD), chromatic dispersion (CD) [23] are considered during the modeling and the implementation of the proposed estimators.

4.2. The ML-Based CFO Estimation

4.2.1 Traditional ML Estimation Methods

For the estimation of the CFO, the received sequence as expressed in (3.6) is considered and rewritten as (4.1), given as

$$y_i(n) = e^{\frac{j2\pi\epsilon n}{N}} e^{j\rho_i(n)} s_i(n) + g_i(n). \quad (4.1)$$

In the absence of noise-interference and phase noise, (4.1) can be expressed in the frequency domain as

$$R_i(m) = e^{\frac{j2\pi\epsilon m}{N}} \sum_{n=0}^{N-1} s_i(n) e^{-\frac{j2\pi n m}{N}}. \quad (4.2)$$

Considering the two consecutive OFDM sequences, which are the same except for a phase difference given as [50]

$$R_2(m) = R_1(m) e^{j2\pi\epsilon}. \quad (4.3)$$

Now including the noise-interference component, then

$$Y_1(m) = R_1(m) + W_1(m) \quad (4.4)$$

$$Y_2(m) = R_1(m) e^{j2\pi\epsilon} + W_2(m) \quad (4.5)$$

Using the observations as expressed in (4.4) and (4.5), it is shown in [50] that the CFO estimation can be obtained by

$$\hat{\varepsilon} = \left(\frac{1}{2\pi}\right) \tan^{-1} \left\{ \left(\sum_{m=0}^{N-1} \text{Im}[Y_2(m)Y_1^*(m)] \right) / \left(\sum_{m=0}^{N-1} \text{Re}[Y_2(m)Y_1^*(m)] \right) \right\}. \quad (4.6)$$

In [63], two training symbols are utilized to derive the ML CFO estimator. This is achieved by obtaining the ratios of two frequency observations, according to [63] as follows

$$D(m) = \frac{X_1(m)Y_2(m)}{X_2(m)Y_1(m)} = e^{j2\pi\varepsilon} + E(m), \quad (4.7)$$

where $E(m)$ is the error term [63], which is assumed to be Gaussian-distributed with zero mean and covariance matrix $\sigma_E^2 I_N$. Therefore, based on the expression in (4.7), the CFO ε is obtained based on the likelihood function $p(D(m)|\varepsilon)$, given as [63, 97]

$$p(D(m)|\varepsilon) = \frac{1}{(\pi\sigma_E^2)^N} \exp \left\{ -\frac{1}{\sigma_E^2} \sum_{m=1}^N |D(m) - e^{j2\pi\varepsilon}|^2 \right\} \quad (4.8)$$

Hence, the CFO is obtained by the following expression

$$\hat{\varepsilon} = \arg \min_{\varepsilon} \sum_{m=1}^N |D(m) - e^{j2\pi\varepsilon}|^2. \quad (4.9)$$

The CFO ML estimator in (4.9) requires the traditional exhaustive search, which increases system complexity, and its performance is highly influenced by channel conditions.

4.2.2. Proposed ML Based CFO Estimation

In order to achieve an enhanced CFO ML estimation using only two training sequences, which are assumed to be identical, this section proposes an efficient ML estimator, which is further implemented in a closed-form. Therefore, considering the observation $Y_1(m)$ and $Y_2(m)$, in (4.4) and (4.5), the value of ε that maximizes the joint conditional probability density function $p(Y_1(m), Y_2(m)|\varepsilon)$ can be obtained by

$$\begin{aligned} \hat{\varepsilon} &= \arg \max_{\varepsilon} p(Y_1(m), Y_2(m)|\varepsilon) \\ &= \arg \max_{\varepsilon} p(Y_2(m)|\varepsilon, Y_1(m))p(Y_1(m)|\varepsilon). \end{aligned} \quad (4.10)$$

Since ε gives no information about $Y_1(m)$, i.e. $p(Y_1(m)|\varepsilon) = p(Y_1(m))$, then

$$\hat{\varepsilon} = \arg \max_{\varepsilon} p(Y_2(m)|\varepsilon, Y_1(m)). \quad (4.11)$$

From (4.4) and (4.5),

$$\begin{aligned} Y_2(m) &= (Y_1(m) - W_1(m))e^{j2\pi\varepsilon} + W_2(m) \\ &= Y_1(m)e^{j2\pi\varepsilon} + W_2(m) - W_1(m)e^{j2\pi\varepsilon} \end{aligned} \quad (4.12)$$

Thus,

$$Y_2(m) - Y_1(m)e^{j2\pi\varepsilon} = W_2(m) - W_1(m)e^{j2\pi\varepsilon} \quad (4.13)$$

In (4.12), $W_1(m)$ and $W_2(m)$ are approximated as Gaussian-distributed, with zero mean and variance $\sigma_W^2 \mathbf{I}_N$ [97], which is independent of ε , so that the probability density function (PDF) $p(Y_2(m)|\varepsilon, Y_1(m))$ has a mean of $Y_1(m)e^{j2\pi\varepsilon}$. Therefore, the PDF $p(Y_2(m)|\varepsilon, Y_1(m))$ is expressed as:

$$p(Y_2|\varepsilon, Y_1) = \frac{1}{(2\pi\sigma_W^2)^{\frac{N}{2}}} \exp\left\{-\frac{1}{2\sigma_W^2} \sum_{m=1}^N |Y_2(m) - e^{j2\pi\varepsilon} Y_1(m)|^2\right\}. \quad (4.14)$$

The ML estimate for CFO ε is obtained as

$$\hat{\varepsilon} = \arg \max_{\varepsilon} \Gamma(\varepsilon), \quad (4.15)$$

where

$$\Gamma(\varepsilon) = \sum_{m=1}^N |Y_2(m) - e^{j2\pi\varepsilon} Y_1(m)|^2. \quad (4.16)$$

The CFO ε can be obtained in a closed-form to avoid the exhaustive ML search. The expression in (4.16) can be expanded and re-written as:

$$\hat{\varepsilon} = \arg \max_{\varepsilon} \Gamma(\varepsilon) = \arg \max_{\varepsilon} \sum_{m=1}^N \left(Y_2(m) - e^{j2\pi\varepsilon} Y_1(m) \right) \left(Y_2(m) - e^{j2\pi\varepsilon} Y_1(m) \right)^*, \quad (4.17)$$

which reduces to

$$\arg \max_{\varepsilon} \Gamma(\varepsilon) = \arg \max_{\varepsilon} \sum_{m=1}^N \Re\{Y_2^*(m)Y_1(m)e^{j2\pi\varepsilon}\} + C, \quad (4.18)$$

where C is independent of the CFO ε . Since ε affects only the phase of $\{Y_2^*(m)Y_1(m)e^{j2\pi\varepsilon}\}$ and not its absolute value, then the maximum of $\Gamma(\varepsilon)$ is achieved when its phase is zero [94]. Thus,

$$2\pi\varepsilon + \angle \sum_{m=1}^N Y_2^*(m)Y_1(m) = 0. \quad (4.19)$$

Then the CFO estimate $\hat{\varepsilon}$ is obtained in a closed-form as:

$$\hat{\varepsilon} = -\frac{1}{2\pi} \cdot \angle \sum_{m=1}^N Y_2^*(m)Y_1(m). \quad (4.20)$$

After obtaining $\hat{\varepsilon}$, the obtained value can be substituted into (3.8) to compensate the CFO i.e.

$$\hat{Y}_i(m) = Y_i(m)e^{-\frac{j2\pi\hat{\varepsilon}m}{N}}. \quad (4.21)$$

Hence, the CFO in the system is effectively estimated and compensated. Also, in the development of the algorithm, σ_w^2 is included due to the dominance of the ASE noise along the optical fiber link, to effectively capture the prevailing fiber characteristics. Table 4.1 shows the summary of the ML-based CFO estimator.

Table 4.1: Summary of the ML-Based CFO Estimator

-
1. For $i = 1, 2, \dots, N$
 2. Obtain $Y_i(m)$ after FFT
 3. Compute $R_i(m)$ using (4.1)
 4. Obtain $Y_1(m)$ using (4.3)
 5. Obtain $Y_2(m)$ using (4.4)
 6. Compute $\hat{\varepsilon} = \arg \max_{\varepsilon} \Gamma(\varepsilon)$ using (4.15) [for ML method 1]
 7. Compute $\hat{\varepsilon} = -\frac{1}{2\pi} \cdot \angle \sum_{m=1}^N Y_2^*(m)Y_1(m)$ using (4.20) [for ML method 2]
 8. Compute $MSE = E[|\hat{\varepsilon} - \varepsilon|^2]$
- End
-

4.3. The Proposed ML-Based CFO and Phase Noise Joint Estimation

This section presents the ML-based estimation methods for the CFO and the phase noise. Figure 4.1 shows the frame structure, highlighting the data and the pilot positions for the joint phase noise and CFO estimation. For the estimation of the phase noise using M_p number of pilot subcarriers, the following are defined. Set $\{m_1, m_2, \dots, m_{M_p}\}$ of pilot tones to be available at each payload OFDM symbol for phase estimation. The CFO is assumed to vary slowly, therefore remains constant across each frame, while the phase is estimated at each frame based on available pilot subcarriers.

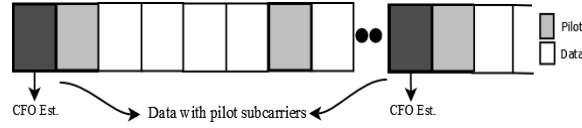


Figure 4.1: The frame structure highlighting the data and the pilot positions.

Hence, from (3.12), the following expression is obtained:

$$Y_i(m_p) = e^{\frac{j2\pi\epsilon m_p}{N}} e^{j\Phi_i} X_i(m_p) Z(m_p) + W_i(m_p), \quad m_p \in M_p \quad (4.22)$$

In order to obtain the estimate of the CFO ϵ , the received sequence is considered. In the absence of noise-interference and by assuming $e^{j\Phi_i} \approx 1$, then in the frequency domain, using the pilot structure as described in Figure 4.1, which shows the pilot position for the CFO estimation i.e. m_{cfo} ,

$$R_i(m_{cfo}) = e^{\frac{j2\pi\epsilon m_{cfo}}{N}} X_i(m_{cfo}) Z(m_{cfo}). \quad (4.23)$$

Assuming two consecutive OFDM sequences are the same except for a phase difference given as [50]

$$R_2(m_{cfo}) = R_1(m_{cfo}) e^{j2\pi\epsilon}. \quad (4.24)$$

By including the noise-interference component, then

$$Y_1(m_{cfo}) = R_1(m_{cfo}) + W_1(m_{cfo}) \quad (4.25)$$

and

$$Y_2(m_{cfo}) = R_1(m_{cfo})e^{j2\pi\varepsilon} + W_2(m_{cfo}) \quad (4.26)$$

Thus, to obtain the CFO ε , the probability density function (PDF) $p(Y_2(m_{cfo})|\varepsilon, Y_1(m_{cfo}))$ is expressed as:

$$p(Y_2(m_{cfo})|\varepsilon, Y_1(m_{cfo})) = \frac{1}{(2\pi\sigma_W^2)^N} \exp\left\{-\frac{1}{2\sigma_W^2} \cdot |Y_2(m_{cfo}) - e^{j2\pi\varepsilon}Y_1(m_{cfo})|^2\right\}. \quad (4.27)$$

The ML estimate for CFO ε is obtained as

$$\hat{\varepsilon} = \arg \max_{\varepsilon} \Gamma(\varepsilon), \quad (4.28)$$

where

$$\Gamma(\varepsilon) = \sigma_W^{-2} |Y_2(m_{cfo}) - e^{j2\pi\varepsilon}Y_1(m_{cfo})|^2. \quad (4.29)$$

The CFO ε can be obtained in a closed-form to avoid the exhaustive ML search. Also, the variance σ_W^2 is included due to the dominance of the ASE noise along the optical fiber link, which cannot be ignored. The expression in (4.29) can be expanded and re-written as:

$$\begin{aligned} & \arg \max_{\varepsilon} \Gamma(\varepsilon) \\ &= \arg \max_{\varepsilon} \left\{ 2\sigma_W^{-2} \left(Y_2(m_{cfo}) - e^{j2\pi\varepsilon}Y_1(m_{cfo}) \right) \left(Y_2(m_{cfo}) - e^{j2\pi\varepsilon}Y_1(m_{cfo}) \right)^* \right\}, \end{aligned} \quad (4.30)$$

which reduces to

$$\arg \min_{\varepsilon} \Gamma(\varepsilon) = \arg \max_{\varepsilon} \left\{ 2\sigma_W^{-2} \cdot \Re\{Y_2^*(m_{cfo})Y_1(m_{cfo})e^{j2\pi\varepsilon}\} \right\} + C, \quad (4.31)$$

where C is independent of the CFO ε . Since ε affects only the phase of the expression on the right hand side of (4.31) and not its absolute value, then the minimum of $\Gamma(\varepsilon)$ is achieved when its phase is zero. Thus,

$$2\pi\varepsilon + \angle\{2\sigma_W^{-2} \cdot Y_2^*(m_{cfo})Y_1(m_{cfo})\} = 0. \quad (4.32)$$

Then the CFO ε is obtained in a closed-form as:

$$\hat{\varepsilon} = -\frac{1}{2\pi} \cdot \angle \{2\sigma_W^{-2} \cdot Y_2^*(m_{cfo})Y_1(m_{cfo})\}. \quad (4.33)$$

Now for the estimation of the phase noise, considering (4.22) with no CFO, having obtained the estimate $\hat{\varepsilon}$ and assuming a perfect compensation, an ML cost function is defined based on (4.22), which is expressed as

$$\Gamma(\Phi) = 2\sigma_W^{-2} \sum_{m_p \in M_p} |Y_i(m_p) - X_i(m_p)Z(m_p)e^{j\Phi_i}|^2 \quad (4.34)$$

The expression in (4.34) can be expanded and re-written as

$$\begin{aligned} \Gamma(\Phi) &= 2\sigma_W^{-2} \sum_{m_p \in M_p} \left((Y_i(m_p) - X_i(m_p)Z(m_p)e^{j\Phi_i})(Y_i(m_p) - X_i(m_p)Z(m_p)e^{j\Phi_i})^* \right), \end{aligned} \quad (4.35)$$

$$\Gamma(\Phi) = 2\sigma_W^{-2} \sum_{m_p \in M_p} \Re\{Y_i(m_p)X_i^*(m_p)Z^*(m_p)e^{-j\Phi_i}\} \quad (4.36)$$

$$\Gamma(\Phi) = 2\sigma_W^{-2} \sum_{m_p \in M_p} \Re\{C_i(m_p)e^{-j\Phi_i}\} \quad (4.37)$$

where $C_i(m_p) = Y_i(m_p)X_i^*(m_p)Z^*(m_p)$ and \Re represents real value.

Hence, the ML estimate for Φ_i is obtained by

$$\hat{\Phi}_i = \arg \max_{\Phi} \sum_{m_p \in M_p} \Re\{C_i(m_p)e^{-j\Phi_i}\}. \quad (4.38)$$

Hence, the range of the CPE can be searched across N_Φ candidate values with step size α_Φ , $[(-N_\Phi/2)\alpha_\Phi, (N_\Phi/2 + 1)\alpha_\Phi, \dots, (N_\Phi/2)\alpha_\Phi]$, to acquire the estimate $\hat{\Phi}_i$. As obtained in (4.33),

Φ_i can also be obtained in a closed-form, which is expressed as

$$\hat{\Phi}_i = \angle \sum_{m_p \in M_p} C_i(m_p). \quad (4.39)$$

Thus, the exhaustive search is no longer required, which drastically reduces the computational burden and the overall complexity of the system.

Furthermore, instead of utilizing the CPE ML estimator derived in (4.39), an efficient data-dependent pilot-aided (DD-PA) technique is implemented for the laser phase acquisition while still utilizing the derived ML scheme of (4.33) for CFO estimation. This approach differs from the conventional pilot aided method where pilot subcarriers are predetermined. In this method, the phases of the pilot subcarriers are selected in a way that their average phase angle is direct opposite of the data carrying subcarriers. This is ensured by the condition expressed as

$$ave\llbracket arg(X_i(m))\rrbracket_{M_p} + ave\llbracket arg(X_i(m))\rrbracket_{data} = 0 \quad (4.40)$$

where $ave\llbracket \cdot \rrbracket$ is the averaging operation and $arg(\cdot)$ denotes the phase angle.

Thus, the average phase angle of the pilot subcarriers is selected by satisfying the condition stated above, where $ave\llbracket arg(X_i(m))\rrbracket_{M_p} = -ave\llbracket arg(X_i(m))\rrbracket_{data}$. The CPE is, therefore, obtained by adding the phases of the M_p pilot subcarriers and the corresponding data carrying subcarriers using the following expression

$$\hat{\Phi}_i = \left(ave\llbracket arg(Y_i(m_p))\rrbracket_{M_p} + ave\llbracket arg(Y_i(m))\rrbracket_{data} \right) / 2. \quad (4.41)$$

Also, by using the expression in (4.41), the CPE is estimated without prior information on the phase of the pilot subcarriers. Table 4.2 shows the summary of the joint ML-based algorithm.

Table 4.2: Summary of the Joint ML-Based Algorithm

-
1. Set pilots $M_p = \{m_1, m_2, \dots, m_{M_p}\}$
 2. For $i = 1, 2, \dots, N$
 3. Obtain $Y_i(m_p)$ using (4.21)
 4. Compute $R_i(m_{cfo})$ using (4.22)
 5. Obtain $Y_1(m_{cfo})$ using (4.24)
 6. Obtain $Y_2(m_{cfo})$ using (4.25)
 7. Compute CFO $\hat{\varepsilon} = \arg \max_{\varepsilon} \Gamma(\varepsilon)$
 8. where $\Gamma(\varepsilon) = \sigma_W^{-2} |Y_2(m_{cfo}) - e^{j2\pi\varepsilon} Y_1(m_{cfo})|^2$
 9. Compute MSE = $E[|\hat{\varepsilon} - \varepsilon|^2]$
 10. Compensate CFO ε
 11. Compute $\Gamma(\Phi)$ using (4.32)
 12. where $\Gamma(\Phi) = \sum_{m_p \in M_p} 2\sigma_W^{-2} \Re\{C_i(m_p)e^{-j\Phi_i}\}$
 13. Obtain phase estimate $\hat{\Phi}_i = \arg \min_{\Phi} \sum_{m_p \in M_p} \Re\{C_i(m_p)e^{-j\Phi_i}\}$ using (4.34)
 14. Obtain $\hat{\Phi}_i$ in a closed-form using (4.35)
 15. Obtain $\hat{\Phi}_i$ using DD-PA method using (4.37)
 16. Compute MSE = $E[|\hat{\Phi}_i - \Phi_i|^2]$
 17. End for
-

4.4. Simulations and Discussion

4.4.1. Proposed ML Based CFO Estimation

The performance as well as the effectiveness of the proposed method is investigated and analyzed. A 20 Gb/s CO-OFDM system, with FFT size 256 and a central wavelength of 1550nm is considered, while a 12.5% cyclic prefix is used. The 16-QAM-modulation format is used while the sampling duration of the OFDM symbol is set to 28.8ns. The optical system model is implemented mimicking a practical scenario with prevailing fiber-link dispersion including PDLs, whose effects on optical links are detailed in [23]. The fiber link is 100 km span distance, standard single mode fiber (SSMF) with fiber dispersion value of 17 ps/km/nm, loss coefficient

of 0.2 dB/km , and differential group delay of $5 \text{ ps}/\sqrt{\text{km}}$. The EDFA has 16 dB gain with noise figure of 4 dB and the non-linear coefficient of the fiber is $1.32/W/\text{km}$.

In Figure 4.2, the BER performance of the proposed ML-based methods is shown in comparison with the existing ML methods. It is clear from the plots that the proposed methods outperform the existing ML methods. The CFO is set to $\varepsilon = 0.2$ while the CD is 1700 ps/nm . From the plot, it is observed that the proposed ML estimator of (4.15) achieves a BER close to its closed-form counterpart as derived in (4.20). This shows that the simplification of the ML method of (4.15) to achieve a closed-form estimation has no conspicuous effect on the BER performance.

The MSE plots of the proposed methods are compared with existing ML methods in Figure 4.3. The impact of the CFO on the MSE performance of the ML methods is verified at different normalized CFO values of 0.1 and 0.2. Generally, all the compared ML methods offer a fairly stable MSE performance at the various CFO values. Also, Moose's method offers a better performance compared to Nguyen-Le's method at lower OSNR values i.e. ($\text{OSNR} < 10 \text{ dB}$). At increased OSNR values beyond 10 dB , Nguyen-Le's method outperforms Moose's ML method. However, the proposed ML method offers a superior performance compared to Nguyen-Le's method. This is due to the weighting factor present in the Nguyen-Le's method, which is greatly influenced by fiber-link characteristics. The impact of increased fiber impairments is investigated in Figure 4.4. The MSE versus OSNR graph is obtained at CD values of 2200 ps/nm and 4000 ps/nm . The plot shows that the ML methods are moderately affected by fiber impairments although Nguyen-Le's method shows instability and high degradation at high OSNR values. Also, from the plots, it can be seen that the proposed ML method of (4.15) achieves similar MSE performance as its closed-form counterpart of (4.20).

Finally, in Figure 4.5, the performance of the ML methods over various values of CFO is shown. The MSE versus CFO plot shows that the proposed closed-form ML method in (4.20) closely approaches its counterpart in (4.15), for all values of CFO. This verifies the fact that the derived

simplified ML expression maintains a performance as good as the proposed method in (4.15). Thus, a similar performance is achieved while avoiding the traditional exhaustive search, to ensure lower computational cost.

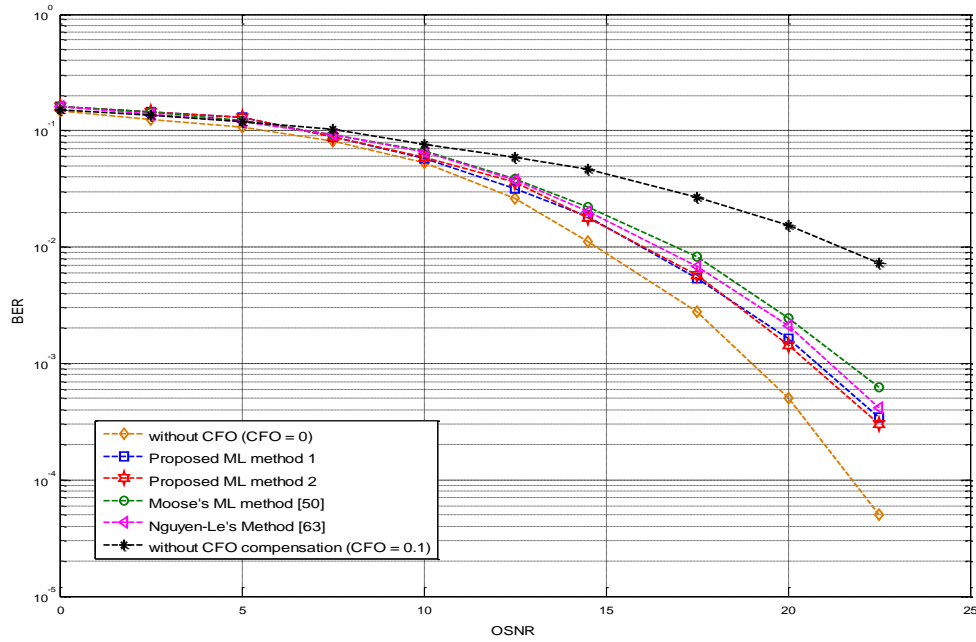


Figure 4.2: BER sensitivity for the proposed ML-based estimation algorithms in comparison with existing methods.

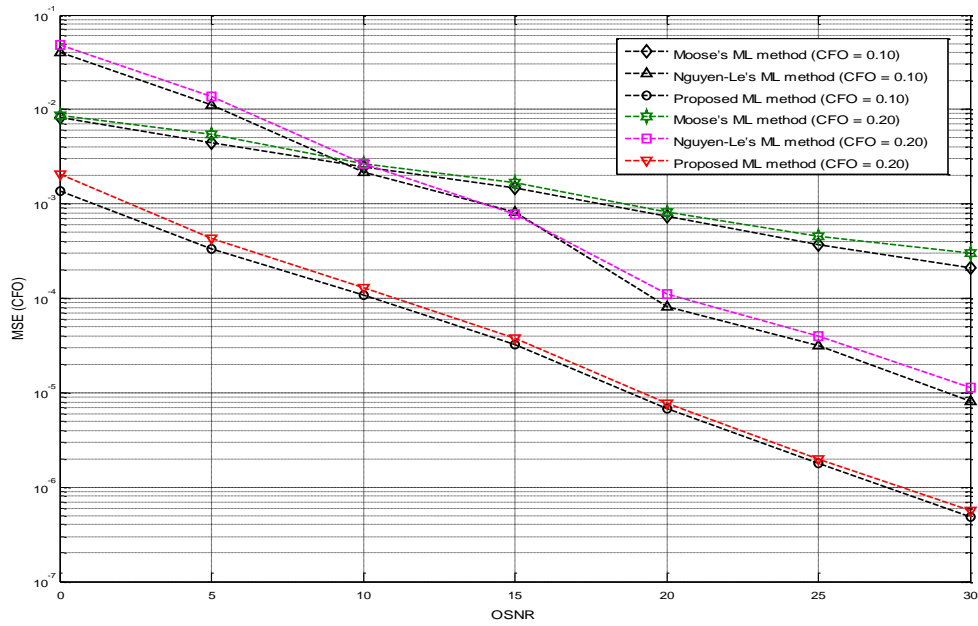


Figure 4.3: MSE comparison of the ML-based estimators at CFO $\varepsilon = 0.10, 0.20$.

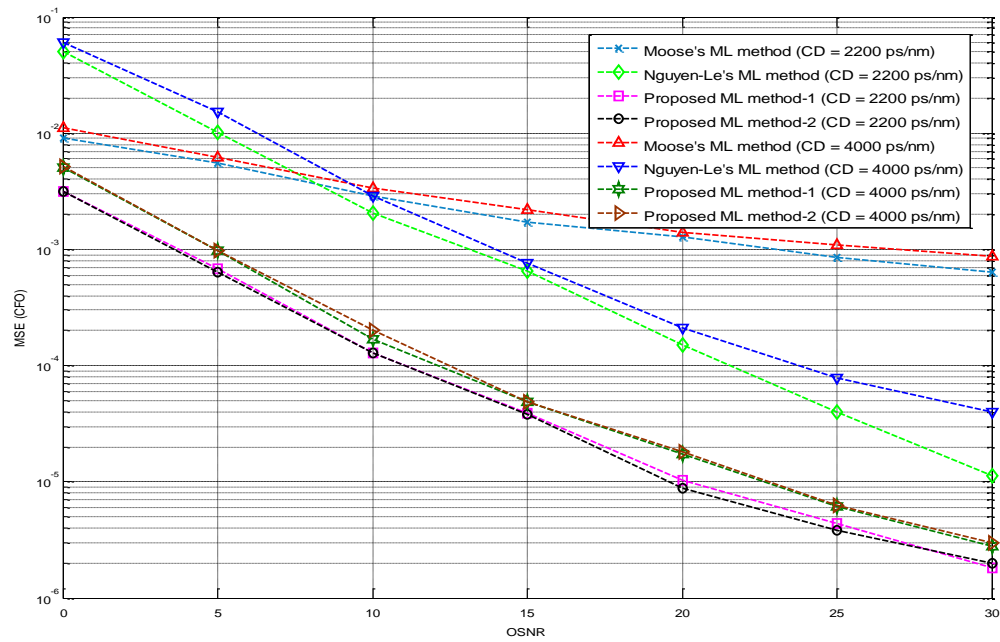


Figure 4.4: MSE performance of the various ML-based estimators under varied fiber impairments

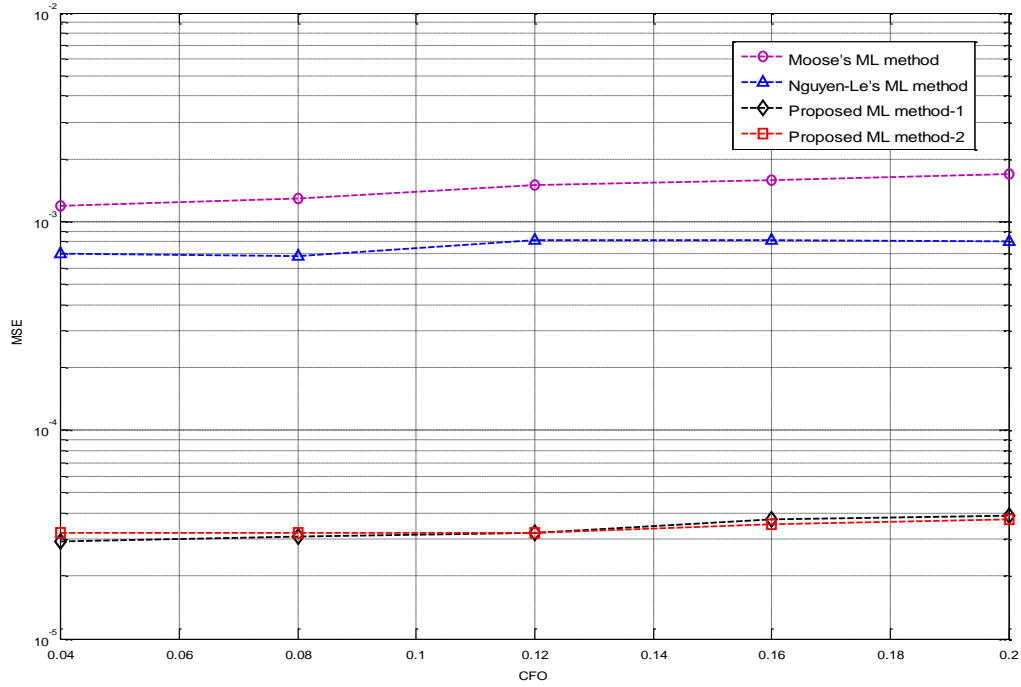


Figure 4.5: MSE versus normalized CFO graph at OSNR = 15 dB

4.4.2. The Proposed ML-Based CFO and Phase Noise Joint Estimation

The mean square error (MSE) plots of the proposed closed-form ML (CML) based schemes are compared with the existing ML scheme [65] in Figure 4.6 and 4.7, where the MSEs of the normalized CFO ε , and the CPE ϕ_i , are defined as $MSE = E[|\hat{\varepsilon} - \varepsilon|^2]$ and $MSE = E[|\hat{\phi}_i - \phi_i|^2]$ respectively. The CML/CML scheme utilizes the closed-form ML technique as derived in (4.33) and (4.39), for the acquisition of both the CFO and laser phase noise respectively. The laser phase noise estimation is performed using four pilot symbols to account for the variation within the frame. Also, the CML/DD-PA scheme employs the DD-PA technique for the estimation of the laser phase noise, followed by the closed-form ML acquisition of the CFO. The plots show the performance of the CML/CML scheme, the CML/DD-PA scheme as well as the existing ML scheme [65]. The laser linewidth is set to 160 KHz while the impact of the proposed schemes verified at different values of CFO (i.e. CFO = 0.10, 0.25). The MSE plots

show that the use of the CML scheme combined with the DD-PA phase acquisition technique (CML/DD-PA) ensures an improved estimation and overall system performance, which is due to the use of pilot subcarriers. The graph in Figure 4.7 also shows the impact of the estimation algorithm with different phase noise values of linewidth 400 KHz and 800 KHz, while the CFO is set to $\varepsilon = 0.10$. As seen from the plots, the proposed methods outperform the existing ML technique. It is noteworthy that despite both the proposed schemes both utilizes the derived CML algorithm for the acquisition of the CFO, the effectiveness of the technique employed for the first stage estimation of the laser phase noise essentially impacts the overall performance and efficiency of the estimation schemes.

In Fig. 4.8, the BER performance of the proposed CML-based schemes is compared with an RF-based joint estimator of [75] and an FFT-based acquisition scheme of [67]. The joint estimation scheme in [75] implements an RF-pilot aided phase recovery and frequency estimation method for the acquisition of both the laser phase noise and the CFO. The RF-based scheme is compared with the proposed CML-based schemes by utilizing a RF-pilot tone with 6.3% of power overhead, which is inserted in the center of the OFDM band. A band pass filter (BPF) with 100 MHz bandwidth is applied to filter out the RF-pilot tone at the receiver. Also, the plot shows the implementation of an FFT-based scheme. Before the acquisition of the CFO using the FFT method, the laser phase noise is estimated using a conventional pilot-based method proposed in [70]. The impact of the CFO, which is set at $\varepsilon = 0.1$ is shown as well as the perfect scenario where CFO $\varepsilon = 0$, to enable a clear comparison of the impact of the CML-based schemes on the CO-OFDM system model used. The combined laser linewidth h is set to 160 KHz. The plots show that the proposed schemes outperform the existing ML scheme as well as the FFT-based method. Furthermore, from the plots, the RF-based joint scheme outperforms the CML/CML scheme. However, the CML/DD-PA scheme, where the DD-PA technique is utilized for the acquisition of the phase noise before using the CML algorithm to obtain the CFO, offers a slightly better system performance as compared to the RF-based technique. Also for comparison,

the CML technique is combined with an RF-pilot phase estimator (CML/RFP). The CML/RFP offers a performance close to both the CML/DD-PA and the RF-based joint schemes. However, the RF-pilot tone in the CML/RFP as well as the RF-based joint schemes in [75] is grossly impacted by the size of the frequency guard band around the DC subcarrier, while the effectiveness degrades further under ASE and other fiber nonlinearity related impairments. Table 4.2 gives the summary of the phase noise and the CFO ML-based algorithm.

Figure 4.9 shows the MSE versus OSNR plot of the impact of fiber impairments on the overall performance of the CML/DD-PA and the RF-based joint estimation schemes. In the scenario where the fiber link is assumed compensated with no influence of fiber dispersions, the RF-based joint scheme tends to outperform the CML/DD-PA scheme. However, at CD of 1700 ps/nm, the CML/DD-PA shows better robustness against dispersion as compared to the RF-based scheme. Although the performance of both the CML/DD-PA scheme and the RF-based scheme steadily degrades as the CD is further increased, the CML/DD-PA offers a superior overall performance in the presence of fiber dispersions.

In Figure 4.10, the MSE plots of the proposed joint estimation schemes in comparison with the existing methods are shown. From the plot, the CML schemes outperform both the FFT-based estimator and the ML scheme in [65]. Also, the CML/DD-PA scheme still offers an enhanced performance than the RF-based scheme and offers better efficiency as mentioned earlier. Figure 4.11 shows the MSEs of the estimation schemes as a function of the CFO at $OSNR = 15 \text{ dB}$. The plots verify the performance of the proposed schemes in comparison with the existing schemes. Also, the RF-based joint estimator closely approaches but slightly outperformed by the CML/DD-PA technique. As a result of the BPF, the complexity of the RF-pilot scheme is significantly higher as compared to the proposed schemes. Thus, the CML/DD-PA offers an overall better performance and efficiency.

4.5. Computational complexity

The complexity of the ML method proposed in [65] requires the traditional search similar to the method in [97]. By referring to (4.38), evaluating the sequence $C_i(m_p) = Y_i(m_p)X_i^*(m_p)Z^*(m_p)$ requires NM_p complex multiplications. The curly bracket in the expression $\sum_{m_p \in M_p} \Re\{C_i(m_p)e^{-j\Phi_i}\}$ in (4.38) also requires NM_p complex multiplications, $N(M_p - 1)$ complex additions while the required exhaustive search is over N candidate values. Thus, the overall complexity of the estimator in (4.38) is of the order $O(N^2M_p)$. Deriving the closed-form expression as in (4.39), the estimator requires NM_p complex multiplications $N(M_p - 1)$ complex additions while the need for the exhaustive search is eliminated. Hence, the complexity of (4.39) is of the order $O(N)$ as the search operation is avoided. This shows that the closed-form expression, which enables the avoidance of the traditional ML search, offers a considerably lower complexity as compared to existing ML scheme. It is noteworthy that despite both the proposed schemes both utilizing the CML estimation approach for the acquisition of the CFO, the effectiveness of the technique employed for the first stage estimation of the laser phase noise essentially impacts the overall performance and efficiency of the estimation schemes. The complexity of the algorithms in terms of complex multiplications and complex additions is presented in Table 4.3. Also, Figure 4.12 shows the complexity graph of the considered ML methods in terms of the required complex multiplication operations.

Table 4.3: Complexity comparison for ML methods

| ML Method | Complex Multiplication | Complex Addition | Search |
|-------------------------|------------------------|------------------|--------|
| ML Method [65] and [97] | $2NM_p$ | $N(M_p - 1)$ | N |
| Proposed method | NM_p | $N(M_p - 1)$ | – |
| Nguyen-Le [63] | $N(M_p + 2)$ | $2(NM_p - 1)$ | N |

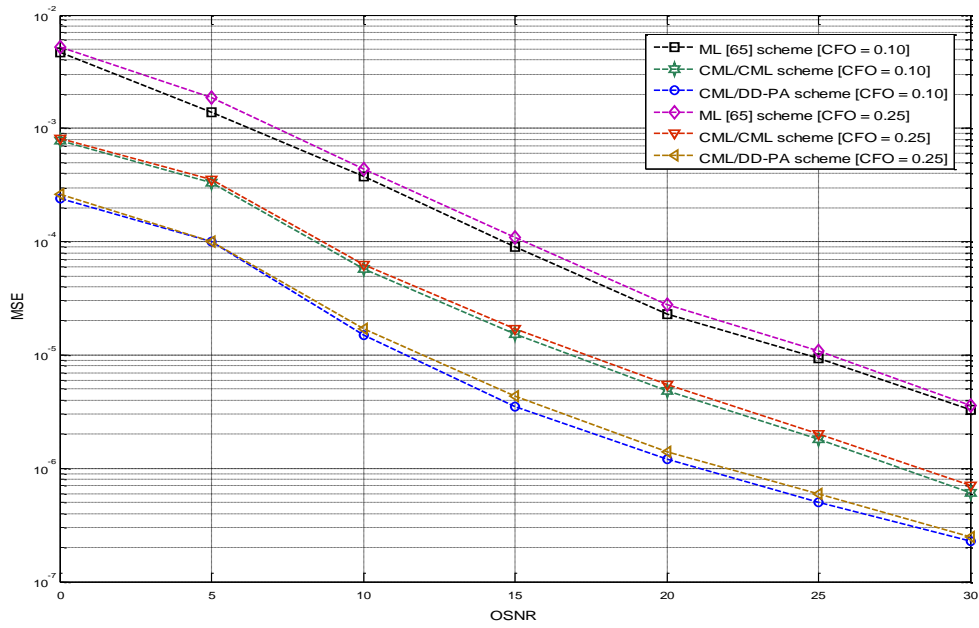


Figure 4.6: CFO estimation MSE for the joint estimation algorithms with laser linewidth of 160 KHz.

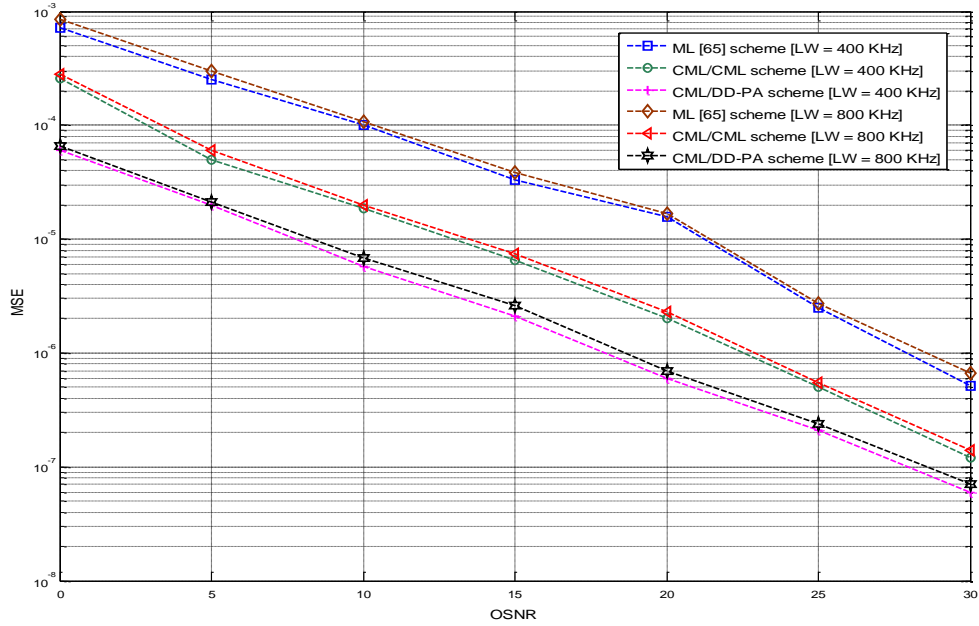


Figure 4.7: Phase noise estimation MSE for the joint estimation algorithms with CFO $\epsilon = 0.10$.

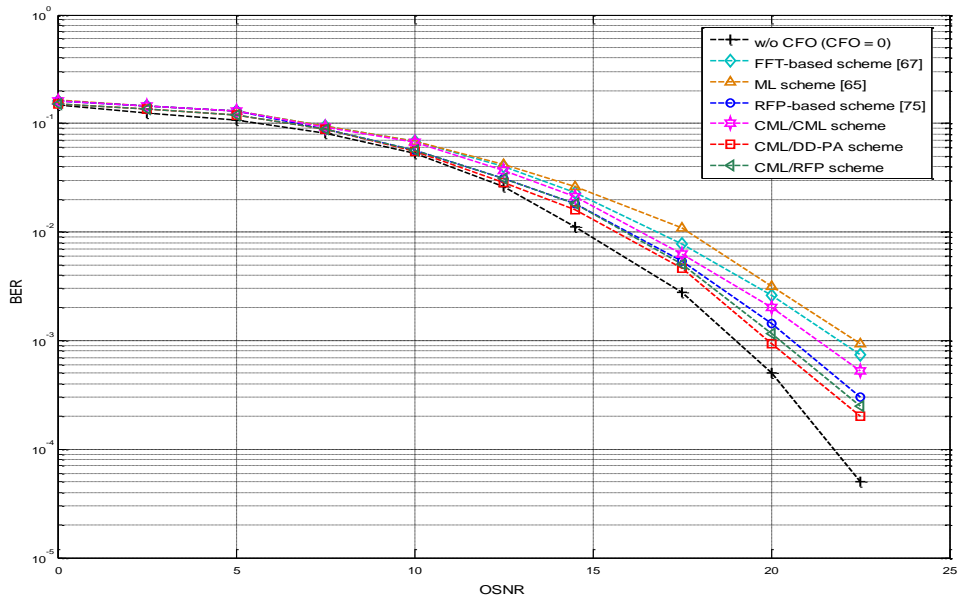


Figure 4.8: BER for the proposed ML-based estimation algorithms in comparison with existing methods.

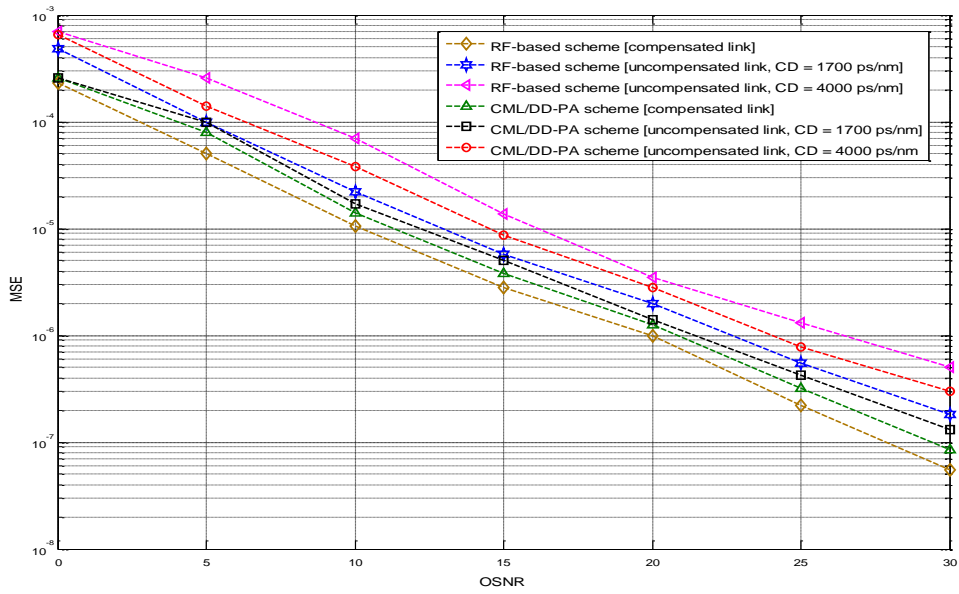


Figure 4.9: MSE performance of the CML/DD-PA and the RF-based joint scheme under fiber impairments.

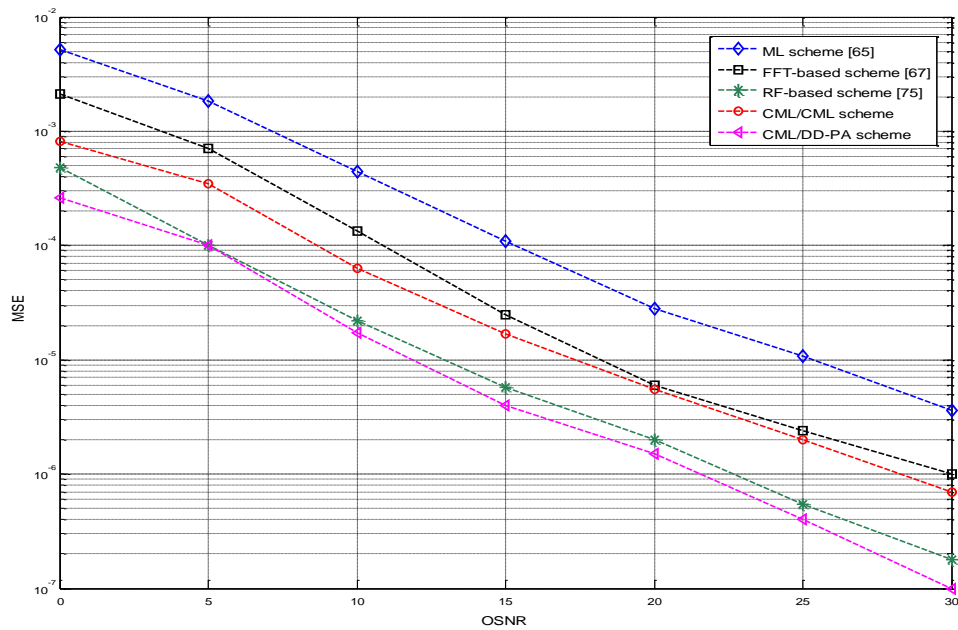


Figure 4.10: CFO estimation MSE comparison at CFO $\varepsilon = 0.25$ with laser linewidth of 250 KHz.

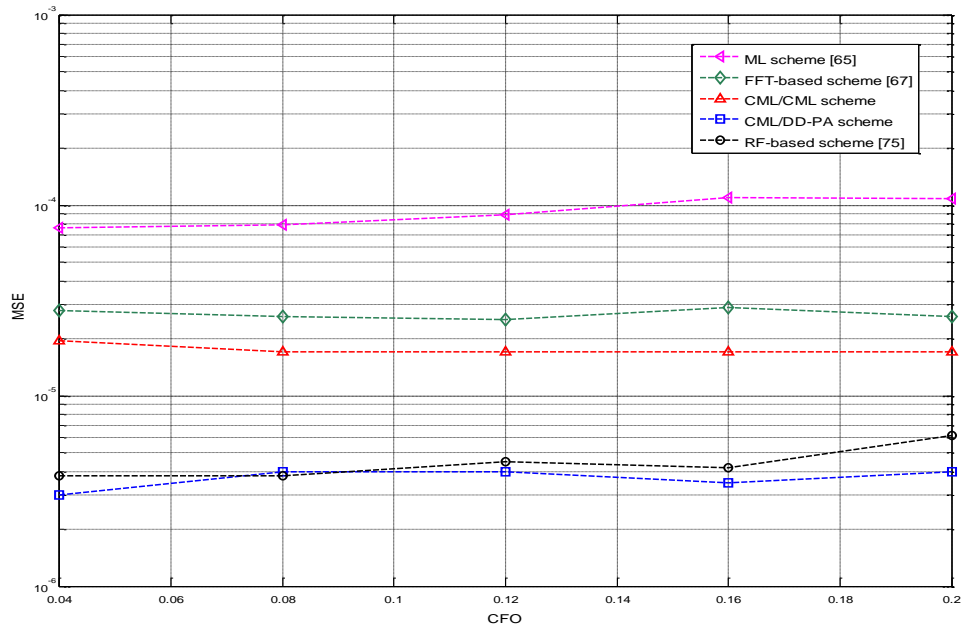


Figure 4.11: CFO estimation MSEs versus normalized CFO with laser linewidth of 250 KHz at SNR = 15 dB.

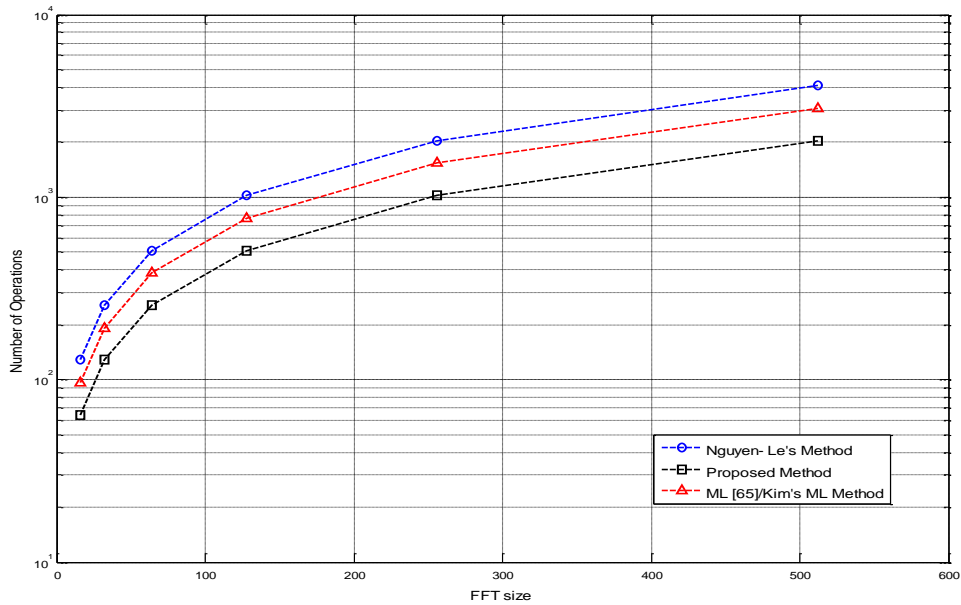


Figure 4.12: Complexity comparison of the ML methods considered in terms of the number of required operations

4.6. Conclusion

A proposed simplified ML-based scheme that is implemented for the joint acquisition of the laser phase noise and the CFO in an all-encompassing optical system model with an uncompensated fiber-link is derived and presented in this Chapter. Existing ML algorithms, which have been said to exhibit better tolerance towards distortion in optical systems, are seen to come with a high computational burden. Thus, a simplified ML estimator, with low complexity, has been adapted, derived and implemented in the optical domain. First, the CML scheme is implemented, where the simplified ML estimator is utilized to acquire both the laser phase noise and the CFO. The second scheme (CML/DD-PA) employed a DD-PA technique for the estimation of the laser phase noise followed by the CML estimator for the acquisition of the CFO. Simulation results show that the proposed closed-form ML-based acquisition schemes perform comprehensively well. However, the CML/DD-PA scheme offers a better overall system performance compared to

the first scheme, where the CML estimator is employed for the estimation of both the laser phase noise and the CFO. In the presence of impairments along the fiber link, the CML/DD-PA approach exhibits a balanced, low-complexity and better performance over the existing RF-pilot based method. Also, it is noteworthy that the effectiveness of the technique employed for the laser phase noise estimation impacts the overall performance of the proposed closed-form ML-based joint acquisition schemes.

CHAPTER FIVE

EFFICIENT CONSTANT MODULUS BASED CARRIER FREQUENCY OFFSET ESTIMATION

5.1. Introduction

In this chapter, a completely blind low-complexity CFO estimation approach for constant modulus constellation CO-OFDM systems is proposed, with a cost function similar to the one utilized for blind channel equalization in [98]. In [89]-[92], constant modulus (CM) schemes are implemented to address the gross performance degradation in [87]. This is achieved by assuming that the channel response of two neighboring subcarriers is the same. However, this assumption is not valid when the CFO is not estimated perfectly. This, therefore, motivates the implementation of the proposed blind CM based CFO estimation algorithm. The approach is implemented in such a way that it becomes independent of the assumptions in [89]-[92], to achieve a more robust performance in the presence of optical channel impairments. The performance of the proposed approach is analyzed and compared with prominent existing methods in a scenario, which mimics the practical optical system with an uncompensated fiber link in terms of the mean square error (MSE), the bit-error-rate (BER) and the convergence speed.

The main contributions in this chapter therefore include

1. The investigation of the performance of prominent constant modulus based blind estimation schemes, which have hitherto not been implemented and analyzed in the optical domain. The work presented in this chapter therefore investigates how these existing constant modulus schemes perform in the optical scenario, with fiber dispersion.
2. A blind low-complexity CFO estimator is proposed and compared with existing constant modulus schemes. In the existing methods, the cost functions are totally dependent on the channel characteristics, where it is usually assumed that the channel slowly varies over

consecutive symbols. However, the proposed estimator is independent of this general assumption. This in fact makes the proposed method robust against channel impairments.

3. In order to achieve low-complexity, the proposed cost function is derived and approximated as a cosine function, so that the CFO estimate is obtained using the curve fitting method, where only three trial values are required.
4. The derived closed-form expression ensures a low complexity similar to the existing schemes while offering a superior overall performance.

5.2. The System Model

Considering a CO-OFDM system as described in Figure 3.1, the i^{th} OFDM transmitted signal is given by $\mathbf{X}_i = [X_i(0), X_i(1) \dots X_i(M-1)]^T$, where data symbols \mathbf{X}_i are uniformly drawn from a constant modulus (CM) constellation. Thus, the received sequence in (3.12), while neglecting the phase noise and for easy analysis as well as comparison with existing schemes, can be rewritten as:

$$\mathbf{y}_i = e^{j\frac{2\pi\varepsilon i}{M}(M+N_g)} \mathbf{W}(\varepsilon) \mathbf{CZ}_i \mathbf{X}_i + \mathbf{g}_i, \quad (5.1)$$

where $\varepsilon \in (-0.5, 0.5)$ is the CFO, $N = M + N_g$ is the total number of subcarriers with M representing the data subcarriers while N_g denotes the cyclic prefix. The accumulated phase shift caused by the CFO on the time domain samples is given by $\mathbf{W}(\varepsilon) =$

$$diag\left(\left[e^{j\frac{2\pi\varepsilon}{M}\times 0}, e^{j\frac{2\pi\varepsilon}{M}\times 1} \dots e^{j\frac{2\pi\varepsilon}{M}\times (M-1)}\right]^T\right),$$

whose i^{th} element is given as $e^{j\frac{2\pi\varepsilon i}{M}(M+N_g)}$. Also, \mathbf{C}

is the normalized $N \times N$ IDFT matrix. The elements of \mathbf{C} are defined by $C_{mn} = \frac{1}{\sqrt{N}} e^{j\frac{2\pi mn}{M}}$, where m and n denote the row and column indices respectively and vary from 0 to $M-1$. The connotation \mathbf{Z}_i is the holistic channel impulse response of the fiber link encompassing the polarization mode dispersion, group velocity dispersion and other polarization dependent losses [20, 23].

The received sequence \mathbf{y}_i is multiplied by $\mathbf{W}^*(\bar{\epsilon})$ for CFO compensation using a trial value of CFO $\bar{\epsilon}$, then fed to the DFT to obtain

$$\mathbf{Y}_i = \mathbf{C}^H \mathbf{W}^*(\bar{\epsilon}) \mathbf{y}_i, \quad (5.2)$$

where \mathbf{C} is a unitary matrix. Also, the m^{th} element of \mathbf{Y}_i can be expressed as:

$$Y_i(m) = \frac{1}{\sqrt{N}} \sum_{n=0}^{N-1} y_i(n) e^{-j \frac{2\pi n}{N} (m - \bar{\epsilon})}, \quad (5.3)$$

where

$$y_i(n) = \frac{e^{j \frac{2\pi \epsilon i}{N} (N + N_g)}}{\sqrt{N}} \sum_{m=0}^{N-1} X_i(m) Z_i(m) e^{j \frac{2\pi n}{N} (m - \epsilon)} + g_i(n). \quad (5.4)$$

Also, as stated earlier, $Z_i(m)$ is the comprehensive channel impulse response of the fiber link, which includes the group velocity dispersion (GVD).

5.3. Blind Constant Modulus Based CFO Estimation Methods

Blind constant modulus based CFO estimation schemes have been proposed in the wireless domain [87]-[93]. A modest kurtosis-type criterion is used for CFO estimation in [87]. The approach exploits the variance of interfering subcarriers and the Gaussianity of a random sequence, to derive the proposed cost function. The kurtosis-type estimator is built on the idea that if the CFO has not been totally compensated, the distribution of the post-DFT sequence is closer to Gaussian than when the CFO has been perfectly compensated. Another blind CFO estimation method is presented in [88], which exploits the smoothing power spectrum. In the approach, the cost function is based on the similarity of the frequency response between two adjacent subcarriers. The method can be utilized for both constant modulus (CM) and non-CM signaling. In [89], an improved method is proposed to address the drawbacks of the kurtosis-based estimators. In this method, CFO estimation is achieved by minimizing an objective function based on the power difference between the received constellation using CM signaling.

The performance of this method is shown to be superior to the method in [87], but with similar computational complexity. However, these schemes suffer from gross degradation under severe channel conditions [90]. The power difference estimator (PDE-T), which is a hybrid time-frequency domain estimator, is proposed in [91]. The cost function minimizes the power difference between subcarriers in two consecutive OFDM symbols and assumes a slowly varying channel in the time domain. Recently, the amplitude difference estimator (ADE-T) method [92], similar to the PDE-T, was proposed. In the ADE-T method, the CFO estimate is obtained by deriving a cost function based on the magnitude of the received sequence with two similar subcarriers having the same indexes. The cost function, which is derived by exploiting the channel coherence in time, has quasi-regular shape and can be further approximated to achieve a closed-form CFO estimation [92]. The ADE-T method is less sensitive to noise and instabilities along the channel. In [93], a CFO estimator is presented, whose cost function is derived based on the powers of non-diagonal elements of covariance matrix. The information on the CFO is embedded in the covariance matrix of the received sequence. The method achieves CFO estimation by minimizing the total off-diagonal power induced by the inter-channel interference (ICI) in the frequency domain. However, the implementation of this scheme requires large number of OFDM symbols, which causes processing delay. Also in [90], a circularly shifted covariance (CSC) matrix method was proposed, where estimation is achieved by forcing the out-of-band elements of the matrix to zero. The covariance matrix obtained has a banded structure and the CFO is estimated by minimizing the power of the elements that are outside the band. The cost function of this method is dependent on the property of the channel matrix, which makes it susceptible to impairments along the channel. The prominent among the existing constant modulus based blind estimation methods in the wireless domain are therefore examined and derived for CFO estimation in the optical scenario. Also, the prominent methods that are examined in the following sub-sections form the basis of comparison with the newly proposed method.

5.3.1. The power difference estimator (PDE)

In [89], a blind CFO estimation scheme for OFDM systems with CM signaling is proposed in the wireless domain. The scheme, which is referred to as PDE-F, is based on the assumption that the channel frequency response is approximately the same for two neighboring subcarriers. Based on this assumption, a cost function is derived and utilized for blind CFO estimation in a closed-form. Also, it is assumed that the CFO has been perfectly compensated before the DFT stage, thus the DFT output is considered to be without ICI. In [91], a similar method, which is referred to as the PDE-T scheme, is implemented for CFO estimation in OFDM systems. The method, which is a hybrid time-frequency-domain estimator, assumes the channel frequency response varies slowly in the time domain. Therefore the resulting sequence after DFT in a noise-free case is described as:

$$\mathbf{Y}_i|_{\bar{\varepsilon}=\varepsilon} = \mathbf{Z}_i \mathbf{X}_i. \quad (5.5)$$

Considering the case of CM signaling, the squared amplitude of the resulting sequence after DFT is taken as the squared amplitude of the optical channel frequency response, which is expressed as:

$$|Y_i(m)|_{\bar{\varepsilon}=\varepsilon}|^2 = |Z_i(m)|^2, \quad (5.6)$$

where $\bar{\varepsilon}$ is the trial value of the CFO as defined earlier.

Also assuming that the channel response slowly changes in the frequency domain so that $|Z_i(m)|$ and $|Z_{i+1}(m)|$ are almost equal, then consecutive subcarriers have equal power [91]. Thus,

$$|Y_i(m)|_{\bar{\varepsilon}=\varepsilon}|^2 \approx |Y_{i-1}(m)|_{\bar{\varepsilon}=\varepsilon}|^2. \quad (5.7)$$

Based on the above expressions, a cost function is formulated, and the CFO estimation is achieved by the following expression

$$\hat{\varepsilon} = \arg \min_{\bar{\varepsilon} \in (-0.5, 0.5)} J_{P_f}(\bar{\varepsilon}), \quad (5.8)$$

where

$$J_{P_f}(\bar{\varepsilon}) = \sum_{i=0}^{M-1} \sum_{m=0}^{N-1} (|Y_i(m)|^2 - |Y_{i-1}(m)|^2)^2, \quad (5.9)$$

and the assumption in (5.7) is valid for all subcarriers. The CFO is assumed constant over M consecutive OFDM symbols and (5.9) can be expanded and further approximated as [89, 91]:

$$J_{P_f}(\bar{\varepsilon}) \approx A \cos[2\pi(\varepsilon - \bar{\varepsilon})] + C, \quad (5.10)$$

where A and C are constants with real values, independent of $\bar{\varepsilon}$ but dependent on the optical channel and symbol realization as detailed in [91].

The curve-fitting method as described in Appendix I [88, 91], can be utilized for the minimization process since the cost-function as approximated in (5.10) is sinusoidal. The curve-fitting method enables a closed-form estimation of the CFO and the cost function in (5.10) can be evaluated at three different points, i.e. $\bar{\varepsilon} = 0, 0.25$, and -0.25 . The estimate of the CFO is therefore obtained according to [88, 90, 91] as

$$\hat{\varepsilon} = \begin{cases} \frac{1}{2\pi} \tan^{-1}(b/a) & \text{for } a \geq 0 \\ \frac{1}{2\pi} \tan^{-1}(b/a) + \frac{1}{2} & \text{for } a < 0 \text{ and } b \geq 0 \\ \frac{1}{2\pi} \tan^{-1}(b/a) - \frac{1}{2} & \text{for } a < 0 \text{ and } b \leq 0 \end{cases} \quad (5.11)$$

where a and b are obtained by the expressions

$$a = \left\{ (1/2)(J_{P_f}(\bar{\varepsilon} = 0.25) + J_{P_f}(\bar{\varepsilon} = -0.25)) - J_{P_f}(\bar{\varepsilon} = 0) \right\}, \text{ and}$$

$$b = \left\{ (1/2)(J_{P_f}(\bar{\varepsilon} = 0.25) - J_{P_f}(\bar{\varepsilon} = -0.25)) \right\}.$$

5.3.2. The amplitude difference estimator (ADE-T)

In [92], another cost function was proposed for blind CFO estimation in the wireless domain. The method is achieved by using a cost-function based on the sum of the products of the signal

amplitudes on each pair of equivalent subcarriers from consecutive OFDM symbols. Considering the case of CM signaling while assuming a slow time-varying channel response, then

$$|Y_i(m)| \approx |Y_{i-1}(m)|, \quad (5.12)$$

and the cost-function is described as

$$J_{A_t}(\bar{\varepsilon}) = \sum_{i=0}^{M-1} \sum_{m=0}^{N-1} (|Y_i(m)| - |Y_{i-1}(m)|)^2. \quad (5.13)$$

Thus, CFO can be estimated by minimizing the cost-function as

$$\hat{\varepsilon} = \arg \min_{\bar{\varepsilon} \in (-0.5, 0.5)} J_{A_t}(\bar{\varepsilon}). \quad (5.14)$$

Since $|Y_i(m)|^2$ and $|Y_{i-1}(m)|^2$ are independent of $\bar{\varepsilon}$ and ε [92], the cost function is modified as

$$J_{A_t}(\bar{\varepsilon}) = \sum_{i=0}^{M-1} \sum_{m=0}^{N-1} |Y_i(m)| |Y_{i-1}(m)|. \quad (5.15)$$

The cost function is further approximated and the closed-form expression of (5.11) is used for the CFO estimation.

5.3.3. The circularly shifted covariance method

A circularly shifted covariance method is proposed in [90] for RF, with the cost-function based on the covariance matrix obtained through circularly shifted OFDM blocks in the time-domain. The method in [90] is achieved by using the covariance matrix obtained by the circular shifts of the received signal. From the banded structure of the covariance matrix in the absence of the CFO, the estimate of the CFO is acquired by minimizing the powers outside the band of the covariance matrix. The elements outside the band of the covariance matrix are referred to as out-of-band elements [90]. The sample covariance matrix is generated using the expression given as

$$R_i(\bar{\varepsilon}) = \frac{1}{N} \mathbf{F}_i \mathbf{F}_i^H, \quad (5.16)$$

where $\mathbf{F}_i = [\mathbf{y}_i, \mathbf{P}\mathbf{y}_i, \dots, \mathbf{P}^{N-1}\mathbf{y}_i]$ and \mathbf{P} is the permutation matrix, which makes \mathbf{y}_i circularly symmetric [90]. Assuming a perfect CFO estimation and compensation, the covariance matrix can be expressed further as:

$$R_i(\bar{\epsilon}) = \sum_{m=0}^{M-1} Z(m) \sum_{m=0}^{M-1} Z^H(m) + e_i, \quad (5.17)$$

where $Z(m)$ is the optical channel frequency response and e_n is the error due to the noise along the fiber link. Since this method is realized through the circular shift of the time-domain received samples, the covariance matrix of the received sample is obtained without time-average, where a large number of OFDM blocks are needed. Thus, the cost function is formulated using the first column of the covariance matrix and the CFO estimation is achieved using the following expression as detailed in [90]

$$J_{C_t}(\bar{\epsilon}) = \sum_{i=0}^{M-1} \|R_i(\bar{\epsilon}) \odot \mathbf{A}\|_F^2, \quad (5.18)$$

where $\|\cdot\|_F$ is a Hilbert-Schmidt norm operation, \mathbf{A} is the matrix whose elements outside the band are 1 and elements inside the band are 0, while \odot denotes the entry-wise product [90]. Also, the cost function can be approximated as shown in Appendix II, according to [90] as

$$J_{C_t}(\bar{\epsilon}) \approx A \cos[2\pi(\epsilon - \bar{\epsilon})] + B, \quad (5.19)$$

where A and B are constants with real values, and the CFO is obtained using the expression in (5.11) as detailed in [90]. Also, the approximation in (5.19) becomes $J_{C_t}(\bar{\epsilon}) \approx A \cos[2\pi(\epsilon - \bar{\epsilon})] - A$, without noise. The proof is given in Appendix II as detailed in [90].

5.4. Proposed Blind CFO Estimation for CO-OFDM Systems

The schemes described in subsection 5.3.1 to 5.3.3 are implemented in the RF-domain for CFO estimation. Also, as summarized above, the various methods are based on a common assumption that the channel varies slowly over consecutive symbols. However, this assumption may not hold

in the case where the CFO is not perfectly estimated. The approach in [90] deviates from this assumption, but is highly dependent on the channel characteristics. Therefore, a cost-function, which is independent of the above assumptions i.e. not dependent on the fast or slow varying characteristics of a channel, is herein presented for the optical OFDM system. The proposed approach is achieved based on the approximation of the constant modulus cost-function similar to the one utilized for blind channel equalization in [98]. Hence, the following cost-function is proposed for the blind CFO estimation

$$J_{GA}(\bar{\varepsilon}) = E\{|Y_i(m)|^2 - R\}^2, \quad (5.20)$$

where R is a constant chosen to guarantee the minimization of $J_{GA}(\bar{\varepsilon})$. Thus, $J_{GA}(\bar{\varepsilon})$ should be minimized with respect to the trial value of ε , denoted as $\bar{\varepsilon}$, and the CFO estimate is obtained by

$$\hat{\varepsilon} = \arg \min_{\bar{\varepsilon} \in (-0.5, 0.5)} J_{GA}(\bar{\varepsilon}). \quad (5.21)$$

In order to achieve a closed-form CFO estimation, the cost-function in (5.20) is therefore expanded and expressed as:

$$J_{GA}(\bar{\varepsilon}) = E\{|Y_i(m)|^4\} - E\{2R \cdot |Y_i(m)|^2\} + R^2, \quad (5.22)$$

Substituting (5.4) into (5.3), while assuming the noise due to the ASE of the optical amplifiers is minimal throughout the fiber-link, gives:

$$Y_i(m) = \frac{e^{j\frac{2\pi\varepsilon i}{M}(M+N_g)}}{M} \sum_{m=0}^{M-1} \hat{B}_i(m) \sum_{n=0}^{M-1} e^{j\frac{2\pi n}{M}(m+\partial-i)}, \quad (5.23)$$

where $\partial = \varepsilon - \bar{\varepsilon}$, $\hat{B}_i(m) = X_i(m)Z_i(m)$

Substituting (5.23) into (5.22) gives

$$J_{GA}(\bar{\varepsilon}) = E \left\{ \left| \frac{e^{j\frac{2\pi\varepsilon i}{M}(M+N_g)}}{M} \sum_{m=0}^{M-1} \hat{B}_i(m) \sum_{n=0}^{M-1} e^{j\frac{2\pi n}{M}(m+\partial-i)} \right|^4 \right\} - E \left\{ 2R \left| \frac{e^{j\frac{2\pi\varepsilon i}{M}(M+N_g)}}{M} \sum_{m=0}^{M-1} \hat{B}_i(m) \sum_{n=0}^{M-1} e^{j\frac{2\pi n}{M}(m+\partial-i)} \right|^2 \right\} + R^2, \quad (5.24)$$

Thus,

$$|Y_i(m)|^4 = \frac{1}{M^4} \sum_{m_1, m_2, m_3, m_4=0}^{M-1} \hat{B}_i(m_1) \hat{B}_i^*(m_2) \hat{B}_i(m_3) \hat{B}_i^*(m_4) \\ \times \sum_{n_1, n_2, n_3, n_4=0}^{M-1} e^{\frac{j2\pi\partial\omega}{M}} e^{j\frac{2\pi}{M}(n_1 m_1 - n_2 m_2 + n_3 m_3 - n_4 m_4)} \times \sum_{i=0}^{M-1} e^{-\frac{j2\pi i\omega}{M}}, \quad (5.25)$$

where $\omega = n_1 - n_2 + n_3 - n_4$.

Also,

$$\sum_{i=0}^{M-1} e^{-\frac{j2\pi i\omega}{M}} = \begin{cases} M, & \omega = M, 0, -M \\ 0, & \text{otherwise.} \end{cases} \quad (5.26)$$

Hence, (5.25) can be simplified as shown below where S_{i_1} is a real constant independent of ∂ , which is obtained by substituting $\omega = 0$, [89]-[92] as defined in (5.25)

$$|Y_i(m)|^4 = \frac{2}{M^3} \operatorname{Re} \left\{ e^{-j2\pi\partial} \sum_{m_1, m_2, m_3, m_4=0}^{M-1} \hat{B}_i(m_1) \hat{B}_i^*(m_2) \hat{B}_i(m_3) \hat{B}_i^*(m_4) \right. \\ \left. \times \sum_{n_1=0}^{M-1} \sum_{n_2=n_1+1}^{M-1} \sum_{n_3=0}^{n_2-n_1-1} e^{j\frac{2\pi}{M}n_1(m_1-m_4)} e^{-j\frac{2\pi}{M}n_2(m_2-m_4)} e^{j\frac{2\pi}{M}n_3(m_3-m_4)} \right\} + S_{i_1}. \quad (5.27)$$

Now define [91]

$$\Phi \triangleq \{m_1, m_2, m_3, m_4\},$$

$$\Phi_1 \triangleq \{\Phi | m_1 = m_2, \text{ or } m_3 = m_4\},$$

$$\Phi_2 \triangleq \{\Phi | m_1 \neq m_2, \text{ and } m_3 \neq m_4\},$$

where the indices $m_1, m_2, m_3, m_4 \in \{0, 1, \dots, M-1\}$, $\Phi = \Phi_1 \cup \Phi_2$.

Therefore, (5.27) can be expressed as:

$$|Y_i(m)|^4 = \frac{2}{M^3} \operatorname{Re}\{e^{-j2\pi\partial} D_i(\Phi_1)\} + \frac{2}{M^3} \operatorname{Re}\{e^{-j2\pi\partial} D_i(\Phi_2)\} + S_{i_1}, \quad (5.28)$$

where

$$\begin{aligned}
D_i(\Omega) &= \sum_{\substack{m_1, m_2, m_3, m_4=0 \\ m_1, m_2, m_3, m_4 \in \Omega}}^{M-1} \hat{B}_i(m_1) \hat{B}_i^*(m_2) \hat{B}_i(m_3) \hat{B}_i^*(m_4) \\
&\quad \times \sum_{n_1=0}^{M-1} \sum_{n_2=n_1+1}^{M-1} \sum_{n_3=0}^{n_2-n_1-1} e^{j\frac{2\pi}{M}n_1(m_1-m_4)} e^{-j\frac{2\pi}{M}n_2(m_2-m_4)} e^{j\frac{2\pi}{M}n_3(m_3-m_4)},
\end{aligned}$$

and $\Omega \in \{\Phi_1, \Phi_2\}$.

Also,

$$\begin{aligned}
|Y_i(m)|^2 &= \frac{1}{M^2} \sum_{m_1, m_2=0}^{M-1} \hat{B}_i(m_1) \hat{B}_i^*(m_2) \\
&\quad \times \sum_{n_1, n_2=0}^{M-1} e^{j\frac{2\pi\partial\omega}{M}} e^{j\frac{2\pi}{M}(n_1 m_1 - n_2 m_2)} \times \sum_{i=0}^{M-1} e^{-j\frac{2\pi i\omega}{M}}. \tag{5.29}
\end{aligned}$$

If $\omega = 0$, and using the condition in (5.26), then (5.29) becomes

$$|Y_i(m)|^2 = \frac{1}{M^2} \sum_{m_1, m_2=0}^{M-1} \hat{B}_i(m_1) \hat{B}_i^*(m_2) \sum_{n=0}^{M-1} e^{\frac{j2\pi nq}{M}}, \tag{5.30}$$

where $q = m_1 - m_2$ and $n_1 = n_2 = n$. The expression in (5.30) is therefore independent of $\bar{\varepsilon}$, as well as the CFO ε , and is denoted as S_{i_2} .

Therefore, substituting (5.30) and (5.28) into the cost function in (5.22) gives:

$$\begin{aligned}
J_{GA}(\bar{\varepsilon}) &= \frac{2}{M^3} \mathcal{R}e\{e^{-j2\pi\partial} D_i(\Phi_1)\} + \frac{2}{M^3} \mathcal{R}e\{e^{-j2\pi\partial} D_i(\Phi_2)\} + S_{i_1} \\
&\quad - 2R \cdot \frac{1}{M^2} \sum_{m_1, m_2=0}^{M-1} \hat{B}_i(m_1) \hat{B}_i^*(m_2) \sum_{n=0}^{M-1} e^{\frac{j2\pi nq}{M}} + R^2, \tag{5.31}
\end{aligned}$$

Recalling that (5.30) is denoted as S_{i_2} , i.e.,

$$S_{i_2} = \frac{1}{M^2} \sum_{m_1, m_2=0}^{M-1} \hat{B}_i(m_1) \hat{B}_i^*(m_2) \sum_{n=0}^{M-1} e^{\frac{j2\pi nq}{M}}, \tag{5.32}$$

therefore,

$$J_{GA}(\bar{\varepsilon}) = \frac{2}{M^3} \mathcal{R}e\{e^{-j2\pi\partial} D_i(\Phi_1)\} + \frac{2}{M^3} \mathcal{R}e\{e^{-j2\pi\partial} D_i(\Phi_2)\} + S_{i_1} - 2R \cdot S_{i_2} + R^2,$$

$$= \frac{2}{M^3} \operatorname{Re}\{e^{-j2\pi\partial}((D_i(\Phi_1) + D_i(\Phi_2)))\} + S_{i_1} - 2R.S_{i_2} + R^2, \quad (5.33)$$

and (5.33) can be reduced to

$$J_{GA}(\bar{\varepsilon}) \approx \mathring{A} \cos(2\pi\partial) + B, \quad (5.34)$$

where $\mathring{A} = -2(D_i(\Phi_1) + D_i(\Phi_2))/M^3$, and $B = S_{i_1} - 2R.S_{i_2} + R^2$. Note that \mathring{A} and B are real values and independent of $\bar{\varepsilon}$ and ε , while $\partial = \varepsilon - \bar{\varepsilon}$.

Therefore, approximating the cost-function in (5.20) eliminates the need for the exhaustive search and the CFO estimate can be obtained using the curve-fitting method as described in [88, 91]. The minimum of the approximated cost-function in (5.34) is evaluated at three distinct points, $\bar{\varepsilon} = 0, 0.25$, and -0.25 . Thus, the estimate of the CFO is obtained by

$$\hat{\varepsilon} = \begin{cases} \frac{1}{2\pi} \tan^{-1}(b/a) & \text{for } a \geq 0 \\ \frac{1}{2\pi} \tan^{-1}(b/a) + \frac{1}{2} & \text{for } a < 0 \text{ and } b \geq 0, \\ \frac{1}{2\pi} \tan^{-1}(b/a) - \frac{1}{2} & \text{for } a < 0 \text{ and } b \leq 0 \end{cases} \quad (5.35)$$

where $a = \{(1/2)(J_{GA}(\bar{\varepsilon} = 0.25) + J_{GA}(\bar{\varepsilon} = -0.25)) - J_{GA}(\bar{\varepsilon} = 0)\}$, and

$b = \{(1/2)(J_{GA}(\bar{\varepsilon} = 0.25) + J_{GA}(\bar{\varepsilon} = -0.25))\}$.

The above method thus enables the closed-form estimation of the CFO and reduces the computational complexity of the proposed cost-function. Table 5.1 gives the summary of the proposed algorithms.

Table 5.1: Summary of the Proposed Algorithm

-
1. Generate \mathbf{X}_i OFDM signal
 2. Compute \mathbf{y}_i
 3. Using a trial value of CFO ε obtain \mathbf{Y}_i (5.2)
 4. Obtain CFO $\hat{\varepsilon}$ for proposed method using three trial values (5.35)
-

5.5. Computational complexity

The proposed method, the PDE method in [89] for CFO acquisition as well as the ADE method are performed using sequences that are obtained as the FFT of the received OFDM symbol with complexity of order $O(M)$. The CSC method in [90] is formulated using the first column of the covariance matrix, which is dependent on the FFT operation, with complexity of order $O(M)$. For the ADE-T method, $2M$ complex multiplications are required, which is the same as the PDE method. The calculation of the norm $\{\|R_i(\bar{\epsilon}) \odot \mathbf{A}\|_F\}$, in the CSC method requires M complex multiplications and $2M + 1$ complex additions [90]. The proposed method involves $2M$ complex multiplications from $\frac{2}{N^3} \text{Re}\{e^{-j2\pi\delta}((D_i(\Phi_1) + D_i(\Phi_2)))\}$ in (5.33), which is the same as the PDE methods as well as the ADE-T method. Thus, the total number of computational operation required by the proposed method is of the same order as the existing methods highlighted in section 5.3. The complexity of the considered CM methods, in terms of the required complex multiplications and complex additions are presented in Table 5.2. Also, Figure 5.9 shows the complexity graph of the CM methods in terms of the required complex addition operations.

Table 5.2: Complexity of the various CM methods

| CM Method | Complex Multiplication | Complex Addition |
|-----------------|------------------------|------------------|
| CSC [90] | M | $2M + 1$ |
| ADE-T [92] | $2M$ | $M + 1$ |
| PDE [89] | $2M$ | $3M + 2$ |
| Proposed Method | $2M$ | $3M + 1$ |

5.6. Simulation and Discussion

The quadrature phase-shift keying CO-OFDM system is utilized in the computer simulations to investigate and analyze the performance of the various estimation methods. The CO-OFDM system is based on a central wavelength of 1550 nm , with $N = 64$ subcarriers and cyclic prefix of length 16. The sampling rate of 10 GS/s is utilized and the OFDM duration is 7.2 ns with fiber link loss coefficient of 0.2 dB/km . Existing schemes are compared with the proposed method

in terms of mean square error and bit-error rate using Monte Carlo simulations while the normalized CFO ϵ , is assumed to be uniformly distributed in the range $(-0.5, 0.5)$. The optical system model is fully implemented mimicking a practical scenario with prevailing fiber-link dispersions, whose effects on optical links are detailed in [23]. The fiber dispersion is 17 ps/km/nm while the erbium-doped fiber amplifier is of 16 dB gain with noise figure of 4 dB and the non-linear coefficient of the fiber is $1.32/W/\text{km}$.

Firstly, an independent analysis is carried out on the performance and the behavior of the proposed cost function. The constant R can be taken as a dispersion coefficient as described in [98, 99], where it becomes dependent on the transmitted data. However, to achieve a blind CFO estimation without a priori knowledge of the transmitted signal, R can be taken as a positive real constant [99]-[101]. To ascertain the value of R at which the proposed method achieve the best performance, the value of R is varied and the MSE plot is shown in Figure 5.1. From the plot, the proposed method achieves the best performance at $R = 1.0$ while $R = 0.5$ gives a degraded output. Also, in Figure 5.2, the MSE is plotted as a function of R at different OSNRs. It can be seen from the plot that $R = 0.9$ offers the best performance at $OSNR = 15 \text{ dB}$. However, at $OSNR = 22 \text{ dB}$, $R = 1.0$ gives the best performance.

In Figure 5.3, the BER performance of existing methods in the literature is compared with the proposed method as implemented in the optical scenario with CFO ϵ , uniformly distributed in the range $(-0.5, 0.5)$. The effectiveness of the algorithms is demonstrated by showing the scenario where there is no CFO in the CO-OFDM system, with the CFO at 0.15. The plot shows the performance of the PDE-T method in [91]. The PDE-T method has been shown to outperform the PDE-F method [89], therefore it is chosen as one of the methods used for performance comparison. Also, the performance of the CSC method [90] and the ADE-T method are shown in the plot. The BER and the MSE plots with varying values of CFO are shown in Figure 5.4 and Figure 5.5 respectively, at $OSNR = 15 \text{ dB}$. It can be seen that the range of the proposed method,

like the other methods considered, is limited by the constant modulus constraint. The methods give acceptable performance up to $CFO \leq 0.25$, beyond which there is fast system degradation. The estimation range can be increased considerably by employing a second stage iterative estimator [102], although this comes with an increased system complexity. The MSE comparison of the various existing methods is compared with the proposed method as shown in Figure 5.6 and Figure 5.7. In Figure 5.6, the plot is obtained with the fiber link of eight optically amplified 80 km fiber spans. From the plot, the ADE-T method achieves a superior performance as compared to the other methods including the proposed method at low OSNRs. However, the performance degrades at high OSNR values, where it is outperformed by the PDE-T method. The CSC method outperforms both the ADE-T and the PDE-T methods at high OSNR values although the ADE-T method offers a superior performance at low OSNR value. The proposed method is outperformed by the ADE-T method at $OSNR < 8$ dB. Also, the proposed scheme offers a superior performance to the PDE-T and the CSC method for these OSNR values. However, at OSNR values greater than 8 dB, the proposed method effectively gives a better performance. The effectiveness of the various methods is further investigated under an uncompensated fiber-link with a total fiber haul of 1.8×10^3 km. Under this fiber condition, the general performance of the various algorithms degrades as shown in Figure 5.7. The plot shows that the CSC method suffers greatly under fiber impairments and its performance becomes inferior to the other blind estimation schemes. The ADE-T outperforms all the other methods at low OSNR values but at increased OSNRs it is outperformed by the PDE-T method and the proposed method.

In Figure 5.8, the plot shows the behavior of various schemes at $OSNR = 15$ dB, as the fiber length is increased up to 2000 km. From the graph, the performance of the proposed method suffers slight degradation with increased dispersion and fiber length. However, it offers a stable and efficient performance across the fiber length, compared to the ADE-T method. The plot

shows the CSC method as very unstable as compared to the other methods under consideration. The performance of the CSC method is greatly influenced by dispersion and impairments along the fiber-link of length L . Also, the proposed method achieves a low-complexity, stable and efficient performance, which is shown to be robust against fiber dispersions.

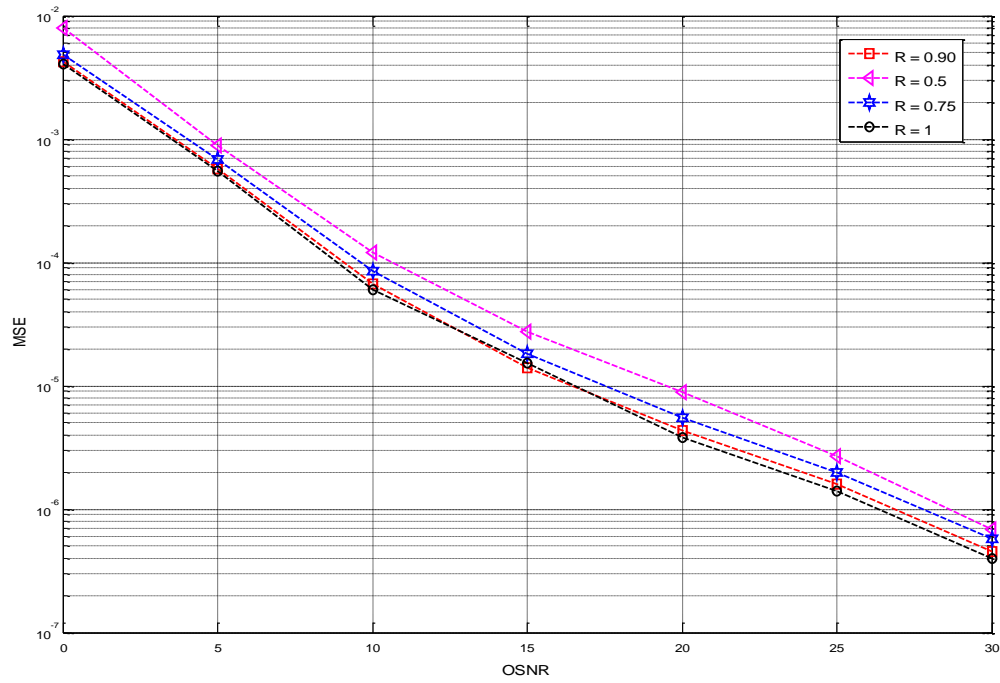


Figure 5.1: The MSE versus OSNR plot for different values of R .

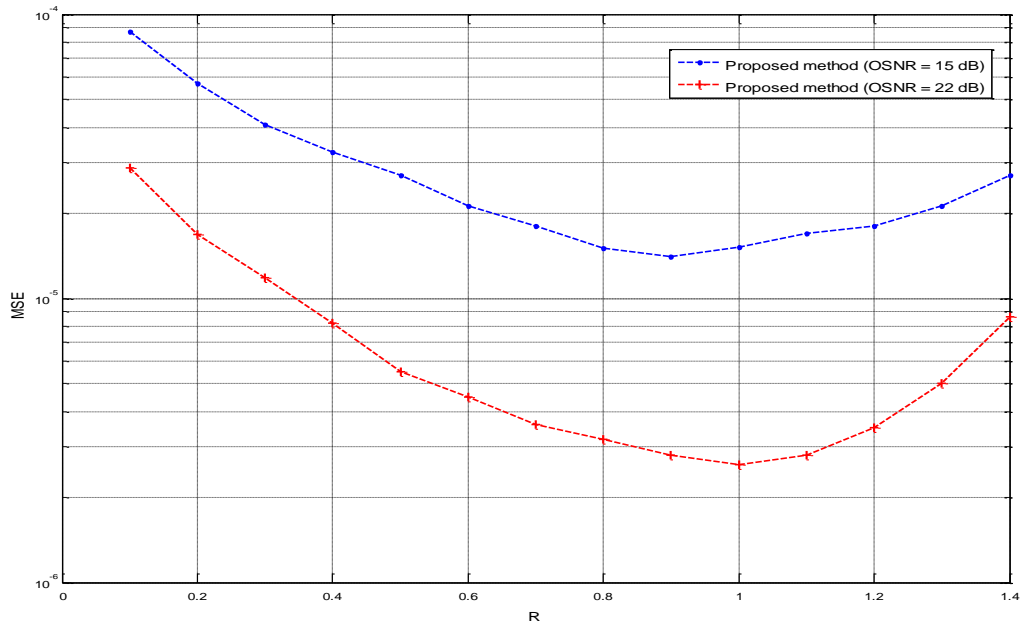


Figure 5.2: MSE plot of the proposed method as a function of R (OSNR = 15 dB, 22 dB).

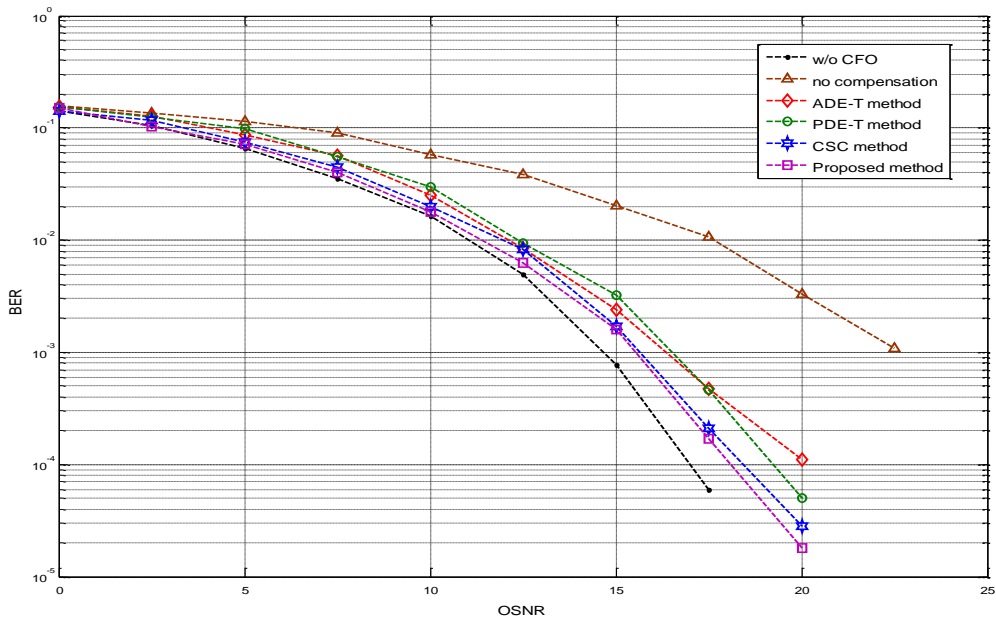


Figure 5.3: BER sensitivity for the proposed estimator in comparison with existing methods using a compensated fiber link.

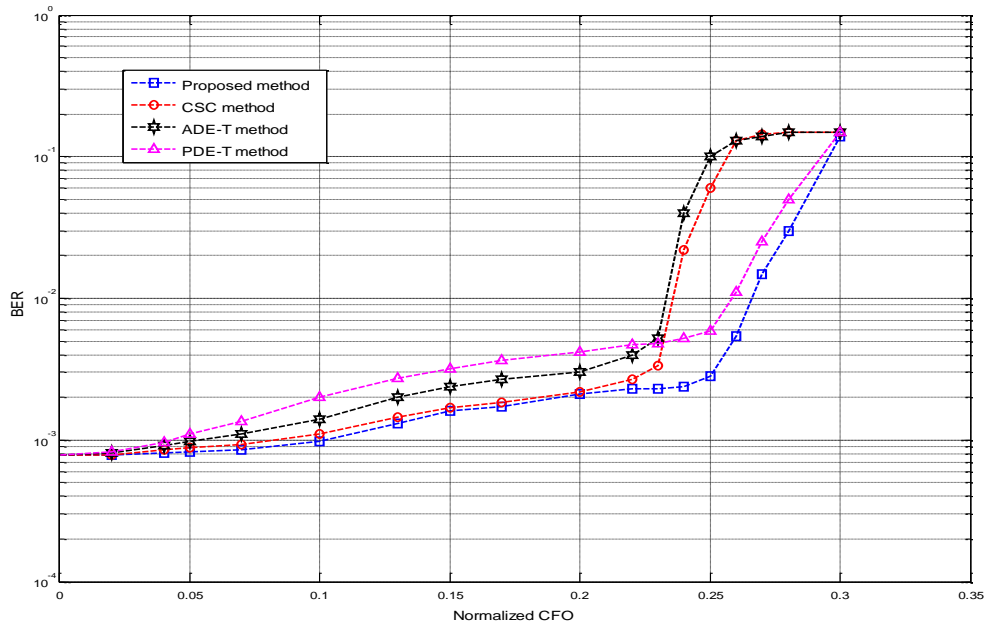


Figure 5.4: BER plot for varying values of CFO at OSNR = 15 dB.

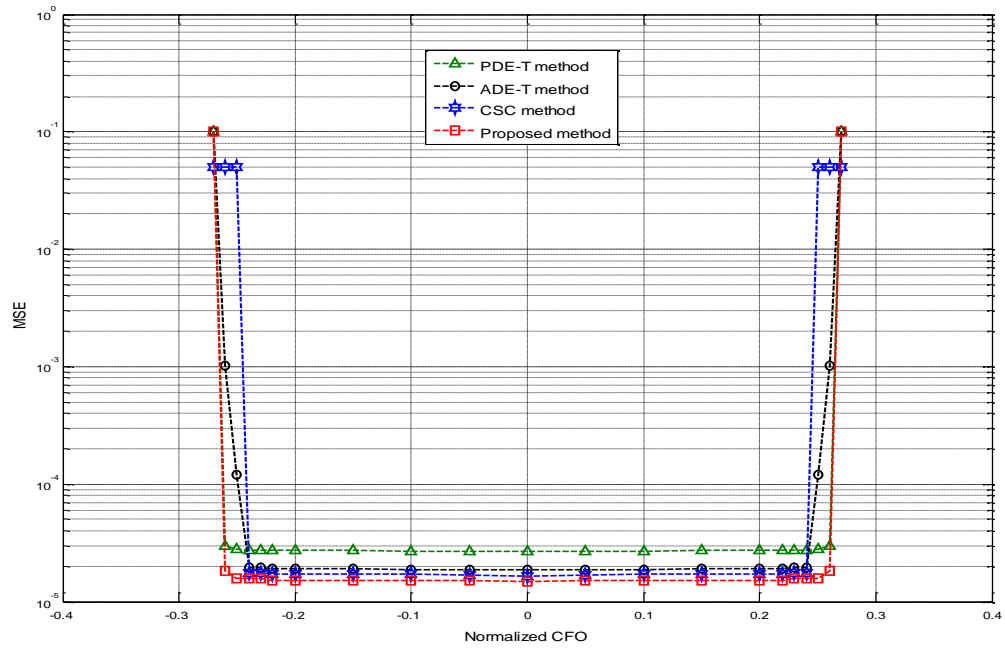


Figure 5.5: MSE plot of the various methods showing range limits (OSNR = 15 dB).

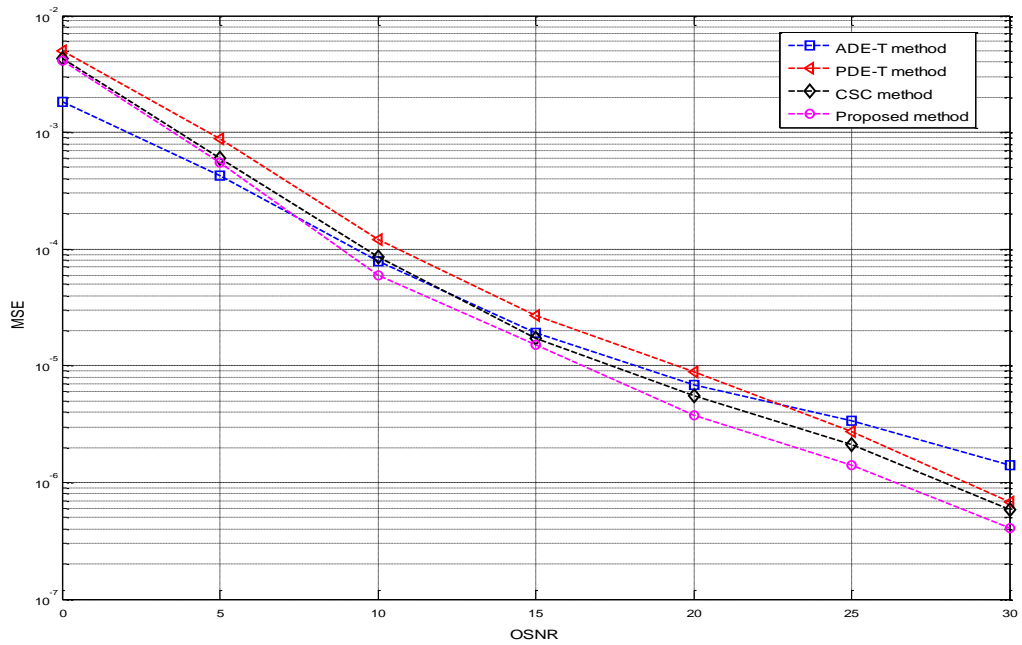


Figure 5.6: MSE performance of the various estimation methods using a fiber link of 8×80 km spans.

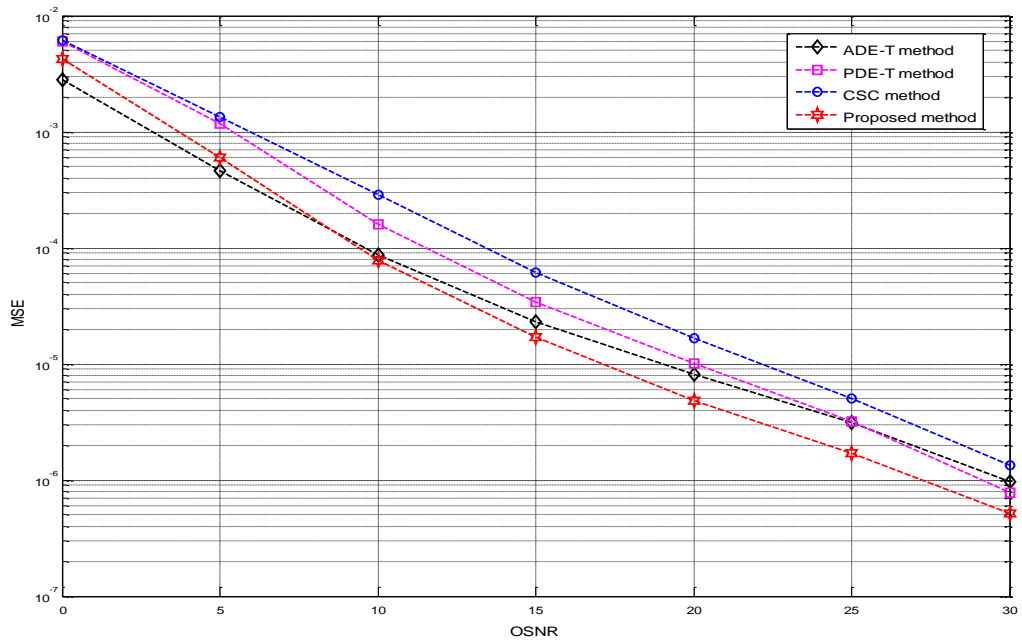


Figure 5.7: MSE performance of the various estimation schemes under fiber impairments with total haul 1.8×10^3 km.

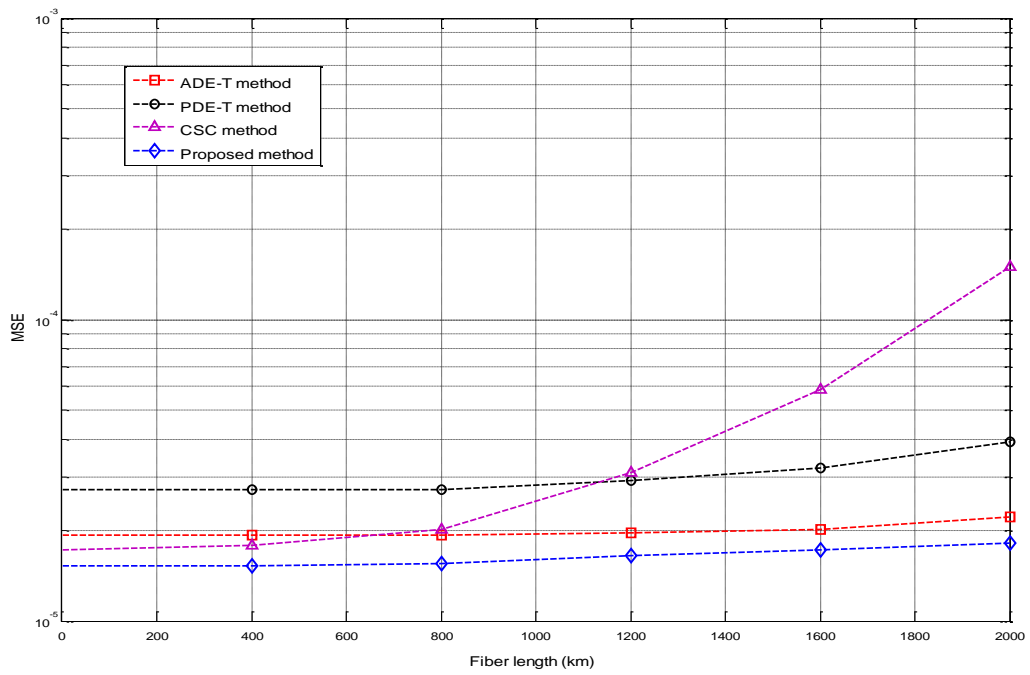


Figure 5.8: MSE performance of the various estimation methods as function of the fiber length at OSNR=15 dB.

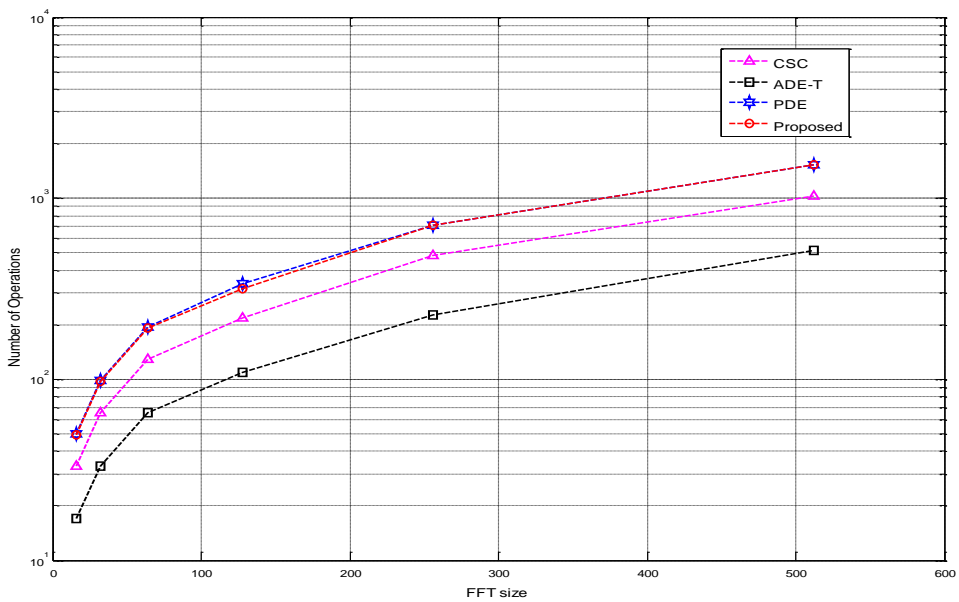


Figure 5.9: Complexity graph of the various CM methods.

5.7. Conclusion

A highly efficient totally blind CFO estimation method has been proposed and implemented for CM-signaling based CO-OFDM systems. First and foremost, existing blind estimation schemes for wireless communication systems in literature have been adapted, derived and implemented in the optical scenario. The performances of these existing schemes are further compared with the proposed blind CFO estimator. The blind CFO estimation method has been proven through analysis and simulation to achieve a superior performance as compared to the prominent existing blind estimation schemes. The proposed estimator shows high stability and performance in the presence of fiber impairments and dispersion. The proposed cost-function is also approximated as a cosine function, thus the CFO is estimated in close-form using only three trial values. This ensures that the proposed method achieves a reduced computational complexity similar to the existing methods. Therefore, the proposed method offers a balanced and efficient overall performance as compared to existing blind estimation methods.

CHAPTER SIX

ADAPTIVE SUBSPACE METHOD FOR PHASE NOISE ESTIMATION IN CO-OFDM SYSTEMS

6.1. Introduction

This chapter focuses on the implementation of subspace-tracking based blind phase noise estimation. An efficient adaptive subspace-tracking method is developed and utilized for phase noise estimation while mimicking a practical CO-OFDM system. There are various subspace-tracking methods in the literature [78]-[83] that have been implemented in the RF domain. A direct way of estimating a subspace of interest is by applying the singular vector decomposition (SVD) on an observation covariance matrix. The direct SVD approach however, results in a high computational complexity. To address this, alternative methods have been studied and proposed, focusing on the signal subspace tracking while little attention is given to the estimation of the noise subspace. A direct modification of the signal subspace, to achieve a low complexity noise subspace tracking is not practicable. This is evident in existing noise subspace tracking methods, where high instability and inefficiency become inevitable [103]-[104].

The fast data projection method (FDPM) as reported in [84], offers a low complexity, numerically stable, and robust noise subspace tracking. Hence, for the purpose of this study, the subspace-tracking method utilized is based on the FDPM. In order to achieve an adaptive implementation and convergence of the FDPM subspace tracking, the selection of the step-size becomes imperative. In [84], the use of a normalized step-size is proposed. Thus, the speed of convergence and the overall performance of the algorithm largely depend on the stringent selection of the step-size. For an enhanced performance, and to achieve a more stable as well as fast convergence, this work therefore proposes the use of a variable step-size. Also, to obtain a simple adaptive estimate of the phase noise, a prediction parameter is introduced using the forward backward linear

prediction (FBLP) technique [107]. The prediction parameter is constructed based on the estimates obtained from the noise subspace-tracking algorithm.

Thus, the main contributions in this chapter include the following

1. The derivation and the implementation of an adaptive method based on fast subspace tracking, for phase noise estimation in optical networks. The method utilizes an observation vector that is a subset of the total OFDM subcarrier, in order to adaptively estimate the phase noise, which constantly changes over an OFDM frame. The proposed method is derived and investigated for CO-OFDM system in a scenario close to practical situation, which considers the impact of dispersions and impairments along the fiber link.
2. Convergence speed and stability are important factors that must be considered while estimating any subspace of interest. Existing subspace methods generally utilize the regular normalized step-size, which is carefully selected to ensure stability and speed of convergence. This work deviates from the use of the normalized step-size by introducing an adaptive step-size, for the implementation of the noise subspace-tracking algorithm. The unique introduction of the adaptive step-size for use in the subspace-tracking algorithm ensures that a stable and faster speed of convergence is achieved while overall system performance is enhanced.
3. To achieve a simple way by which the phase noise can be adaptively obtained based on initial estimates of the subspace-tracking algorithm, a prediction parameter is introduced. The weighting parameter is derived using the forward backward linear prediction (FBLP) technique. The novel combination of the FBLP technique with the subspace-tracking algorithm ensures low-complexity and also improves the robustness of the estimation algorithm. Thus, the proposed approach is called SS-FBLP and the case where the variable step-size is introduced is called SS-FBLP-VSS.

6.2. The Subspace Tracking Algorithm

The subspace-tracking scheme has been studied with wide variety of approaches, and computational complexities. Various subspace-tracking algorithms have been employed in different applications such as source localization, spectral analyses, antenna array processing, system identification, wireless communication systems, adaptive filtering, among others. Subspace-tracking algorithms are mainly centered on the estimation of either singular vectors or orthogonal basis for a subspace of interest [77]. The particular ability of subspace tracking scheme to estimate the subspace corresponding to both the largest and the smallest singular values is of paramount interest especially in telecommunication system applications. Also, the complexity of the subspace tracking algorithm as well as their numerical stability must be put into consideration for optimum and cost effective performance.

A very pertinent method in the actualization of the subspace tracking algorithms is the Singular Value Decomposition (SVD). The SVD is useful in various applications to identify the spectrum of a matrix, to carefully resolve the matrix rank problem as well as to determine a certain subspace of interest. In [78], an adaptive procedure to update signal subspace estimates was proposed. The method is based on an orthogonal iteration variant, which utilizes the exponentially windowed sample autocorrelation matrix as an estimate of a covariance matrix \mathbf{R} . The method employed in [78] was also utilized in [79, 80] while adopting the Rayleigh-Ritz approximation in [81]. In [82], a subspace algorithm known as the low rank adaptive filter is introduced. This method is achieved by projecting the observed data unto the signal subspace instead of the complete data subspace. The Data Projection Method is detailed in [83] and the iterative technique is described in the next section. This method provides orthonormal estimates and its variant, called the Fast DPM, forms the basis of the subspace method adopted in this thesis.

6.2.1 Iterative subspace computation technique

There are various iteration techniques employed to determine singular values and their corresponding singular vectors. The power method is considered popular, together with its variants. Considering a case with received sequence \mathbf{y}_n and let $\mathbf{R} = E[\mathbf{y}_n \mathbf{y}_n^H]$ be a symmetric, non-negative definite matrix of size N , with SVD that satisfies the following expression [84, 85]:

$$\mathbf{R} = \mathbf{Q}\mathbf{\Lambda}\mathbf{Q}^H = [\mathbf{q}_1, \mathbf{q}_2, \dots, \mathbf{q}_N] \begin{bmatrix} \tau_1 & & & \\ & \tau_2 & & \\ & & \ddots & \\ & & & \tau_N \end{bmatrix} \begin{bmatrix} \mathbf{q}_1^H \\ \mathbf{q}_2^H \\ \vdots \\ \mathbf{q}_N^H \end{bmatrix} \quad (6.1)$$

where $\tau_1 \geq \tau_2 \geq \dots \geq \tau_N \geq 0$ are the singular values of \mathbf{R} and $\mathbf{q}_1, \mathbf{q}_2, \dots, \mathbf{q}_N$ the associated singular vectors. The task therefore is to determine the singular vector corresponding to the dominant singular value. Although the power method [86] presents a simple way out, an even more easier and encompassing method, which computes the subspace corresponding to the V major singular values is the orthogonal iteration. Hence, a sequence of matrices $[\mathbf{Q}(n)]$, will therefore be obtained using the orthogonal iteration technique as shown below, while satisfying the condition $1 \leq V \leq N$.

In Table 6.1, ortho'norm represents the orthonormalization, which is achieved using the modified Gram-Schmidt (MGS) procedure. There are other methods such as the QR decomposition and variations like the Householder, Givens transformations and the Gram-Schmidt orthogonalization. However, the MGS procedure is more desirable because of its enhanced performance and numerical stability [85]. The QR factorization and decomposition as well as the orthogonal iteration technique using the MGS, are detailed in [86].

Table 6.1: The Modified Gram-Schmidt (MGS) Orthonormalization Procedure

```

Initialize with a random orthonormal matrix  $\mathbf{Q}(0)$ 
for  $n= 1,2,\dots$ 
  ▪  $\mathbf{Q}(n) = \text{ortho'norm}[\mathbf{RQ}(n - 1)]$ 
  ▪  $\mathbf{\Pi}(n) = \text{diag}[\mathbf{Q}(n)^H \mathbf{RQ}(n)]$ 
end

```

6.2.2 Modifications of the orthogonal iteration

The focus here is the adaptive implementation of the subspace-tracking scheme. However, there are three variations derived from the power method and its orthogonal iteration derivative [85].

Variation 1: The focus is on the estimation of the largest singular vectors of a matrix. The variant is depicted in Table 6.2

Table 6.2: Orthogonal Iteration Variant 1

```

Initialize with a random orthonormal matrix  $\mathbf{Q}(0)$ 
for  $n= 1,2,\dots$ 
  ▪  $\mathbf{Q}(n) = \text{ortho'norm}[(\mathbf{I} + \beta\mathbf{R})\mathbf{Q}(n - 1)]$ 
end

```

Looking at Table 6.2, the matrix $\mathbf{I} + \beta\mathbf{R}$ has the same singular vectors as \mathbf{R} and the associated singular values are $1 + \beta\tau_v$.

Variation 2: This presents the iteration, which can be used for obtaining the subspace associated with the smallest singular values as opposed to Variation 1 as shown in Table 6.3.

Table 6.3: Orthogonal Iteration Variant 2

```

Initialize with a random orthonormal matrix  $\mathbf{Q}(0)$ 
for  $n= 1,2,\dots$ 
  ▪  $\mathbf{Q}(n) = \text{ortho'norm}[\mathbf{R}^{-1}\mathbf{Q}(n - 1)]$ 
end

```

The iteration in Table 6.3 converges to

$$\lim_{n \rightarrow \infty} \mathbf{Q}(n) = \mathbf{Q} = [\mathbf{q}_N, \dots, \mathbf{q}_{N-V+1}] \quad (6.2)$$

when the condition $\tau_1 \geq \tau_2 \geq \dots \geq \tau_{N-V} \geq \tau_{N-V+1} \geq \dots \geq \tau_N \geq 0$, is satisfied and provided $\mathbf{Q}^H(0)\mathbf{Q}$ is non-singular.

Variante 3: The iteration for Variante 3 is illustrated in Table 6.4. The focus also is on the computation of the subspace corresponding to the smallest singular values. Hence, if $\tau_1 \geq \tau_2 \geq \dots \geq \tau_{N-V} \geq \tau_{N-V+1} \geq \dots \geq \tau_N \geq 0$, then $(\mathbf{I} - \beta\mathbf{R})$ has singular values $1 - \beta\tau_N \geq \dots \geq 1 - \beta\tau_{N-V+1} \geq 1 - \beta\tau_{N-V} \geq \dots \geq 1 - \beta\tau_1 \geq 0$, and singular vectors $[\mathbf{q}_N, \mathbf{q}_{N-1}, \dots, \mathbf{q}_1]$.

Table 6.4: Orthogonal Iteration Variante 3

| |
|---|
| Initialize with a random orthonormal matrix $\mathbf{Q}(0)$ for $n= 1,2,\dots$ <ul style="list-style-type: none"> ▪ $\mathbf{Q}(n) = \text{ortho'norm}[(\mathbf{I} - \beta\mathbf{R})\mathbf{Q}(n - 1)]$ end |
|---|

The first and the third variants are more dynamic as it is convenient to toggle between the largest and the smallest singular values by just a change in sign. Therefore, these two variants form the basis for the actualization of the subspace adaptive technique for estimation as adopted in this thesis.

6.3. Blind Subspace Phase Noise Estimation for CO-OFDM Systems

6.3.1 The subspace problem

The subspace problem as described in subsection 6.2.1 is generally approached by assuming a condition where the parameter to be estimated remains constant over the entire OFDM frame. Thus, the received signal $Y_i(m)$ described in (3.8), while assuming perfect CFO synchronization can be rewritten as:

$$Y_i(m) = B_i(0)X_i(m)Z(m) + W_i(m), \quad (6.3)$$

where

$$B_i(0) = \frac{1}{N} \sum_{n=0}^{N-1} e^{j\rho_i(n)} \cong e^{j\Phi_i}, \quad (6.4)$$

and Φ_i is the CPE, while $W_i(m) = ICI_i(m) + G_i(m)$. Also, in the general subspace problem, the estimation converges after several OFDM symbols. However, such assumption does not hold in the case of phase noise, which is constantly changing within an OFDM frame. Thus, the adaptive algorithm has to converge within an OFDM symbol. In order to overcome the difficulty of adaptively estimating the phase noise, an observation vector, which is a subset of the total OFDM subcarrier, is utilized. The observation vector is defined as a portion of the received signal, which is denoted as $Y(j)$ with length L , where $L < N$. This enables the frequently changing phase noise to be effectively estimated across $Y(j) \dots Y(L+j)$. Hence, the observation sequence on which the phase noise subspace tracking problem is based can be defined as

$$\mathbf{S}_j = [S_j(1) \dots S_j(L)] = [Y(j) \dots Y(L+j)], \quad (6.5)$$

Therefore, considering a non-negative covariance \mathbf{P} with size L of the received data sequence \mathbf{S}_j , by applying singular value decomposition on \mathbf{P} , the following expression is obtained

$$\mathbf{P} = \mathbb{E}[\mathbf{S}_j \mathbf{S}_j^H] = \mathbf{U} \mathbf{\Lambda} \mathbf{U}^H \quad (6.6)$$

where $\mathbf{\Lambda} = \text{diag}\{\gamma(1), \dots, \gamma(L)\}$ denotes the diagonal matrix of singular values of \mathbf{P} , whose elements are the singular values of \mathbf{P} satisfying $\gamma(1) \geq \gamma(2) \geq \dots \geq \gamma(D) > \gamma(D+1) \geq \dots \geq \gamma(L) \geq 0$ ($D < L$), while \mathbf{U} contains the corresponding singular vectors with elements $u(1) \dots u(L)$. A simple orthogonal iterative method can be used to estimate the subspace of interest, in order to obtain the singular vectors corresponding to the singular values of the matrix \mathbf{P} . Since L represents the rank of the subspace of interest, then the sequence of matrices $\mathbf{U}(j)$ is described by the iteration [105]

$$\mathbf{U}(j) = \text{orthonorm}\{\mathbf{P}\mathbf{U}(j-1)\}, \quad j = 1, 2, \dots \quad (6.7)$$

where orthonorm represents an orthogonal procedure using the QR decomposition, and given that the matrix $\mathbf{U}^H(j)[u(1) \dots u(D)]$ is not singular, then

$$\lim_{i \rightarrow \infty} \mathbf{U}(j) = [u(1) \dots u(D)]. \quad (6.8)$$

As mentioned above, since the aim is to estimate the subspace that contains the smallest singular values corresponding to the smallest singular vectors, two variants of the orthogonal iteration are presented. These orthogonal iterative methods ensure the realization of such estimates and also enable adaptive implementations. The variants are described as follows

$$\mathbf{U}(j) = \text{orthonorm}\{\mathbf{P}^{-1}\mathbf{U}(j-1)\}, \quad (6.9)$$

$$\mathbf{U}(j) = \text{orthonorm}\{(I_L - \mu\mathbf{P})\mathbf{U}(j-1)\}, \quad j = 1, 2, \dots \dots \dots \quad (6.10)$$

where $\mu > 0$ is the step-size, which is relatively small, while I_L is the identity matrix. For the purpose of this work, (6.10) is adopted since it has a lower complexity compared to (6.9), which has a higher complexity due to the matrix inversion.

In order to achieve an adaptive implementation at an instance where \mathbf{P} is not available, the received vector is obtained sequentially and the matrix \mathbf{P} is substituted with an adaptive estimate $\hat{\mathbf{P}}_j$, which satisfies the condition $E[\hat{\mathbf{P}}_j] = \mathbf{P}$. An orthogonal iterative process is then used to compute the singular vectors associated with its singular values. The adaptive orthogonal iterative algorithm is expressed as:

$$\mathbf{U}(j) = \text{orthonorm}\{(I_L - \mu\hat{\mathbf{P}}_j)\mathbf{U}(j-1)\}. \quad (6.11)$$

The parameter μ used above represents the constant step-size. However, to achieve a better stability and speed of convergence, an adaptive step-size $\mu(j)$ is utilized, which is defined as [106]:

$$\mu(j) = \delta \cdot \text{erf}\left(1 - e^{-\alpha|\tau_j|}\right), \quad (6.12)$$

where $\text{erf}(x) = 2/\sqrt{\pi} \int_0^x e^{-\sigma^2} d\sigma$ represents the error function operation. The variation rate of the adaptive step-size is controlled by adjustment factors δ and α , while $\tau_j = B_j - B_{j-1}$ is the error term. Also, the range of $\mu(j)$ is given as $0 < \mu(j) < 2/\gamma(1)$ [106], where $\gamma(1)$ is the maximum singular value of the covariance matrix. Also, the range of δ is within the boundary

$0 < \delta < 2/\gamma(1)$ (since $\gamma(1)$ is the maximum singular value of the covariance matrix), given that $0 < \operatorname{erf}(1 - e^{-\alpha|\tau_j|}) < 1$ [106].

6.3.2 The prediction parameter

As $\mathbf{U}(j)$ is obtained using the adaptive iterative method, its corresponding L columns with vectors $[u(1) \dots u(D)]$ are therefore utilized to construct the prediction parameter \mathbf{W} . In order to achieve this, a method based on the minimum-norm solution of the forward-backward linear property in [107] is employed. Using the singular values as well as the singular vectors of the estimate $\mathbf{U}(j)$, the relationship between the prediction parameter and the covariance matrix is derived as follows.

Considering a linear prediction parameter described by the column vector \mathbf{W}_j

$$\mathbf{W}_j = [w_j(1), w_j(2) \dots w_j(D)]^T, \quad (6.13)$$

with $[\cdot]^T$ denoting transpose and $D \leq L$. Utilizing the prediction parameter in both forward and backward direction, the prediction equation can be expressed as [107]:

$$\begin{bmatrix} S_j(D) & S_j(D-1) & \dots S_j(1) \\ S_j(D+1) & S_j(D) & \dots S_j(2) \\ \vdots & \vdots & \vdots \\ S_j(L-1) & S_j(L-2) & \dots S_j(L-D) \\ S_j^*(2) & S_j^*(3) & \dots S_j^*(D+1) \\ S_j^*(3) & S_j^*(4) & \dots S_j^*(D+2) \\ \vdots & \vdots & \vdots \\ S_j^*(L-D) & S_j^*(L-D+1) & S_j^*(L) \end{bmatrix} \begin{bmatrix} w_j(1) \\ w_j(2) \\ \vdots \\ w_j(D) \end{bmatrix} = - \begin{bmatrix} S_j(D+1) \\ S_j(D+2) \\ \vdots \\ S_j(L) \\ \dots \dots \dots \\ S_j^*(1) \\ S_j^*(2) \\ \vdots \\ S_j^*(L-D) \end{bmatrix}, \quad (6.14)$$

which can be written in a condensed form as:

$$\mathbf{R}_j \mathbf{W}_j = -\mathbf{a}_j \quad (6.15)$$

Thus, the minimum-norm solution to the expressions in (6.13)-(6.14) is expressed as:

$$\mathbf{W}_j = -\mathbf{R}_j^{-1} \mathbf{a}_j, \quad (6.16)$$

where \mathbf{R}_j^{-1} denotes the pseudo-inverse of \mathbf{R}_j , which can be expressed as

$$\mathbf{R}_j^{-1} = (\mathbf{R}_j^* \mathbf{R}_j)^{-1} \mathbf{R}_j. \quad (6.17)$$

The correlation matrix \mathbf{P} is also expressed as

$$\mathbf{P} = \mathbf{R}_j^* \mathbf{R}_j; \quad \hat{\mathbf{P}}_j = -\mathbf{R}_j \mathbf{a}_j, \quad (6.18)$$

in linear prediction representation, where $\hat{\mathbf{P}}_j$ is determined from the received data sequence, while “*” denotes complex conjugate transpose. From (6.14), the prediction parameter \mathbf{W}_j can be expressed as:

$$\mathbf{W}_j = (\mathbf{R}_j^* \mathbf{R}_j)^{-1} \mathbf{R}_j \cdot \mathbf{a}_j \Rightarrow \mathbf{W}_j = \mathbf{P}^{-1} \hat{\mathbf{P}}_j. \quad (6.19a)$$

Therefore from (6.19) and recalling the SVD expression in (6.6), \mathbf{W}_j can be further expressed as

$$\mathbf{W}_j = (\mathbf{U} \mathbf{\Lambda} \mathbf{U}^H)^{-1} \hat{\mathbf{P}}_j \quad (6.19b)$$

Thus, the prediction parameter is obtained as:

$$\mathbf{W}_j = \sum_{l=1}^D \frac{u(l)}{\gamma(l)} \cdot (u^H(l) \cdot \hat{\mathbf{P}}_l). \quad (6.20)$$

As $u(l)$ is the efficient estimates of the singular vectors, \mathbf{W}_j also constitutes the estimate of the singular vectors corresponding to the smallest singular values of the subspace of interest. Thus, the adaptive phase noise estimation is therefore obtained using (6.10), which is expressed as [105]:

$$\hat{\mathbf{B}}_j = \text{normalize}\{B_{j-1} - \mu \cdot w_j(1) B_{j-1}\}, \quad (6.21)$$

$$\hat{\Phi}_j = \angle \hat{\mathbf{B}}_j \quad (6.22)$$

where \angle represents the phase angle and B_j is related to the CPE as expressed in (6.4). Finally, the compensation is obtained using the following expression

$$\hat{Y}(j) = e^{-j\hat{\Phi}_j} Y(j) \quad (6.23)$$

6.4. Pilot Aided Subspace Phase Noise Estimation

Now considering the case where M_p number of pilot subcarriers are introduced, where $\{m_1, m_2, \dots, m_{M_p}\}$ of pilot tones are available at each payload OFDM symbol. The phase is estimated based on pilot subcarriers in OFDM symbols. Hence, the pilot-based estimate is obtained as reported in [74] as:

$$\hat{B}_i(0) = \frac{1}{M_p} \sum_{m \in \{m_p\}} \frac{Y_i(m)|X_i(m)|}{X_i(m)|Y_i(m)|}. \quad (6.24)$$

Therefore, from (6.24), if $Q_i(m)$ is expressed as $Q_i(m) = Y_i(m)\hat{B}_i(0)$, then sequence for the subspace algorithm with pilot subcarriers becomes $\mathbf{S}_j = [S_j(1) \dots \dots S_j(L)] = [Q(j) \dots \dots Q(L + j)]$. Thus, the initial phase is obtained using the pilot subcarriers before the final estimation is obtained using the subspace approach as described from (6.6)-(6.23).

Also, the relationship between the prediction parameter and the covariance vector is shown in (6.13)-(6.19). It is seen that the prediction parameter is a linear combination of the singular vectors of the subspace of interest.

6.5. Computational complexity

Using the direct SVD, the number of operations required is generally of order $O(L^3)$. The SVD method generally results in high computational complexity with $L^2(L + 2D + 2)$ multiplication operations and $L(3D^2 + 2D)$ addition operations [84, 85]. However, the proposed method, which is based on the FDPM approach, using the normalization process described in Table 6.2, ensures

a reduced complexity. The sequence $\{\mathbf{U}(j) = \text{norm}[\mathbf{H}(j)]\}$ have computational complexity of $O((L + D)D)$ since the normalization of a vector requires $O(L + D)$ operations. Using the normalization operation (“norm”) reduces the complexity and ensures that an order of magnitude is gained as the use of the “orthonormalize” operation is of complexity $O((L + D)^2D)$ [105]. Thus, the proposed SS-FBLP method requires $L(3D + 1)$ multiplication operations and $L(5D + 1)$ addition operations. Also, considering the adaptive estimator in (6.21), the complexity is of order $O(D^2)$ due to the fact that the adaptive expression in (6.10) is used rather than (6.9). Using (6.9) would have resulted in $O(D^3)$ due to the matrix inversion [105]. The comparison of the considered subspace methods in terms of the required multiplication and addition operations is presented in Table 6.5. Also, the complexity graph of the subspace methods is presented in Figure 6.9.

Table 6.5: Computational Complexity of the Subspace Methods

| Subspace Method | Multiplication | Addition |
|-----------------|-------------------|----------------|
| SVD | $L^2(L + 2D + 2)$ | $L(3D^2 + 2D)$ |
| SS-FBLP | $L(3D + 1)$ | $L(5D + 1)$ |
| SS-FBLP-VSS | $L(5D + 2)$ | $L(7D + 2)$ |

The summary of the proposed phase noise estimation algorithm is as shown in Table 6.6.

Table 6.6: Summary of the Proposed Estimation Algorithm

-
-
1. For $i = 1, 2, \dots, 10^3$
 2. Compute $Y_i(m)$ (3.12)
 3. For $j = 1, 2, \dots, L; L < N$ [FDPM to obtain $\mathbf{U}(j)$]
 4. Obtain sequence $\mathbf{S}_j = [S_j(1) \dots S_j(L)] = [Y(j) \dots Y(L + j)]$
 5. Obtain covariance $\mathbf{P} = \mathbb{E}[\mathbf{S}_j \mathbf{S}_j^H]$
 6. Initialize with a random orthonormal matrix $\mathbf{U}(0)$
 7. Available from previous instant: $\mathbf{U}(j - 1)$
 8. Compute μ
 9. $\mathbf{c}(j) = \mathbf{U}^H(j - 1) \mathbf{S}_j$
 10. $\mathbf{T}(j) = \mathbf{U}(j - 1) \pm \mu \mathbf{S}_j \mathbf{c}^H(j)$
 11. $\mathbf{b}(j) = \mathbf{c}(j) - \|\mathbf{c}(j)\| \mathbf{e}'$, where $\mathbf{e}' = [\mathbf{1}, \dots, \mathbf{0}]^T$
 12. $\mathbf{H}(j) = \mathbf{T}(j) - \frac{2}{\|\mathbf{b}(j)\|^2} [\mathbf{T}(j) \mathbf{b}(j)] \mathbf{b}^H(j)$
 13. $\mathbf{U}(j) = \text{norm}[\mathbf{H}(j)]$,
where $\text{norm}[\cdot]$ is the normalization of each column of $\mathbf{H}(j)$
 14. Obtain singular vectors $[u(1) \dots u(D)]$ from $\mathbf{U}(j)$ for the construction of \mathbf{W}_j
 15. Construct the weighting parameter $\mathbf{W}_j = \sum_{l=1}^D \frac{u(l)}{\gamma(l)} \cdot (u^H(l) \cdot \hat{\mathbf{P}}_l)$ (6.16)
 16. Compute $\hat{\mathbf{B}}_j$ (6.17)
 17. Compute $\hat{\Phi}_j$ (6.18)
 18. End for
 19. Compute MSE
 20. End
-
-

6.6. Simulation and Discussion

The performance of the proposed algorithm is investigated in a 20 Gb/s CO-OFDM system. In the simulation, the sampling frequency of the OFDM symbol is 28.8ns, with the length of the IFFT/FFT chosen as 256, $L = 128$, $D = 96$ while a 12.5% cyclic prefix is used. The quadrature phase shift keying modulation format is adopted. The mimicked practical fiber link consists of ten spans of 80 km standard single mode fiber (SSMF) with fiber dispersion 17 ps/km/nm, differential group delay of 5 ps/ $\sqrt{\text{km}}$ as well as loss coefficient of 0.2 dB/km. A total number

of 1000 OFDM symbols is used for each bit-error-rate simulation result. Also, optical amplifier, EDFA has 16 dB gain with noise figure of 4 dB and the non-linear coefficient of the fiber is 1.32/W/km. The parameters are as shown in Table 6.6.

Table 6.7: Simulation parameters

| PARAMETER | SPECIFICATIONS |
|------------------------------|-------------------|
| FFT size | 256 |
| Modulation format | QPSK |
| Data rate | 20 Gb/s |
| Cyclic prefix | 12.5 % |
| Sampling frequency | 28.8 ns |
| Fiber dispersion | 17 ps/km/nm |
| Differential group delay | 5 ps/ \sqrt{km} |
| Loss coefficient | 0.2 dB/km |
| Wavelength | 1550 nm |
| Amplifier gain | 16 dB |
| Noise figure | 4 dB |
| Non-linear fiber coefficient | 1.32/W/km |

Table 6.8: Acronyms and the description of techniques

| ACRONYM | DESCRIPTION OF TECHNIQUE |
|-------------|--|
| SVD | Singular Vector Decomposition |
| SS-FBLP | Subspace Forward Backward Linear Projection Technique |
| SS-FBLP-VSS | Subspace Forward Backward Linear Projection Variable Step Size Technique |

The FDPM subspace-tracking algorithm depends on the selection of the step-size for stability and convergence. In [84], it has been suggested that a value close to unity ensures the needed stability and speed of convergence. Therefore, with the range $0 < \mu < 1$, the constant step-size parameter is varied in this simulation between values of 0.90 and 1.0, to ascertain the most suitable value for the SS-FBLP method. Figure 6.1 shows the mean square error (MSE) plot for the SS-FBLP method, with varied values of step-size. The MSE of the phase noise is defined as $MSE = \mathbb{E} \left[\left| \angle \hat{B}_j - \angle B_j \right|^2 \right]$. Although the step-size value $\mu = 1.0$ gives a desirable performance, especially for lower values of OSNR, the preferred selection is $\mu = 0.98$, due to the consistent and stable

MSE performance offered at high values of OSNR. Hence, the step-size value $\mu = 0.98$ is utilized for subsequent analysis of the SS-FBLP method. Also, the introduced adaptive step-size as described in (6.12) brings new dynamics such as the selection of the appropriate value for the adjustment variables δ and α . For the purpose of this study, the value of the variable δ is set to unity i.e. $\delta = 1$, in order to achieve good steady-state performance. The value selected for the factor α has a more prominent influence on the variation rate of the step-size and the overall stability of the SS-FBLP-VSS method. Thus, the most suitable selection for α is investigated as shown in Figure 6.2, where the value of α is varied, starting from $\alpha = 1$. It becomes evident that the MSE performance is improved as the value of α increases. However, at some point, the MSE performance ceases to show any further marked improvement. Hence, the selection of $\alpha = 50$ is considered appropriate and this value is used for the subsequent analysis and comparison with the SS-FBLP method.

Figure 6.3 shows the BER performance of the proposed SS-FBLP and the SS-FBLP-VSS estimation methods. These methods are compared with the direct SVD method and from the plot it is seen that the SS-FBLP follows the performance of the direct SVD method closely. However, it should be noted that the SS-FBLP exhibits a significantly lower computational cost in comparison to the direct SVD method [85]. The SS-FBLP-VSS at $\alpha = 50$ offers a superior performance compared to the SS-FBLP and the SVD methods. This shows that, along with the desired stability that the adaptive step-size in the SS-FBLP-VSS method offers, it also comes with a more favorable overall performance as compared to the other methods. A direct comparison of the proposed algorithms is as shown in Figure 6.4. The methods are implemented with the linewidth set to 100 KHz and 400 KHz. In Figures 6.5 and 6.6, the convergence behaviors of the proposed methods are shown. In addition, Figure 6.6 also shows the performance of the algorithm using pilot subcarriers. From the plot, it can be seen that the MSE performances of the proposed methods decrease monotonically and then converge to a steady state. The SS-

FBLP-VSS converges and attain steady-state faster than the SS-FBLP method. Thus, it can be stated that the variable step-size used, accounts for this acceptable convergence behavior. Also, the superior MSE performance exhibited by the SS-FBLP-VSS method could be attributed to its fast convergence as a result of the adaptive step-size utilized instead of the fixed step-size used in the other method.

In Figure 6.7, the MSE versus the linewidth plot is shown. The performance of the SS-FBLP method is compared to the SS-FBLP-VSS method across different linewidth values. It is seen that both methods exhibit moderate robustness with increasing linewidth. Also, the graph in Figure 6.8 shows the behavior of the proposed methods, as the length of the optical channel is increased. Although the performances of the proposed methods are affected by the length of the optical channel, the methods especially the SS-FBLP-VSS, exhibit smooth decline and fair stability across the distance.

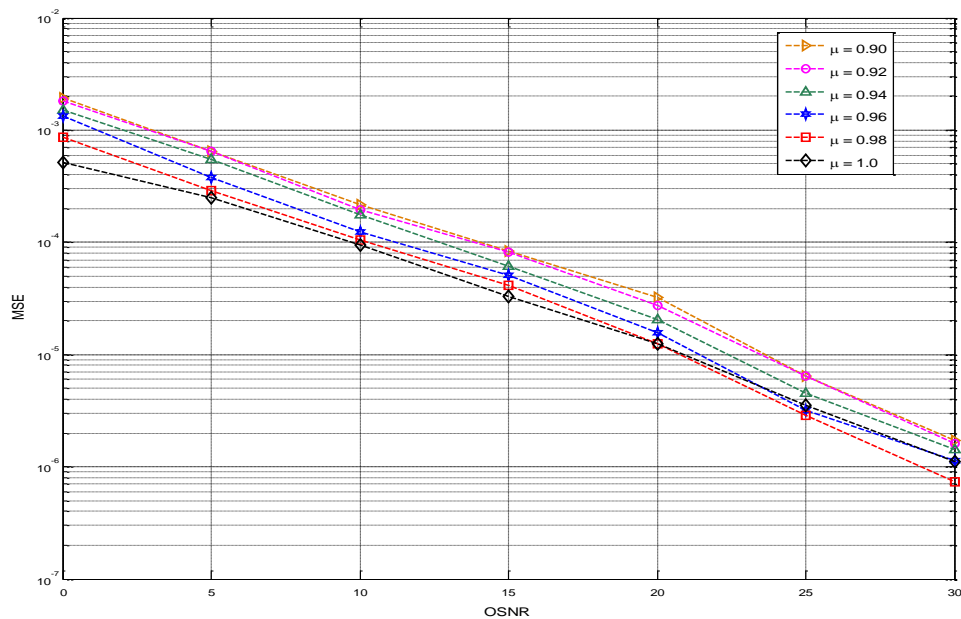


Figure 6.1: MSE versus OSNR plot for the SS-FBLP method with varied values of the step-size.

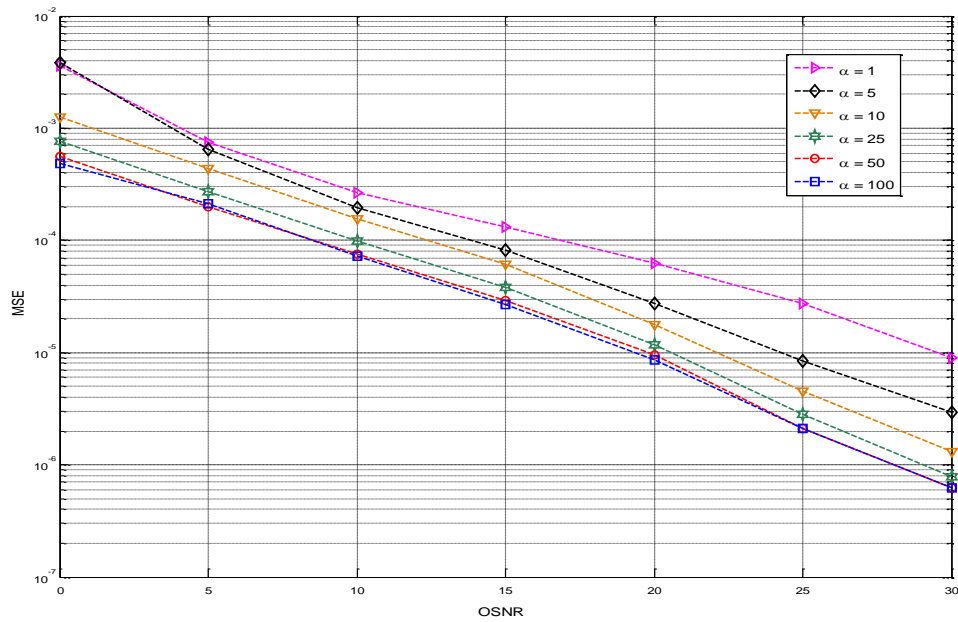


Figure 6.2: MSE performance of the SS-FBLP-VSS method with varied values of the adjustment variable α .

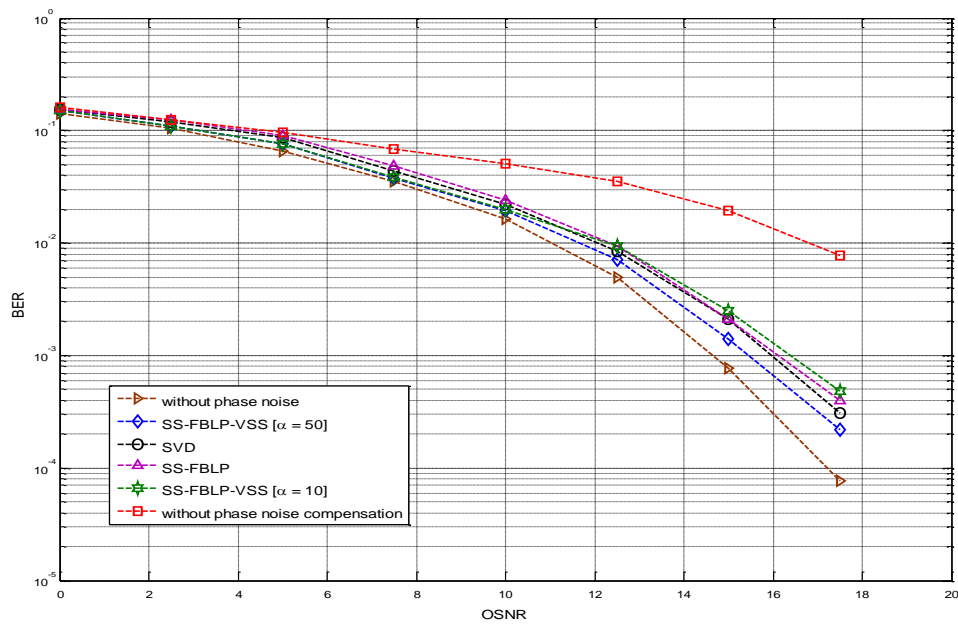


Figure 6.3: BER sensitivity for the proposed estimation algorithms in comparison with the direct SVD method.

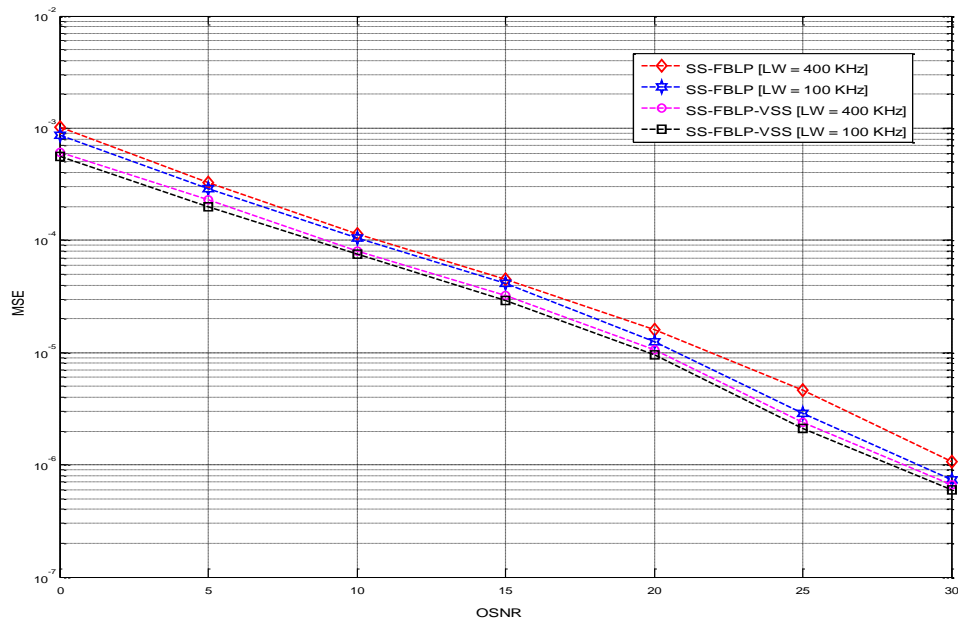


Figure 6.4: MSE performance of the proposed algorithms with linewidth set to 100 KHz and 400 KHz.

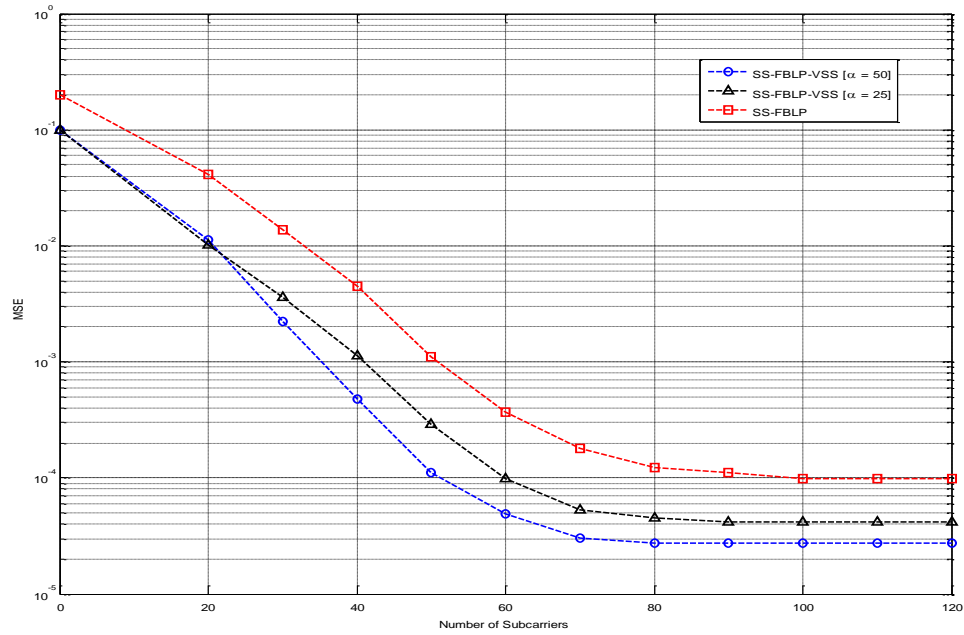


Figure 6.5: MSE plot showing the convergence behavior of the proposed algorithms.

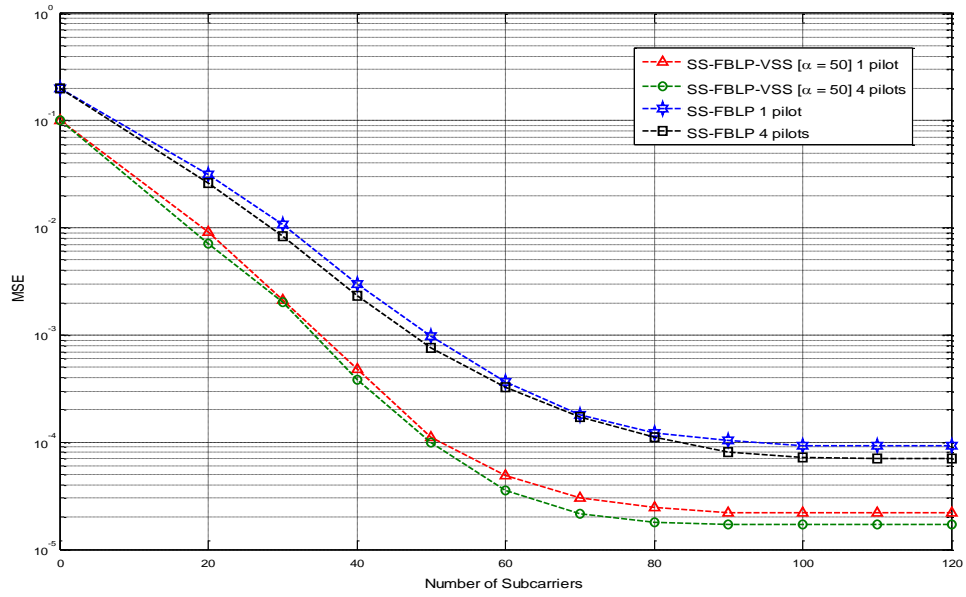


Figure 6.6: MSE plot showing the convergence behavior of the proposed algorithms with pilots.

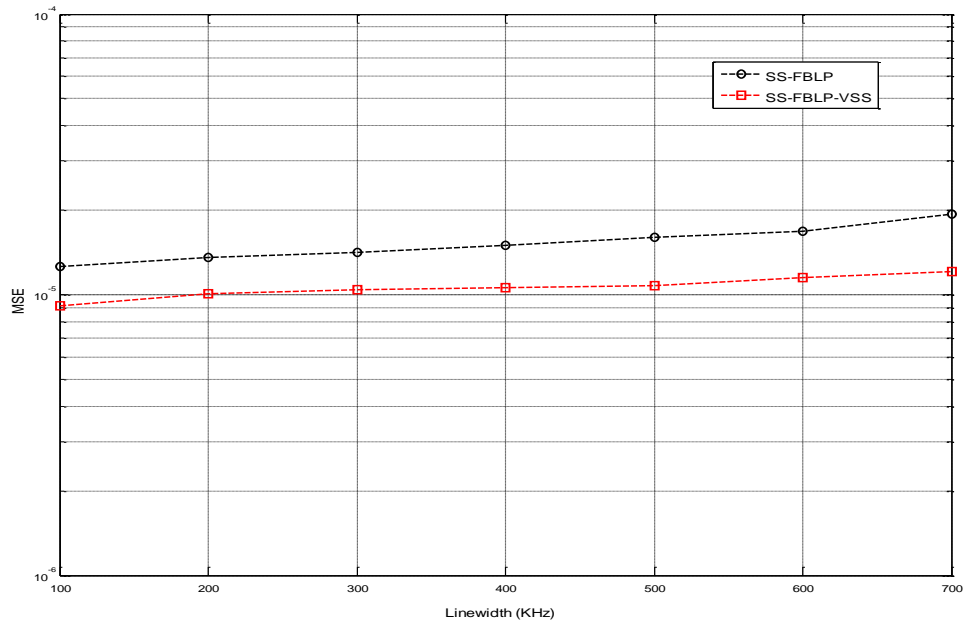


Figure 6.7: MSE versus linewidth plot for the proposed estimation algorithms.

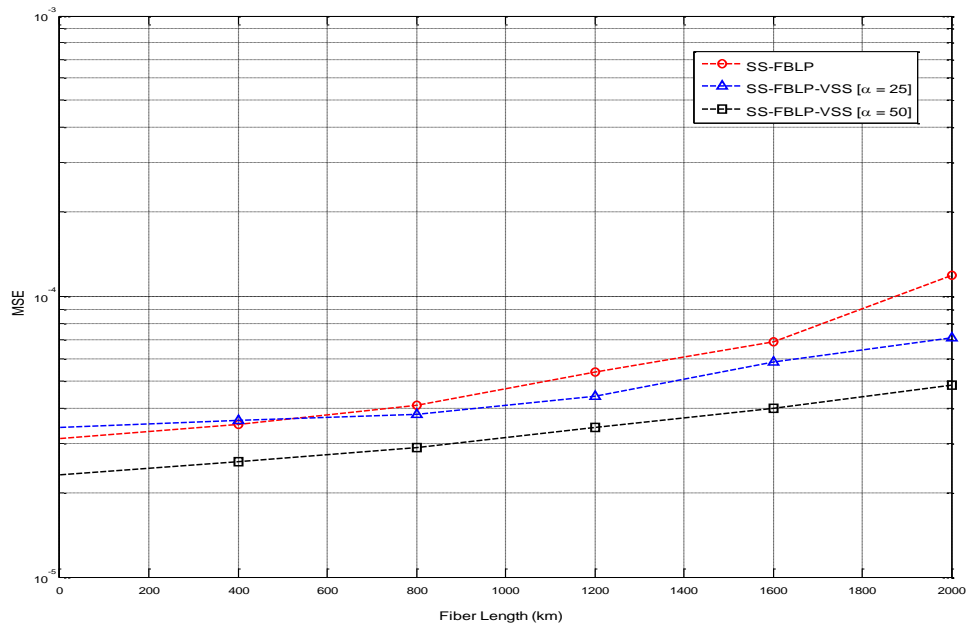


Figure 6.8: Performance of the proposed estimation algorithms with varying fiber length.

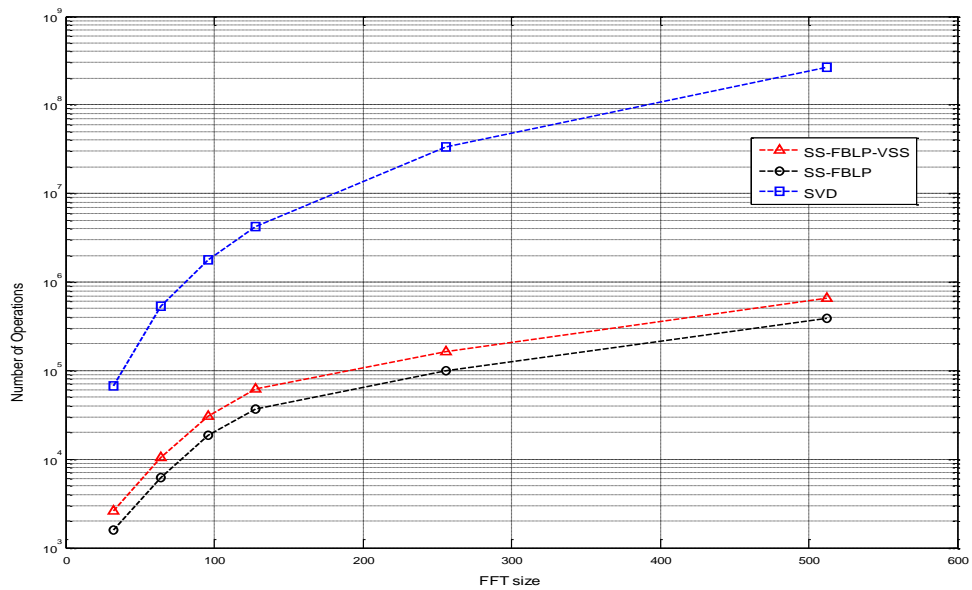


Figure 6.9: Complexity graph of the proposed methods as compared to the SVD method.

6.7. Conclusion

A blind estimation method, based on the subspace-tracking approach, has been proposed and implemented for phase noise estimation in CO-OFDM systems. The proposed SS-FBLP method

is derived in such a way that the estimate of the phase noise, which is constantly changing over an OFDM frame, is estimated adaptively. The adaptive implementation of the phase noise algorithm is enhanced by the FBLP method, which ensures low complexity. Also, a variable step-size is introduced in the SS-FBLP-VSS method, to achieve better convergence and stability. Results show that the proposed methods perform considerably well in the CO-OFDM system, implemented in a scenario close to practical environment. The proposed methods achieve superior performances as compared to the direct SVD method. Also, the results show that the SS-FBLP-VSS method offers an enhanced overall system performance compared to its SS-FBLP counterpart. Thus, in addition to the better convergence and stability that comes with the introduction of the adaptive step-size, an improved overall system performance is also achieved.

CHAPTER SEVEN

CONCLUSION AND FUTURE WORK

This final chapter gives the summary of all the research works that have been carried out, as well as possible areas of research for future consideration.

7.1. Conclusion

This thesis has focused on methods by which the adverse effects of phase noise and carrier frequency offset can be effectively addressed in an OFDM-based optical system.

In chapter one, the general background and the direction of the research work has been provided, highlighting the pertinent research questions, research objectives and the original contributions resulting from the research work.

Detailed discussion and overview of the optical communication system has been provided in chapter two. The major constituents of the optical transport networks, which include the optical transmitter, the optical receiver and the optical channel have been highlighted and discussed. Also, the chapter has discussed the principles of the OFDM, as well as the challenges associated with the OFDM scheme. The chapter concludes by discussing the major contrasts between the optical OFDM system and the RF OFDM system.

A detailed survey on the various methods that have been utilized for phase noise and CFO estimation in optical OFDM systems has been provided in chapter three. Pilot-aided techniques, the RF-based methods, the ML method as well as blind estimation techniques such as the constant modulus method and the subspace algorithm have been reviewed. These reviewed algorithms form the basis of the methods that are proposed for phase noise and CFO estimation in this research work.

In chapter four, the maximum likelihood approach for phase noise and CFO estimation has been discussed, analyzed and implemented. The contributions in this chapter are twofold. First, the

estimation of only the CFO is considered. Two identical training symbols are utilized to achieve CFO estimation. Thereafter, a simplified ML approach, which eliminates the need for the exhaustive search associated with traditional ML methods, is derived and utilized for the estimation of CFO and laser phase noise in CO-OFDM systems. Furthermore, to obtain an improved performance, the proposed simplified low-complexity ML estimator is uniquely combined with an efficient data-dependent pilot-aided (DD-PA) technique, for the acquisition of both the CFO and the laser phase noise. The performance of the simplified ML-based estimators is compared with existing methods and verified in a 16-ary quadrature amplitude modulation (16-QAM) CO-OFDM system with PMD, chromatic dispersion and other polarization dependent losses along the fiber link.

Chapter five proposes a blind carrier frequency offset estimation method for coherent optical orthogonal frequency division multiplexing (CO-OFDM) systems, using constant modulus signaling. The proposed scheme is based on a robust cost-function, which deviates from the common assumption that the channel frequency response slowly varies either in time or frequency domain. The proposed method adopts a cost-function similar to the Godard's method for blind channel equalization [98]. Using Monte Carlo simulations, the proposed method is shown to offer a superior performance compared to prominent existing methods, in a mimicked practical optical link scenario. Also, it is shown that the proposed cost-function can be approximated and expressed in a closed-form in such a way that the CFO estimate is obtained using only three trial values.

In chapter six, a blind phase noise estimation method for coherent optical orthogonal frequency division multiplexing (CO-OFDM) system is considered. Based on the subspace approach, a simple and robust method is proposed to adaptively estimate and track phase noise in CO-OFDM systems. The idea behind this novel technique is to estimate the singular vectors that correspond to the smallest singular values of the noise subspace. A weighting parameter, which is derived based on the forward backward linear prediction technique, is subsequently constructed using the

obtained singular vectors of the noise subspace, to adaptively estimate the phase noise in the system. In addition, a variable step-size is introduced to ensure an improved performance as well as stable convergence. Simulation results were shown to demonstrate the effectiveness as well as the efficiency of the proposed methods.

7.2. Future work

Although this research work has focused on the pertinent issues of phase noise and CFO, which adversely affects the OFDM-based optical system, there are other issues and possible areas for future considerations.

Further investigations can be carried out to determine if the subspace algorithm can be effectively combined with other algorithms, such as MUSIC and ESPRIT, to achieve improved performance especially in OFDM-based optical transport networks. The MUSIC algorithm has hitherto been unattractive in OFDM systems as it involves spectrum searches, which leads to high computational complexity. However, the ESPRIT algorithm, which is an Eigen-decomposition based algorithm like its MUSIC counterpart, is known to offer efficient estimation because of its high resolution and computational efficiency. These algorithms, especially the ESPRIT can be effectively adapted and utilized for phase noise and CFO estimation in CO-OFDM systems.

Although there are some works in the literature that have addressed the issue of peak-to-average power ratio, more investigations needs to be carried out in the optical domain to improve the efficiency of the optical amplifiers, thereby enhancing the overall performance of the optical system.

Also, for enhanced system diversity as well as robustness, the possibility of efficiently incorporating the multiple-input-multiple-output (MIMO) technique can be thoroughly investigated and implemented. The polarization modes supported in the fiber presents an attractive avenue to double the fiber capacity. In [20], the possibility of utilizing a 2 by 2 MIMO OFDM transmission in the optical domain, in a bid to achieve an enhanced capacity without

sacrificing the receiver sensitivity, is reviewed. In [108], a multi-gigabit real-time dual polarization CO-OFDM in a 2 by 2 MIMO configuration is implemented. The demonstration shows the possibility of the integration of the MIMO configuration into the existing CO-OFDM system. However, the few research works reported in literature have hitherto neglected the impact of phase noise and CFO on the performance of the proposed system. Therefore, future research work can focus effectively on investigating the extent at which the phase noise and the CFO impact the CO-MIMO-OFDM system and how they can be efficiently addressed.

APPENDIX I

As mentioned in subsection 5.3.1, a CFO estimate can be obtained by minimizing the function

$$J_{P_f}(\bar{\varepsilon}) \approx A \cos[2\pi(\varepsilon - \bar{\varepsilon})] + C, \quad (AI.1)$$

Although this can be achieved by using line search, the regularity of $J_{P_f}(\bar{\varepsilon})$ as expressed in (5.10) makes it possible to design estimators with low complexity using the curve-fitting closed-form solution [88, 91]. Thus, $J_{P_f}(\hat{\varepsilon})$ can be evaluated on different points to obtain the values of A, C and ε that satisfy (5.10). For instance, if $J(x)$ is to be evaluated at $x = -0.25, 0, -0.25$, it can be seen from (5.10) that an estimate \hat{x} can be obtained as follows [88, 91]

$$\hat{x} = \begin{cases} \frac{1}{2\pi} \tan^{-1}(b/a) & \text{for } a \geq 0 \\ \frac{1}{2\pi} \tan^{-1}(b/a) + \frac{1}{2} & \text{for } a < 0 \text{ and } b \geq 0, \\ \frac{1}{2\pi} \tan^{-1}(b/a) - \frac{1}{2} & \text{for } a < 0 \text{ and } b \leq 0 \end{cases} \quad (AI.2)$$

where a is obtained as

$$a = \{(1/2)(J(0.25) + J(-0.25)) - J(0)\} \quad (AI.3)$$

and

$$b = \{(1/2)(J(0.25) + J(-0.25))\}. \quad (AI.4)$$

Therefore, compared with the exhaustive line search, the curve-fitting method has a much lower complexity. Also, results have shown that it achieves almost the same performance to that of the more demanding line search [88, 91].

APPENDIX II

Since the calculated covariance matrix is circulant due to the circular shifts, the cost function in (5.18) is obtained by calculating only the first row of the covariance matrix. Thus, the following shows the approximation of (5.19), starting from $(1, p + 1)$ -th element $\varphi_{1,p+1}$ of the covariance matrix [90].

$$\begin{aligned}
\varphi_{1,p+1} &= \sum_{m=0}^{N-1} e^{j\frac{2\pi\partial m}{N}} h_m e^{j\frac{2\pi\partial(m+p)N}{N}} h_{(m+p)N}^* \\
&= \sum_{m=0}^{N-1} e^{-j\frac{2\pi\partial p}{N}} h_m h_{(m+p)N}^* - \sum_{m=0}^{p-1} e^{-j\frac{2\pi\partial p}{N}} h_{N-p+m} h_m^* - e^{j\frac{2\pi\partial(N+p)}{N}} h_{N-p+m} h_m^* \\
&= e^{-j\frac{2\pi\partial p}{N}} \alpha_p + e^{-j\frac{2\pi\partial(N/2+p)}{N}} 2j \sin(\pi\partial) \beta_p \tag{AII.1}
\end{aligned}$$

where h_m represents the time domain received signal without CFO, $\alpha_p = h_m h_{(m+p)N}^*$, $\beta_p = h_{N-p+m} h_m^*$ and $\partial = \varepsilon - \bar{\varepsilon}$. From the above equation, the power, $|\varphi_{1,p+1}|^2$, is expressed as

$$\begin{aligned}
|\varphi_{1,p+1}|^2 &= 4 \left(|\beta_p|^2 + \text{Re}\{\alpha_p \beta_p^*\} \right) \sin^2(\pi\partial) + 4 \text{Im}\{\alpha_p \beta_p^*\} \cos(\pi\partial) \sin(\pi\partial) + |\alpha_p|^2 \\
&= -2 \left(|\beta_p|^2 + \text{Re}\{\alpha_p \beta_p^*\} \right) \cos(2\pi\partial) + 2 \text{Im}\{\alpha_p \beta_p^*\} \sin(2\pi\partial) + \gamma_p \tag{AII.2}
\end{aligned}$$

where $\gamma_p = |\alpha_p|^2 + 2 \left(|\beta_p|^2 + \text{Re}\{\alpha_p \beta_p^*\} \right)$. $\text{Re}\{\cdot\}$ and $\text{Im}\{\cdot\}$ represent the real and the imaginary parts respectively. To obtain (AII.2), we use the fact that $\alpha_p \beta_p^* e^{j\pi\partial} - \alpha_p^* \beta_p e^{-j\pi\partial} = 2j \text{Im}\{\alpha_p \beta_p^*\} \cos(\pi\partial) + 2 \text{Re}\{\alpha_p \beta_p^*\} \sin(\pi\partial)$, $\cos^2(\pi\partial) = (1 - \cos(2\pi\partial))/2$ and $\cos(\pi\partial) \sin(\pi\partial) = \sin(2\pi\partial)/2$. Also, since α_p for $M < p \leq N - M + 1$ denotes the element of the covariance matrix without CFO, it can be approximated as zero at high SNR, and the cost function in (5.18) approximated as $A \cos(2\pi\partial) + B$. Likewise, if the OFDM system is noise-free, α_p for $M < p \leq N - M + 1$, which is the $(1, p + 1)$ -th element of CFO-free covariance matrix is zero from (5.17). As it follows from (AII.2), it is obvious that $A = -B$. Hence, the cost function can be expressed as $A \cos(2\pi\partial) - A$ without any approximation [90].

REFERENCES

- [1] T. H. Maiman, “Stimulated optical radiation in ruby,” *Nature*, vol. 187(4736), pp. 493–494, 1960.
- [2] K. Kao and G. Hockman, “Dielectric-fiber surface waveguides for optical frequencies,” *Proc. IEEE*, vol. 113, pp. 1151–1158, 1966.
- [3] L. Kazovsky, “Multichannel coherent optical communications systems,” *J. Lightw. Technol.*, vol. 5, pp. 1095–1102, 1987.
- [4] T. Okoshi, “Heterodyne and coherent optical fiber communications: Recent progress,” *IEEE Trans. on Microw. Tech.*, vol. 82, pp. 1138–1149, 1982.
- [5] A. H. Gnauck, R. W. Tkach, A. R. Chraplyvy and T. Li, “High-capacity optical transmission systems,” *J. Lightw. Technol.*, vol. 26, pp. 1032–1045, 2008.
- [6] L. Gruner-Nielsen, M. Wandel, P. Kristensen, C. Jorgensen, L.V. Jorgensen, B. Edvold, B. Palsdottir, D. Jakobsen, “Dispersion-compensating fibers,” *J. Lightw. Technol.*, vol. 23, NO. 11, pp. 3566–3379, 2005.
- [7] A. E. Willner, K. M. Feng, S. Lee, J. Peng, H. Sun, “Tunable compensation of channel degrading effects using nonlinearly chirped passive fiber Bragg gratings,” *IEEE Journal on select topics, quantum electron*, vol. 5, no. 5, pp. 1298–1311, 1999.
- [8] B. J. Eggleton, A. Ahuja, P. S. Westbrook, J. A. Rogers, P. Kuo, T. N. Nielsen, B. Mikkelsen, “Integrated tunable fiber gratings for dispersion management in high-bit rate systems,” *J. Lightw. Technol.*, vol. 18, no. 10, pp. 1418–1432, 2000.
- [9] H. Bulow, F. Buchali and A. Klekamp, “Electronic dispersion compensation,” *J. Lightw. Technol.*, vol. 26, pp. 158–167, 2007.
- [10] H. Bulow, F. Buchali, W. Baumert, R. Ballentin and T. Wehren, “PMD mitigation at 10 Gbit/s using linear and nonlinear integrated electronic equalizer circuits,” *IET Elect. Lett.*, vol. 36, pp. 163–164, 2000.

- [11] R. I. Killey, P. M. Watts, V. Mikhailov, M. Glick and P. Bayvel, "Electronic dispersion compensation by signal predistortion using digital processing and a dual-drive Mach-Zehnder modulator," *IEEE Photon. Technol. Lett.*, vol. 17, pp. 714–716, 2005.
- [12] J. P. Elbers, H. Wernz, H. Griesser, C. Glingener, A. Faerbert, S. Langenbach, N. Stojanovic, C. Dorschky, T. Kupfer, C. Schulien, "Measurement of the dispersion tolerance of optical duobinary with an MLSE-receiver at 10.7 Gb/s," in Optical fiber communications conference, paper no. OThJ4, Los Angeles, 2005.
- [13] J. Han, W. Li, Z. Yuan, Y. Zheng, and Q. Hu, "A simplified implementation method of Mth-power for frequency offset estimation," *IEEE Photon. Technol. Lett.*, vol. 28, no. 12, pp. 1317–1320, June, 2016.
- [14] X. Zhou, X. Chen, and K. Long, "Wide-range frequency offset estimation algorithm for optical coherent systems using training sequence," *IEEE Photon. Technol. Lett.*, vol. 24, no. 1, pp. 82–84, Jan. 1, 2012.
- [15] J. Han, W. Li, Z. He, Q. Hu, and S. Yu, "Multiplier-free carrier phase estimation for optical coherent systems," *IEEE Photon. Technol. Lett.*, vol. 28, no. 20, pp. 2168–2171, Oct. 15, 2016.
- [16] D. Ives, B. Thomsen, R. Maher and S. Savory, "Estimating OSNR of equalized QPSK signals," *Opt. Express*, vol. 19, no. 26, B661-B666, 2011
- [17] I. B. Djordjevic and B. Vasic, "Orthogonal frequency division multiplexing for high-speed optical transmission," *Opt. Express*, vol. 14, pp. 3767–3775, 2006.
- [18] W. Shieh, C. Athaudage, "Coherent optical orthogonal frequency division multiplexing," *Electron. Lett.*, vol. 42, pp. 587–589, 2006.
- [19] W. Shieh, X. Yi, Y. Ma and Y. Tang, "Theoretical and experimental study on PMD-supported transmission using polarization diversity in coherent optical OFDM systems," *Opt. Express*, vol. 15, pp. 9936–9947, 2007.

- [20] W. Shieh and I. Djordjevic, "OFDM for optical communications," Academic Press, 2010.
- [21] E. Forestieri and L. Vincetti, "Exact evaluation of the Jones matrix of a fiber in the presence of polarization mode dispersion of any order," *J. Lightw. Technol.*, vol. 17, pp. 1898–1909, Dec. 2001.
- [22] G. P. Agrawal, "Lightwave Technology: Components and Devices," Wiley-Interscience, New York, 2004.
- [23] N. Gisin, B. Huttner, "Combined effects of polarization mode dispersion and polarization dependent losses in optical fibers," *Opt. Commun.*, vol.142, pp. 119–125, 1997.
- [24] R. W. Chang, "High-Speed Multichannel Data Transmission with Bandlimited Orthogonal Signals," *Bell Sys. Tech. J.*, vol. 45, pp. 1775–1796, 1966.
- [25] B. R. Saltzberg, "Performance of an Efficient Parallel Data Transmission System," *IEEE Trans. Commun. Tech.*, vol. 15, no. 6, pp. 805–811, 1967.
- [26] S. B. Weinstein and P. M. Ebert, "Data Transmission for Frequency-Division Multiplexing Using the Discrete Fourier Transform," *IEEE Trans. Commun. Tech.*, vol. 19, no. 5, pp. 628–634, 1971.
- [27] Peled and A. Ruiz, "Frequency domain data transmission using reduced computational complexity algorithms," *Int. Conf. on Acoustics, Speech and Sig. Proc.*, vol. 5, pp. 964–967, 1980.
- [28] L. Cimini, "Analysis and Simulation of a Digital Mobile Channel Using Orthogonal Frequency Division Mutiplexing," *IEEE Trans. Commun.*, vol. 33, no. 7, pp. 665–675, 1985.
- [29] IEEE Std. 802.11a-1999, Wireless LAN Medium Access Control (MAC) and Physical Layer (PHY) Specification: Highspeed Physical Layer in the 5 GHz Band, the Institute of Electrical and Electronics Engineers, Inc.

- [30] R. van Nee and R. Prasad, "OFDM Wireless Multimedia Communications," Artech House, Boston, 2000.
- [31] T. Keller and L. Hanzo, "Adaptive Multicarrier Modulation: A Convenient Framework for Time-Frequency Processing in Wireless Communications," *Proc. IEEE*, Vol. 88, no.5, pp. 611-640, May 2000.
- [32] A. Molisch, "Orthogonal Frequency Division Multiplexing (OFDM)," Wiley-IEEE Press eBook Chapters, second edition, pp. 417–443, 2011.
- [33] L. Wang and C. Tellambura, "An overview of peak-to-average power ratio reduction techniques for OFDM systems," *Signal Processing and Information Technology*, 2006 IEEE International Symposium on, pp. 840–845, Aug. 2006.
- [34] H. Ochiai and H. Imai, "Performance of the deliberate clipping with adaptive symbol selection for strictly band-limited OFDM systems," *IEEE Journal Select. Areas Commun.*, vol. 18, no. 11, pp. 2270-2277, Nov. 2000.
- [35] Armstrong, "Peak-to-average power reduction for OFDM by repeated clipping and frequency domain filtering," *IET Elect. Lett.*, vol. 38, no. 5, pp. 246-247, Feb. 2002.
- [36] A. E Jones, T. A Wilkinson and S. K Barton, "Block coding scheme for reduction of peak to mean envelope power ratio of multicarrier transmission schemes", *Electron. Lett.*, vol. 30, No. 25, pp. 2098-2099, Dec. 1994
- [37] A. D. Jayalath and C. Tellambura, "The use of interleaving to reduce the peak-to-average power ratio of an OFDM signal," *Proc. IEEE GLOBECOM 2000*, vol. 1, pp. 82-86, Nov. 2000.
- [38] R. Van Nee and A. De Wild, "Reducing the peak-to-average power ratio of OFDM," *IEEE Vehicular Technology Conferences*, vol. 3, pp. 2072-2076, May 1998.
- [39] A. R. Bahai and B. R. Saltzberg, "Multi-Carrier Digital Communications: Theory and Applications of OFDM," Kluwer Academic/Plenum, 1999.

- [40] B. Lu and X. Wang, "Bayesian Blind Turbo Receiver for Coded OFDM Systems With Frequency Offset and Frequency-Selective Fading," *IEEE Journal on Select. Areas Commun.*, vol. 19, no.12, pp. 2516-2527, Dec 2001.
- [41] M. Necker and G. Stuber, "Totally Blind Channel Estimation for OFDM over Fast Varying Mobile Channels," in Proc. of IEEE International Conference on communications (NY, USA), Apr. 28-May 2, 2002.
- [42] G. B. Giannakis and C. Tepedelenlioglu, "Basis expansion models and diversity techniques for blind identification and equalization of time-varying channels," *Proc. IEEE*, pp. 1969–1986, 1998.
- [43] S. Coleri, M. Ergen, A. Puri and A. Bahai, "Channel Estimation Techniques Based on Pilot Arrangement in OFDM Systems," *IEEE Trans. Broadcast.*, vol.48, no. 3, September 2002.
- [44] C. Shin, J. G. Andrews, and E. J. Powers, "An efficient design of doubly selective channel estimation for OFDM systems," *IEEE Trans. Wireless Commun.*, vol. 6, no. 10, pp. 3790–3802, Oct. 2007.
- [45] O. Edfors and M. Sandell et al., "OFDM channel estimation by singular value decomposition," *IEEE Trans. Commun.*, vol. 46, no. 7, pp. 931-939, Jul. 1998.
- [46] Y. Li, L. J. Cimini, Jr., and N. R. Sollenberger, "Robust channel estimation for OFDM systems with rapid dispersive fading channels," *IEEE Trans. Commun.*, vol. 46, no. 7, pp. 902–915, Jul. 1998.
- [47] T. Kella, "Decision-directed channel estimation for supporting higher terminal velocities in OFDM based WLANs," in Proc. IEEE 2003 Global Telecommunications Conf. (GLOBECOM '03), pp. 1306–1310, 2003.
- [48] J. Akhtman and L. Hanzo, "Decision Directed Channel Estimation Aided OFDM Employing Sample-Spaced and Fractionally-Spaced CIR Estimators," *IEEE Trans. on Wireless Commun.*, vol. 6, no 4, pp. 1171-1175, April 2007.

- [49] O. O. Oyerinde and S. H. Mneney, "Decision Directed Channel Estimation for OFDM Systems employing Fast Data Projection Method Algorithm," in Proc. of IEEE International Conference on Communication (ICC), Dresden, Germany, pp. 14-18, June 2009.
- [50] P. H. Moose, "A technique for orthogonal frequency division multiplexing frequency offset correction," *IEEE Trans. Commun.*, vol.42, pp. 2908-2914, October 1994.
- [51] M. Sandell, J. J. Van De Beek, and P. Borjesson, "Timing and frequency synchronization in OFDM systems using the cyclic prefix," in Proc. Int. Symp. Synchronization, Essen, Germany, pp. 16-19, 1995.
- [52] W. D. Warner and C. Leung, "OFDM/FM frame synchronization for mobile radio data communication," *IEEE Trans. Veh. Technol.*, vol. 42, pp. 302-313, Aug. 1993.
- [53] M. Wu and W. Zhu, "A Preamble-aided Symbol and Frequency Synchronization Scheme for OFDM Systems," Circuits and Systems, ISCAS 2005., IEEE International Symposium on, Vol. 3, pp. 2627-2630, 23-26 May 2005.
- [54] D. Huang, T. Cheng and C. Yu, "Accurate Two-Stage Frequency Offset Estimation for Coherent Optical Systems," *IEEE Photon. Technol. Lett.*, vol. 25, no. 2, pp. 179-182, Jan. 2013.
- [55] X. Yang, Y. Wang, Z. Dou and L. Feng, "A Proposed Joint Timing and Frequency Synchronization Method for IEEE 802.16d OFDM Systems," IEEE International Conference on Commun. Systems (ICCS) 2008, pg. 34 -38, 2008.
- [56] G. Agrawal, "Nonlinear Fiber Optics," 3rd edition, Academic Press, San Diego, 2001.
- [57] C. Demir, A. Mehrotra, and J. Koychowdhury, "Phase noise in oscillators: a unifying theory and numerical methods for characterization," *IEEE Trans. on Fundamental Theory and Applications*, vol. 47, pp. 655 -674, May 2000.

- [58] W. Shieh, Q. Yang, Y. Ma, "107 Gb/s coherent optical OFDM transmission over 1000-km SSMF fiber using orthogonal band multiplexing," *Opt. Express*, vol. 16, pp. 6378–6386, 2008.
- [59] S. Jansen, I. Morita, H. Tanaka, "10 x121.9-Gb/s PDM-OFDM transmission with 2-b/s/Hz spectral efficiency over 1000 km of SSMF," in *Opt. Fiber Commun. Conference*, paper no. PDP2, San Diego, 2008.
- [60] S. Hara, R. Prasad, "Multicarrier Techniques for 4G Mobile Communications," Boston: Artech House, 2003.
- [61] L. Hanzo, M. Munster, B. J. Choi, T. Keller, "OFDM and MC-CDMA for Broadband Multi-User Communications, WLANs and Broadcasting," Wiley, New York, 2003.
- [62] S. T. Le, P. A. Haigh, A. D. Ellis and S. K. Turitsyn, "Blind Phase Noise Estimation for CO-OFDM Transmissions," *J. Lightw. Technol.*, vol. 34, no. 2, pp. 745-753, 2016.
- [63] H. Nguyen-Le, T. Le-Ngoc, and C. C. Ko, "RLS-based joint estimation and tracking of channel response, sampling, and carrier frequency offsets for OFDM," *IEEE Trans. Broadcast.*, vol. 55, pp. 84–94, Mar. 2009.
- [64] S. Wu and Y. Bar-Ness, "A phase noise suppression algorithm for OFDM-based WLANs," *IEEE Commun. Lett.*, vol. 6, no. 12, pp. 535–537, Dec. 2002.
- [65] W. Shieh, "Maximum-likelihood phase and channel estimation for coherent optical OFDM," *IEEE Photon. Technol. Lett.*, vol. 20, no. 8, pp. 605–607, 2008.
- [66] X. Zhou, K. P Long, R. Li, X. L. Yang, and Z. S. Zhang, "A simple and efficient frequency offset estimation algorithm for high-speed coherent optical OFDM systems," *Opt. Express*, vol. 20, no. 7, pp. 7350–7361, Mar. 2012.
- [67] Y. Liu, Y. Peng, S. Wang, and Z. Chen, "Improved FFT-based frequency offset estimation algorithm for coherent optical systems," *IEEE Photon. Technol. Lett.*, vol. 26, no. 6, pp. 631-616, 2014.

- [68] S. Yu, Y. Cao, H. Leng, G. Wu, and W. Gu, "Frequency estimation for optical coherent M-QAM system without removing modulated data phase," *Opt. Commun.*, vol. 285, no. 18, pp. 3692–3696, Aug. 2012.
- [69] X. Yi, W. Shieh, and Y. Tang, "Phase estimation for coherent optical OFDM," *IEEE Photon. Technol. Lett.*, vol. 19, no. 12, pp. 919–921, 2007.
- [70] S. Cao, C. Yu, and P. Y. Kam, "Decision-aided, pilot-aided, decision-feedback phase estimation for coherent optical OFDM systems," *IEEE Photon. Technol. Lett.*, vol. 24, no. 22, pp. 2067–2069, 2012.
- [71] S. T. Le, T. Kanesan, E. Giacomidis, N.J. Doran, and A.D. Ellis, "Quasi-pilot aided phase noise estimation for coherent optical OFDM systems," *IEEE Photon. Technol. Lett.*, vol. 26, no. 5, pp. 504–507, 2014.
- [72] J. G. Proakis, *Digital Communications*, 4th ed. Boston, MA: Mc-Graw-Hill, 2000, ch. 5.
- [73] W. Shieh and C. Athaudage, "Coherent optical orthogonal frequency division multiplexing," *Electron. Lett.*, vol. 42, no. 10, pp. 587–589, May 2006.
- [74] S. Randel, S. Adhikari, and S. L. Jansen, "Analysis of RF-pilot-based phase noise compensation for coherent optical OFDM systems," *IEEE Photon. Technol. Lett.*, vol. 22, no. 17, pp. 1288–1290, 2010.
- [75] X. Zhou, X. Yang, R. Li, and K. Long, "Efficient joint carrier frequency offset and phase noise compensation scheme for high-speed coherent optical OFDM systems," *J. of Lightw. Technol.*, vol. 31, no. 11, pp. 1755–1761, 2013.
- [76] T. N Schmidl and D. C. Cox, "Robust frequency and timing synchronization for OFDM," *IEEE Trans. Commun.*, vol. 45, no. 12, pp. 1613–1621, Dec. 1997.
- [77] I. Karasalo, "Estimating the covariance matrix by signal subspace averaging," *IEEE Trans. Acoust., Speech, Signal Process.*, vol. 34, pp. 8–12, Feb. 1986.
- [78] N. L. Owsley, "Adaptive data orthogonalization," in *ICASSP '78*, pp. 109–112, 1978.
- [79] G. Xu and T. Kailath, "Fast subspace decomposition," *IEEE Trans. Signal Process.*, vol.

- 42, no. 3, pp. 539–551, Mar. 1994.
- [80] G. Xu and T. Kailath, “Fast estimation of principal Eigen-space using Lanczos algorithm,” *SIAM J. Matrix Analysis Appl.*, vol. 15, no. 3, pp. 974–994, Jul. 1994.
- [81] B. N. Parlett, “The Symmetric Eigenvalue Problem. Englewood Cliffs,” NJ: Prentice-Hall, 1980.
- [82] P. Strobach, “Low-rank adaptive filters,” *IEEE Trans. Signal Process.*, vol. 44, pp. 2932–2947, Dec. 1996.
- [83] J. F. Yang and M. Kaveh, “Adaptive Eigen-subspace algorithms for direction or frequency estimation and tracking,” *IEEE Trans. Acoust., Speech, Signal Process.*, vol. 36, pp. 241–251, Feb. 1988.
- [84] X. Doukopoulos and G. Moustakides, “Fast and stable subspace tracking,” *IEEE Trans. Signal Process.*, vol. 56, no. 4, pp. 1452–1465, Apr. 2008.
- [85] X. G. Doukopoulos, “Power techniques for blind channel estimation in wireless communication systems,” Ph.D. dissertation, IRISA-INRIA, Univ. Rennes 1, Rennes, France, 2004.
- [86] G. H. Golub and C. F. Van Loan, *Matrix Computations*, 3rd ed., The John Hopkins University Press, 1996.
- [87] Y. Yao and G. B. Giannakis, “Blind carrier frequency offset estimation in SISO, MIMO, and multiuser OFDM systems,” *IEEE Trans. Commun.*, vol. 53, pp. 173–183, 2005.
- [88] L. Wu, X. D Zhang, P. S. Li, and Y. T. Su, “A blind CFO estimator based on smoothing power spectrum for OFDM systems,” *IEEE Trans. Commun.*, vol. 57, no. 7, pp. 1924–1927, July 2009.
- [89] X. N. Zeng and A. Ghrayeb, “A blind carrier frequency offset estimation scheme for OFDM systems with constant modulus signaling,” *IEEE Trans. Commun.*, vol. 56, no. 7, pp. 1032–1037, July 2008.

- [90] J. Oh, J. Kim, and J. Lim, "Blind carrier frequency offset estimation for OFDM systems with constant modulus constellations," *IEEE Commun. Lett.*, vol. 15, no. 9, pp. 971–973, Sep. 2011.
- [91] A. Al-Dweik, A. Hazmi, S. Younis, B. Sharif, and C. Tsimenidis, "Carrier frequency offset estimation for OFDM systems over mobile radio channels," *IEEE Trans. Veh. Commun.*, vol. 59, no. 2, pp. 974–979, Feb. 2010.
- [92] S. Lmai, A. Bourre, C. Laot, and S. Houcke, "An efficient blind estimation of carrier frequency offset in OFDM systems," *IEEE Trans. Veh. Commun.*, vol. 63, no. 4, pp. 1945–1950, May 2014.
- [93] T. Roman, S. Visuri, and V. Koivunen, "Blind frequency synchronization in OFDM via diagonality criterion," *IEEE Trans. Signal Process.*, vol. 54, no. 8, pp. 3125–3135, Aug. 2006.
- [94] X. Wang and B. Hu, "A low-complexity ML Estimator for carrier and Sampling Frequency Offsets in OFDM Systems," *IEEE Commun. Lett.*, vol. 18, no. 3, pp. 503–506, Mar. 2014.
- [95] J. J. Vande Beek, M. Sandell, and P. O. Borjesson, "ML estimation of time and frequency offset in OFDM systems," *IEEE Trans. Signal process.*, vol. 43, pp. 761–766, August 1997.
- [96] T. M. Schmidl and D. C. Cox, "Robust frequency and timing synchronization for OFDM," *IEEE Trans. Commun.*, vol. 45, pp. 1613–1621, December 1997.
- [97] Y. Kim and J. Lee, "Joint maximum likelihood estimation of carrier and sampling frequency offsets for OFDM systems," *IEEE Trans. Broadcast.*, vol. 57, pp. 277–283, June 2011.
- [98] D. N. Godard, "Self-recovering equalization and carrier tracking in two dimensional data communication systems," *IEEE Trans. Commun.*, vol. 28, pp. 1867–1875, November 1980.

- [99] J. Whitehead and F. Takawira, "Performance analysis of the linearly constrained constant modulus algorithm-based multiuser detector," *IEEE Trans. Signal Process.*, vol. 53, no. 2, pp.643 -653, 2005.
- [100] J. Du, Q. Peng, and H. Zhang, "Adaptive blind channel identification and equalization for OFDM-MIMO wireless communication systems," in Proc. 14th IEEE PIMRC 2003, pp. 2078-2083, 2003.
- [101] Y. Chen, T. Le-Ngoc, B. Champagne, and C. Xu, "Recursive least squares constant modulus algorithm for blind adaptive array," *IEEE Trans. Signal Process.*, vol. 52, no. 5, pp.1452-1456, May 2004.
- [102] A. Al-Dweik, A. Hazmi, S. Younis, B. Sharif and C. Tsimenidis, "Blind iterative frequency offset estimator for orthogonal frequency division multiplexing systems," in *IET Commun.*, vol. 4, no. 16, pp. 2008-2019, 2010.
- [103] S. Attallah and K. Abed-Meraim, "Low cost adaptive algorithm for noise subspace estimation," *Electron. Lett.*, vol. 38, pp. 609–611, June 2002.
- [104] T. Gustaffson and C. S. MacInnes, "A Class of Subspace Tracking Algorithms Based on Approximation of the Noise Subspace," *IEEE Trans. Signal Process.*, vol. 48, no. 11, pp. 3231-3235, Nov. 2000.
- [105] X. G. Doukopoulos and G. V. Moustakides, "Blind adaptive channel estimation in OFDM systems," *IEEE Trans. on Wireless Commun.*, vol. 5, no. 7, pp. 1716-1725, July 2006.
- [106] F. Zhang, Y. Wang and B. Ai, "Variable step-size MLMS algorithm for digital predistortion in wideband OFDM systems," *IEEE Trans. Consumer Electron.*, vol. 61, no. 1, pp. 10-15, February 2015.
- [107] D. W. Tufts and R. Kumaresan, "Estimation of frequencies of multiple sinusoids: Making linear predictions perform like maximum likelihood," *Proc. IEEE*, vol. 70, no. 9, pp. 975-989, Sept. 1982.

- [108] S. Chen, Q. Yang, Y. Ma and W. Shieh, "Real-Time multi-gigabit receiver for coherent optical MIMO-OFDM signals," *J. of Lightw. Technol.*, vol. 27, no. 16, pp. 3699-3704, August 2009.